Centre d'Études Doctorales : Sciences et Techniques
Formation Doctorale : Mathématique et physiques appliquées

THÈSE

Présentée par

Mustapha Zekraoui

Pour l'obtention du grade de
DOCTEUR

Spécialité : …..

Mechatronic modeling and control of a wind turbine system & Role of VANETs in managing Smart Cities.

Soutenue le / /2017 à h devant la commission d'examen composée de :

Président :
Rapporteurs :

Examinateurs :

Directeurs de thèse :

ACKNOWLEDGEMENT

I would like to express my deep gratitude towards my colleagues and friends:

- *Mr. Nourreddine Kouider, this Thesis Supervisor and Head of the Beni Mellal University of Science and Technology's Mechanical Engineering Department.*
- *Mr. Mustapha Mabrouki, Head of the Beni Mellal University of Science and Technology's Engineering Industrial Lab.*
- *Mr. Abdelilah Maach, Professor of Computer Networks and Head of the Mohammadia Engineering School's Intelligent Systems Lab in Rabat.*

Special thanks go to my students, namely:

- *Mr. Zakaria Khaouch, from the Beni Mellal University of Science and Technology's Engineering Industrial Lab,*
- *Mr. Ayoub Bouroumine, from the Mohammadia Engineering School's Intelligent Systems Lab.*

My family has played a supporting role in this endeavor. I would like to thank all of them:

- *My Mother and Father*
- *My Wife and Children.*

Mustapha Zekraoui

DEDICATION

My Mother Rabiha Oujaoura.

My Father Salah Zekraoui,

My Wife Raja Bacim,

My Children:

Ahmad, Muhammad, Essraa and Rayyaan.

Mustapha Zekraoui

Abstract

As wind turbines increased in size and power, control specifications became more challenging and regulation mechanisms more sophisticated. More and more reliable and powerful model control strategies are needed not only to keep the turbine within its safe operating region but also to improve efficiency and quality of power conversion. This paper mainly focuses on the mechatronic modeling and control of a 5MW Variable-Speed Variable-Pitch Wind Turbine (VS-VP WT) for the above-rated power operating condition. The principal parts of the wind turbine are modeled by using the Bond-Graph approach and the control strategy is realized by combining a torque control with a blade pitch control strategy by means of bicausality of the bond graph. The robustness of the proposed model control is verified and the simulation of the complete model is conducted for variable wind speed operation conditions.

Contents

Liste of figures

Liste of tables

INTRODUCTION

This “Thesis of Works” summarizes the research activities of the author for almost the past two and half years. The topics covered in this report are two-fold:

The first one deals with a mechatronic modeling of the dynamic behavior of the popular Wind Turbine Systems. The Beni Mellal University of Science and Technology’s Industrial Engineering Lab harbored this subject’s works. It gave rise to two publications which make the main content of this report.

The second one, conducted in the Mohammadia School of Engineers’ Intelligent Systems’ Lab, features the new trend in modeling the so-called Smart City Infrastructure by means of the wireless communication Vehicular Ad-hoc Networks (VANETs). This research produced three publications which constitute the second part of this report.

The following lines provide the reader with an overview of both topics.

Wind turbines are electric power generation systems that involve dynamic behaviors that are difficult to control. These behaviors are mainly related to poorly controlled couplings between certain subsystems. A state of the art on the existing modeling practices highlights a lack of consideration of energetic interactions between the subsystems, making it hard to analyze and control these phenomena and leading to point solutions. This contribution introduces a mechatronic approach to multiphysical and multilevel representation applied to wind power systems, that is to say, considering the wind system as a multi-domain mechatronics system including various areas of physics such as Aerodynamics, Mechanics, Electromechanics, Power Electronics and Electrical Sub-systems. This approach offers an energetic, global and structural vision to master the dynamics of this complex system. A reflection on the existing tools of representation led to the choice of the Bond Graph as a fundamental tool for: modeling the various elements, the analyzing the models properties and the design of inverse model control laws using the Bicausality. The proposed model’s reliability and the control robustness were validated by simulations.

The Smart City concept may be considered as a complex urban environment managing and controlling several complex systems including infrastructure, human behavior, technology, social, political structures, communication tools and the economy. A Smart City provides an intelligent way to manage components such as transport, health, energy, homes, buildings and the environment. The data collected by these components are usually generated by wireless networks data collectors. The wireless communication Vehicular Ad-hoc Networks (VANETs) within the Smart City are an essential tool that benefits the network in the Smart City by providing opportunistic communication to the different intelligent systems without the need of pre-installed infrastructures.

Chapter 1 is an introduction to the Wind Systems. It goes through the most popular existing technologies in the field. Chapter 2 exposes the fundamental tool used here: The Bond Graph Approach. Chapter 3 and 4 constitute two different applications of this BGA to Wind Energy Conversion Systems.

Chapter 5 deals entirely with the crucial function carried out by the VANETs in dealing with this futuristic concept of Smart City.

Chapter 1. Background and Literature Review

1.1 . Introduction

Since the beginnings of wind turbine development (~1980) until today, where wind energy is seen as a mature technology and has become an important participant in the power generation branch, various wind turbine concepts and designs have been developed. The marketable wind turbine concepts can be distinguished by different electrical design and control and can be classified by their speed range (variable speed, fixed speed) and power controllability (stall, pitch control) [1]. In the following, a general overview of wind turbine components and topology is given. Then the characteristics of different wind turbine concepts are presented. Finally the wind turbine concepts are assessed with respect to their controllability.

This chapter aims presenting a review on the wind turbines' state of the art technologies.

1.2 . Definition of a Wind Turbine

A wind turbine is a machine for converting the kinetic energy in the wind into mechanical energy. If the mechanical energy is used directly by machinery, such as a pump or grinding stones, the machine is called a windmill. If the mechanical energy is then converted to electricity, the machine is called a wind generator. Utility-scale turbines range in size from 100 kilowatts to several megawatts [2].

1.3 . Aerodynamic Lift and Aerodynamic Drag Wind Turbines

There are two different types of wind energy conversion devices: those which depend mainly on aerodynamic lift and those which use mainly aerodynamic drag. High speed turbines rely on lift forces to move the blades. To generate electricity from a wind turbine, it is usually desirable that the driving shaft of the generator operates at considerable speed (1500 revolutions per minute). This, together with the higher aerodynamic efficiency of lift devices, means that turbines which rely on aerodynamic drag are not commonly used [3].

1.4 . Horizontal-axis and Vertical-axis Wind Turbines

Wind turbines can further be classified into horizontal-axis or vertical-axis. The earliest windmills in antiquity rotated around a vertical axis and they were driven by drag. Modern vertical-axis turbines use vertical symmetrical airfoils and the driving force is produced by the lift developed by the blade in the moving air stream. The only vertical-axis turbine which has been manufactured commercially at any volume is the Darrieus machine, named after the French engineer Georges Darrieus who patented the design in 1931. The conventional Darrieus turbine has curved blades connected at the top and at the bottom and rotates like an "egg whisk" [4], as illustrated in Figure 1.

Figure 1.1. Vertical-axis wind turbine

Vertical-axis wind turbines have the advantages that no tower is needed. They operate independently of the wind direction (a yawning mechanism is not needed) and heavy gearboxes and generators can be installed at ground level. But they suffer many shortcomings: they are not self-starting, the torque fluctuates with each revolution as the blades move into and away from the wind, and speed regulation (or control) in high winds can be difficult. Vertical-axis turbines were developed and commercially produced in the 1970s until the end of the 1980s. But since then the research and production of vertical-axis wind turbines has practically stopped worldwide [5].

Nowadays, horizontal axis wind turbines (Figure 1.2.) dominate the majority of the wind industry. Horizontal axis means the rotating axis of the wind turbine is horizontal, or parallel with

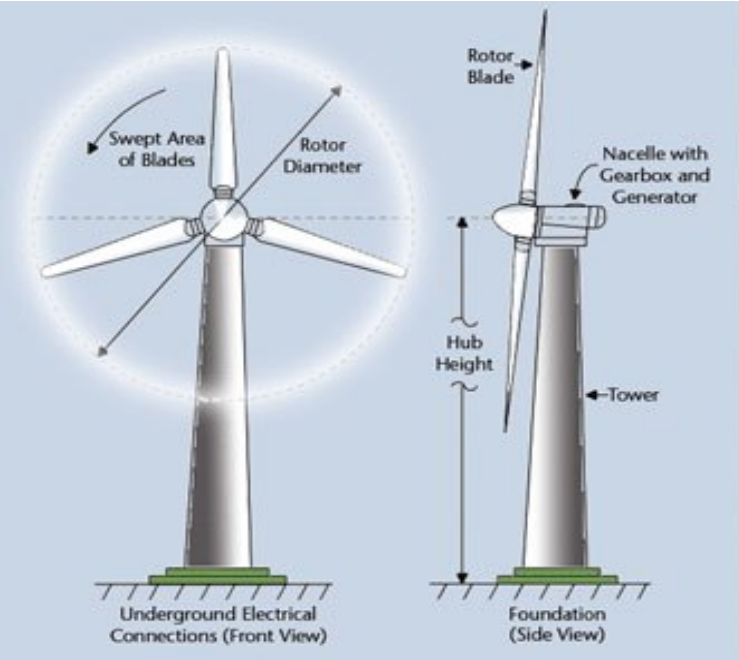

Figure 1.2. Horizontal-axis and vertical-axis wind turbines configurations

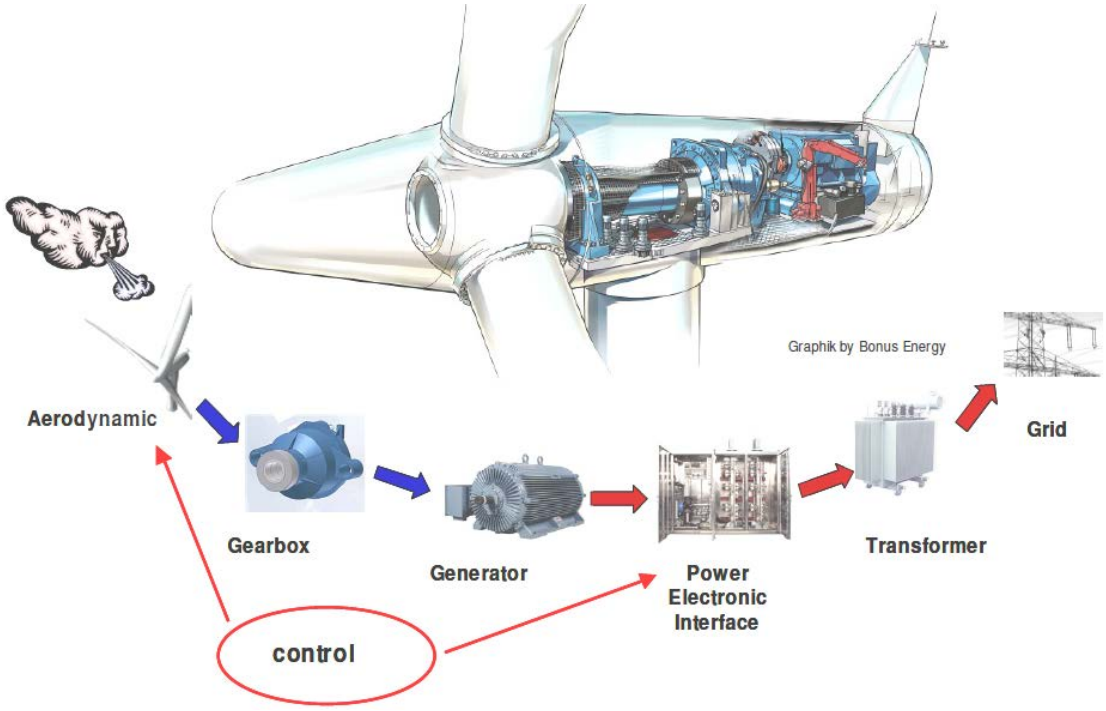

Figure 1.3. Wind turbine components

the ground. In big wind applications, horizontal axis wind turbines are almost all you will ever see. However, in small wind and residential wind applications, vertical axis turbines have their place. The advantage of horizontal wind is its ability to produce more electricity from a given amount of wind. So, if you are trying to produce as much wind as possible at all times, horizontal axis is likely the choice for you. The main shortcoming of horizontal axis however is its tremendous weight: it is generally heavier and its output power goes sharply down turbulent winds.

1.5 . 3.Wind Turbine Components

The entire system of a grid connected wind turbine includes several components, which contribute with their specific function in the energy conversion process from wind energy into electrical energy. Figure 1.3 illustrates the main components of a modern wind turbine, which are - to a greater or lesser extent - common for all wind turbine concepts.

The figure illustrates from left to right the aerodynamic and mechanical part of the wind turbine (aerodynamic rotor and gearbox), the electrical system (generator, power electronic interface and transformer) and finally its connection to the grid. An interaction with the control system is indicated as well. The turbine's different components can be listed under four main groups [6]:

1. Mechanical and aerodynamic components:
   - Rotor effective wind
   - Turbine rotor
   - Blade pitching mechanism
   - Drive train (flexible shaft, bearings)
   - Emergency breaks
   - Gear

- Tower

2. Electrical components
   - Generator types
   - Squirrel cage induction generator
   - Wound rotor induction generator
   - Doubly-fed induction generator
   - Permanent magnet synchronous generator Electrical excited synchronous generator
   - Power electronic interface
   - Soft starter
   - Capacitor bank
   - Static compensator Frequency converter
   - Protection system
   - Transformer
   - Cable
3. Control system
   - Converter controller
   - Blade angle controller
   - Overall controller

The fourth main group -called “grid components”- contains components, which do not directly belong to the wind turbine itself; however, when the impact of wind turbines with the power system is investigated the grid components play a major role.

4. Grid components – interacting with grid connected wind turbines
   - Conventional power plants (synchronous generators)
   - Frequency and voltage controller
   - Consumer load
   - Transformer
   - Cable

1.6 . Wind Turbine Systems

Wind turbines can operate with either fixed speed (actually within a speed range about 1 %) or variable speed. For fixed-speed wind turbines, the generator (induction generator) is directly connected to the grid. Since the speed is almost fixed to the grid frequency, and most certainly not controllable, it is not possible to store the turbulence of the wind in form of rotational energy. Therefore, for a fixed-speed system the turbulence of the wind will result in power variations, and thus affect the power quality of the grid [7]. For a variable-speed wind turbine the generator is controlled by power electronic equipment, which makes it possible to control the rotor speed. In this way the power fluctuations caused by wind variations can be more or less absorbed by changing the rotor speed [8] and thus power variations originating from the wind conversion and the drive train can be reduced. Hence, the power quality impact caused by the wind turbine can be improved compared to a fixed-speed turbine [9].

The rotational speed of a wind turbine is fairly low and must therefore be adjusted to the electrical frequency. This can be done in two ways: with a gearbox or with the number of pole pairs of the generator. The number of pole pairs sets the mechanical speed of the generator with respect to the electrical frequency and the gearbox adjusts the rotor speed of the turbine to the mechanical speed of the generator. In this section the following wind turbine systems will be presented:

1. Fixed-speed wind turbine with an induction generator.
2. Variable-speed wind turbine equipped with a cage-bar induction generator or synchronous generator.
3. Variable-speed wind turbine equipped with multiple-pole synchronous generator or multiple-pole permanent-magnet synchronous generator.
4. Variable-speed wind turbine equipped with a doubly-fedinduction generator.

There are also other existing wind turbine concepts; a description of some of these systems can be found in [10].

1.6.1. Fixed-Speed Wind Turbine

For the fixed-speed wind turbine, the induction generator is directly connected to the electrical grid according to Figure 1.4. The rotor speed of the fixed-speed wind turbine is generally determined by a gearbox and the pole-pair number of the generator.

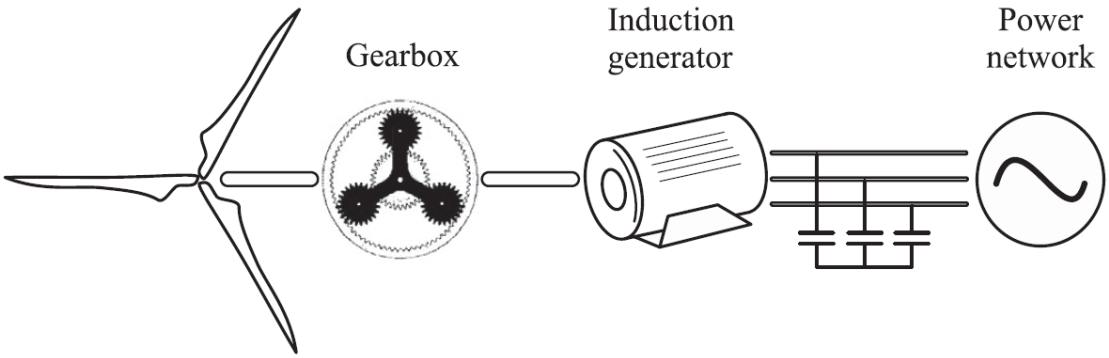

Figure 1.4. Fixed-speed wind turbine with an induction generator.

The fixed-speed wind turbine system has often two fixed speeds. This is accomplished using two generators with different ratings and pole pairs; or it can be a generator with two windings having different ratings and pole pairs. This leads to increased aerodynamic capture as well as reduced magnetizing losses at low wind speeds. This system (one or two-speed) was the “conventional” concept used by many Danish manufacturers in the 1980s and 1990s [10].

1.6.2. Variable-Speed Wind Turbine with a synchronous/induction generator.

The system presented in Figure 1.5 consists of a wind turbine equipped with a converter connected to the stator of the generator. The generator could either be a cage-bar induction generator or a synchronous generator. The gearbox is designed so that the maximum rotor speed corresponds to rated speed of the generator. Synchronous generators or permanent-magnet synchronous generators can be designed with multiple poles which implies that there is no need for

a gearbox (see Figure 1.6). Since this “full-power” converter/generator system is commonly used for other applications, one advantage with this system is its well-developed and robust control [11]. A synchronous generator with multiple poles as a wind turbine generator is successfully manufactured by Enercon [12].

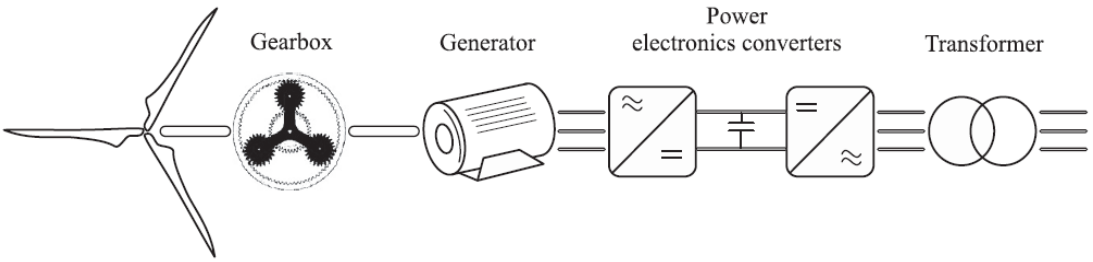

Figure 1.5. Variable-speed wind turbine with a synchronous/induction generator.

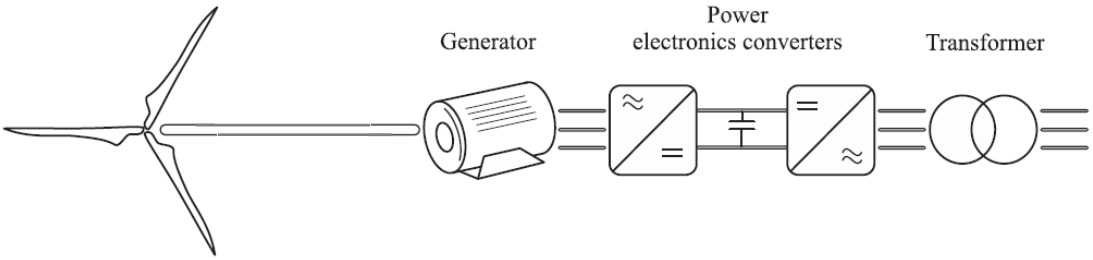

Figure 1.6. Variable-speed direct-driven (gearless) wind turbine with a synchronous generator (SG).

1.6.3. Variable-Speed Wind Turbine with Doubly-Fed Induction Generator

This system (Figure 1.7) consists of a wind turbine with doubly-fed induction generator. This means that the stator is directly connected to the grid while the rotor winding is connected via slip rings to a converter. This system has recently become very popular as generators for variable-speed wind turbines [10]. This is mainly due to the fact that the power electronic converter only has to handle a fraction (20–30%) of the total power [10]. Therefore, the losses in the power electronic converter can be reduced, compared to a system where the converter has to handle the total power. In addition, the cost of the converter becomes lower.

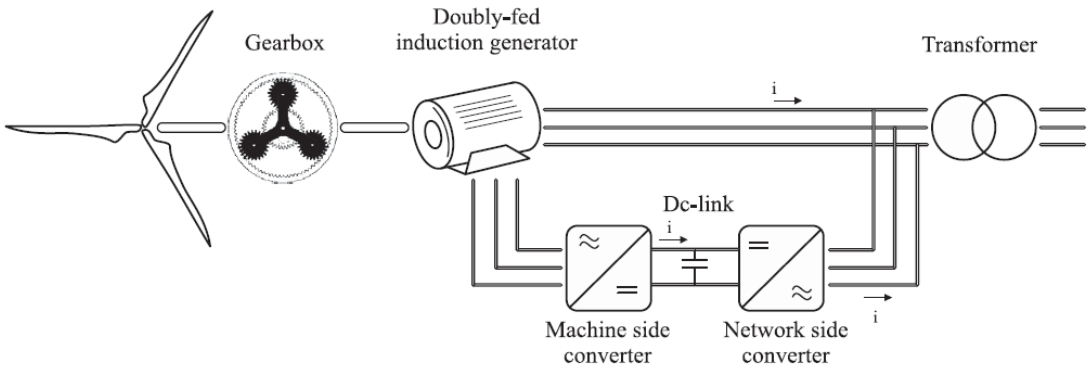

Figure 1.7. Variable-speed wind turbine with a doubly-fed induction generator (DFIG).

There exists a variant of the DFIG method that uses controllable external rotor resistances (compare to slip power recovery). Some of the drawbacks of this method are that energy is unnecessarily dissipated in the external rotor resistances and that it is not possible to control the reactive power.

Manufacturers, that produce wind turbines with the doubly-fed induction machine as generator are, for example, DeWind, GE Wind Energy, Nordex, and Vestas [13].

1.7 . Power Control

The power in the wind is equal to:

$$P = \frac{1}{2}\rho A v^3 \tag{1.1}$$

Where ρ is the air density (kg/m^3), A the area (m^2) and v the wind speed (m/s), and

P: the power of the wind (watts or J/s).

From equation (1.1), the power available from the wind is a function of the cube of the wind speed. That means that doubling the wind speed gives eight times the power output from the turbine. Therefore, turbines have to be designed to support higher wind loads than those from which they can generate electricity, to prevent them from damage.

Wind turbines reach the highest efficiency at a wind speed between 10 and 15 m/s. Above this wind speed, the power output of the rotor must be controlled to reduce driving forces on the rotor blades as well as the load on the whole wind turbine structure [14]. High winds occur only for short periods and hence have little influence in terms of energy production; but, if not controlled, they would dominate the design and cost of the drive train and the generator [15]. Accordingly, all wind turbines are designed with a type of power control. There are different ways to control aerodynamic forces on the turbine rotor and therefore limit the power in high winds in order to avoid damage to the wind turbine [16].

Three options for the power output control are currently used:

1.7.1. Stall Control

Stall control is the simplest, cheapest and most robust control method [16]. It has long been the preferred control method for small and medium sized Danish commercial turbines [15] and it is also known as passive control, since there are no moving parts to adjust: it is the inherent aerodynamic properties of the blade which determine power output. The twist and thickness of the rotor blade vary along its length in a way that turbulence occurs behind the blade whenever the wind speed becomes too high. This turbulence means that less of the energy in the air is transferred, minimizing power output in higher speeds. In other words, the design of the blades aerodynamic causes the rotor to stall (lose power) when the wind speed exceeds a certain level. Thus, the aerodynamic power of the blades is limited.

The main setback of this control method is its low efficiency at low wind speeds, and no assisted start-up [16]. Besides, this type of control requires the use of a constant speed turbine which has lower energy efficiency than the variable speed turbine.

1.7.2. Pitch Control

The blades of pitch controlled wind turbines can be turned out or into the wind as the power output becomes too high or too low, respectively. The rotor blades' angle can be actively adjusted by the control system in order to shed the unwanted power. Pitch control is relatively fast and can be used to limit the rotor speed by regulating input aerodynamic power flow [17].

The main advantages of this type of control are good power control (power kept close to the rated power in high winds), assisted start-up and emergency stop. Besides, stall controlled turbines have to be shut down beyond a certain speed, whereas pitch controlled turbines can adjust the blades' angle to reduce the aerodynamic forces.

A disadvantage that may be put forward is the complexity arising from the pitching mechanism of the blades [16].

In Figure 1.8, the change of the $Cp(\lambda,\beta)$ curve as the pitch angle is adjusted is shown. In low and medium wind speeds, the pitch angle is controlled to allow the wind turbine to operate at its optimum condition. In high wind speeds, the pitch angle is increased in order to shed some of the aerodynamic power and maintain the rotor speed within a controllable limit. As pitch angle increases, the wind turbine operates at lower efficiency [17].

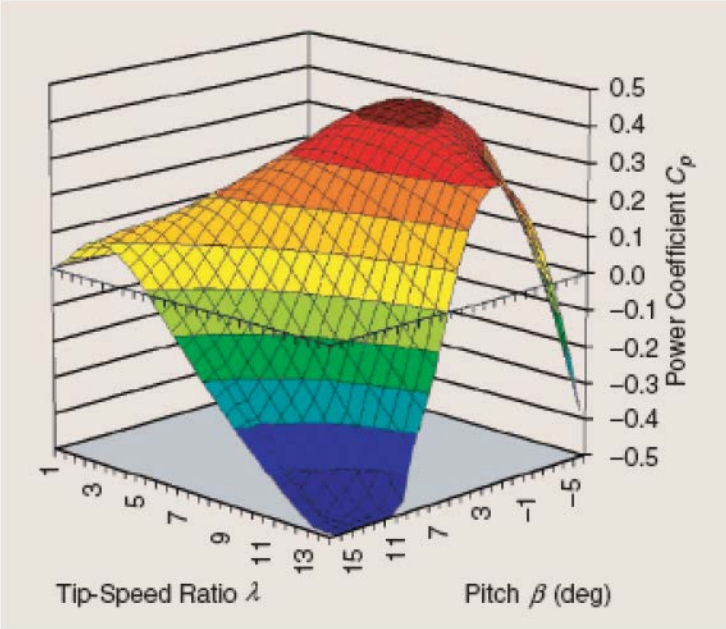

Figure 1.8. Cp vs. Tip-Speed Ratio and Pitch angle for a typical wind turbine with pitch control.

Nowadays, large wind turbines are increasingly being operated with pitch control systems [15].

1.7.3. Active Stall Control

As the name indicates, active stall control is a combination of the two techniques explained above. At low and medium wind speeds, the blades are pitched similar to a pitch-controlled turbine. When the wind turbine reaches rated capacity, the turbine will pitch in the opposite direction in order to make the blades go into a deeper stall [14].

1.8 . Conclusion

This introductory chapter presented a general overview about the marketable wind turbine concepts and emphasizes their various features. Four types of wind turbine concepts prevail in the market nowadays. The most conventional wind turbine concept is the fixed speed stall controlled wind turbine with induction generator, the so-called Danish concept. The variable speed pitch controlled wind turbine concept with doubly-fed induction generator and partial-scale frequency converter has increased its market penetration enormously, being the most popular generator concept in wind turbines today. The main trend in wind turbine technology is recently the variable speed option using pitch control and power electronic interface. This development is due to increased grid requirements for wind turbines in systems with high amount of wind power. In the subsequent chapters, an overview of the modeling tools of wind turbine systems is presented, with the focus being stressed on the so-called the Bond Graph Approach.

References

[1]. A. Hansen, G. Michalke, “Modelling and control of variable speed multi-pole PMSG wind turbine”, accepted for Wind Energy, submitted in September 2007.

[2]. EERE (2007) Wind Power. [Online] Available from: www1.eere.energy.gov/windandhydro/wind_how.html [Accessed in January 2007].

[3]. Jenkins, N. Walker, J. (1997) Wind Energy Technology. Wiley, England.

[4]. Harrison, R. Hau, E. Snel, H. (2000) Large Wind Turbines. Wiley, England.

[5]. Ackermann, T. Söder (2000) Wind energy technology and current status: a review. Renewable and Sustainable Energy Reviews, [Online] 315-374 Available from: www3.imperial.ac.uk/library/digitallibrary/electronicjournals [Accessed December 2006].

[6]. Pierik J., Morren J., de Haan S., van Engelen T., Wiggelinkhuizen E., Bozelie J., ”Dynamic models of wind farms for grid-integration studies”, Nordic Wind Power Conference NWPC, 1-2 March, Chalmers University, Sweden, 2004.

[7]. M. P. Papadopoulos, S. A. Papathanassiou, N. G. Boulaxis, and S. T. Tentzerakis, “Voltage quality change by grid-connected wind turbines,” in European Wind Energy Conference, Nice, France, 1999, pp. 783–785.

[8]. T. Petru and T. Thiringer, “Active flicker reduction from a sea-based 2.5 MW wind park connected to a weak grid,” in Proc. Nordic Workshop on Power and Industrial Electronics, Aalborg, Denmark, June, 13–16, 2002.

[9]. A . Larsson, P. Sørensen, and F. Santjer, “Grid impact of variable speed wind turbines,” in Proc. of European Wind Energy Conference and Exhibition (EWEC´99), Nice, France, Mar., 1–5, 1999.

[10]. L. H. Hansen, L. Helle, F. Blaabjerg, E. Ritchie, S. Munk-Nielsen, H. Bindner, P. Sørensen, and B. Bak-Jensen, “Conceptual survey of generators and power electronics for wind turbines,” Risø National Laboratory, Roskilde, Denmark, Tech. Rep. Risø-R-1205(EN), ISBN 87-550-2743-8, Dec. 2001.

[11]. I. Boldea and S. A. Nasar, Electric Drives. CRC Press LCC, 1999.

[12]. (2004) Enercon website. [Online]. Available: http://www.enercon.de/

[13]. DEWIND. (2005, Jan.) The D8 series. Brochure. [Online]. Available: http: //www.dewind.de/en/downloads/D8-2000-100-eng.pdf

[14]. Ackermann, T. (ed). (2005) Wind Power in Power Systems. Wiley, England.

[15]. Harrison, R. Hau, E. Snel, H. (2000) Large Wind Turbines. Wiley, England.

[16]. Ackermann, T. Söder (2000) Wind energy technology and current status: a review. Renewable and Sustainable Energy Reviews, [Online] 315-374 Available from: www3.imperial.ac.uk/library/digitallibrary/electronicjournals [Accessed December 2006].

[17]. Butterfield, C. Muljadi, E. (2001) Pitch-Controlled Variable-Speed Wind Turbine Generation. IEEE Transactions on Industry Applications.

Chapter 2. Mechatronic Systems Modeling Tools Overview

2.1 . Introduction

Modeling goals: The physical modeling of mechatronic systems is predominantly characterized by the multidisciplinary (multi-domain) character of the different component systems. Naturally, the goal is a complete abstract model, representing overall system behavior a domain-independent model. In this and following sections, this will be accomplished by transferring and simplifying fundamental physical model equations (differential equations, algebraic equations) into linear time-invariant (LTI) models in a frequency-domain representation (transfer functions). Using such models, a series of significant analyses of system behavior can be efficiently worked through using established (commercial) computational tools. However, to deal with more complex high-fidelity models, further modeling must be undertaken.

Modeling approaches: Starting from the view of a system using lumped system elements and generally valid statements of energy conservation, there are fundamentally two modeling approaches which emerge (Figure 2.1):

- energy-based modeling employing scalar energy functions (LAGRANGE formalism, HAMILTON's equations)
- multi-port modeling employing component-based system models with power-conserving network rules (KIRCHHOFF networks, bond graphs).

In both modeling approaches, the aspects of back-effect arising from mutual power exchanges between interacting system components is taken into account in different ways. In the case of

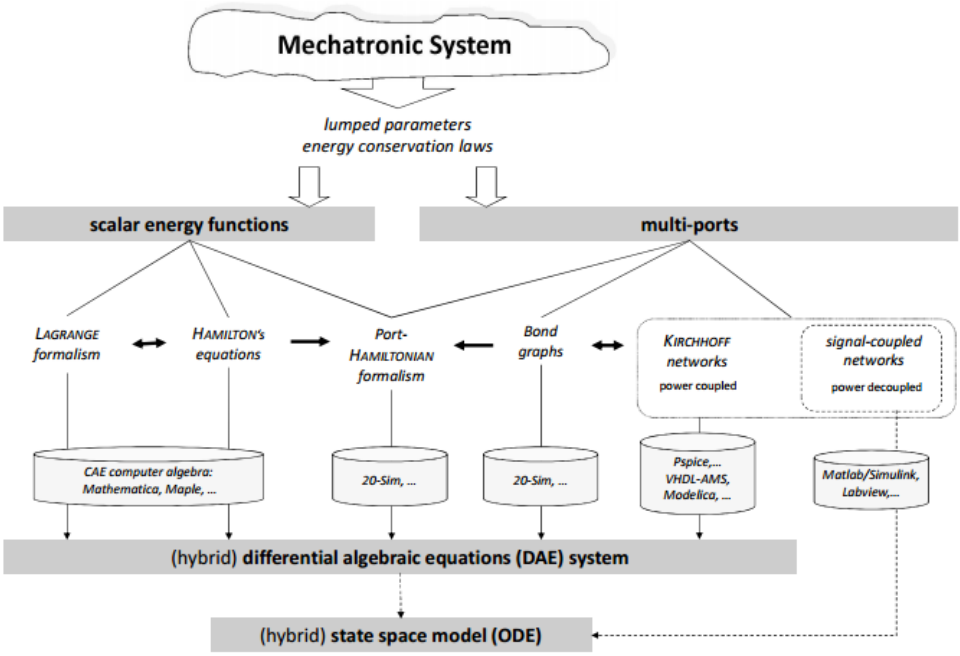

Figure 2.1. Paradigms and commercial computational tools for multi-domain modeling of mechatronic systems using lumped system elements

unidirectional KIRCHHOFF networks, modeling can be simplified using signal-coupled networks (e.g. control system signal-oriented diagrams). The port-HAMILTONIAN formulation an interesting, relatively new approach combines properties of energy-based and multi-port modeling and enables a specific type of mathematical model which is particularly useful for nonlinear controller design.

Among those modeling tools, the Bond Graph (BG) [1-5] Approach is, by far, the most suitable for multi-domain mechatronic systems such as Wind Turbines. Therefore, the following section deals entirely with a relatively detailed introduction to this BG Tool.

2.2 . Introduction to the Bond Graph Approach

Bond graphs are a domain-independent graphical description of dynamic behavior of physical systems. This means that systems from different domains (cf. electrical, mechanical, hydraulic, acoustical, thermodymanic, material) are described in the same way. The basis is that bond graphs are based on energy and energy exchange. Analogies between domains are more than just equations being analogous: the used physical concepts are analogous. Bond-graph modeling is a powerful tool for modeling engineering systems, especially when different physical domains are involved. Furthermore, bond-graph submodels can be re-used elegantly, because bond-graph models are non-causal. The submodels can be seen as objects; bond-graph modeling is a form of object-oriented physical systems modeling. Bond graphs are labeled and directed graphs, in which the vertices represent submodels and the edges represent an ideal energy connection between power ports. The vertices are idealized descriptions of physical phenomena: it are concepts, denoting the relevant (i.e. dominant and interesting) aspects of the dynamic behavior of the system. It can be bond graphs itself, thus allowing hierarchical models, or it can be a set of equations in the variables of the ports (two at each port). The edges are called bonds. They denote point-to-point connections between submodel ports. When preparing for simulation, the bonds are embodied as two-signal connections with opposite directions. Furthermore, a bond has a power direction and a computational causality direction. Proper assigning the power direction resolves the sign-placing problem when connecting submodels structures. The internals of the submodels give preferences to the computational direction of the bonds to be connected. The eventually assigned computational causality dictates which port variable will be computed as a result (output) and consequently, the other port variable will be the cause (input). Therefore, it is necessary to rewrite equations if another computational form is specified then is needed. Since bond graphs can be mixed with block-diagram parts, bond-graph submodels can have power ports, signal inputs and signal outputs as their interfacing elements. Furthermore, aspects like the physical domain of a bond (energy flow) can be used to support the modelling process. The concept of bond graphs was originated by Paynter (1961). The idea was further developed by Karnopp and Rosenberg in their textbooks (1968, 1975, 1983, 1990), such that it could be used in practice (Thoma, 1975; Van Dixhoorn, 1982). By means of the formulation by Breedveld (1984, 1985) of a framework based on thermodynamics, bond-graph model description evolved to a systems theory. In the next section, we will introduce the bond graph method by some examples, where we start from a given network composed of ideal physical models. Transformation to a bond graph leads to a domain independent model. In section 3, we will introduce the foundations of bond graphs, and present the basic bond graph elements in section 4. We will discuss a systematic method for deriving bond graphs from engineering systems in section

5. How to enhance bond–graph models to generate the model equations and for analysis is presented in section 6, and is called Causal Analysis. The equations generation and block diagram expansion of causal bond graphs is treated in sections 7 and 8. Section 9 discusses simulation issues. In section 10 we review this chapter, and also include some hints for further reading.

2.3 . Foundations of bond graphs

Analogies between different systems were shown in the previous section: Different systems can be represented by the same set of differential equations. These analogies have a physical foundation: the underlying physical concepts are analogous, and consequently, the resulting differential equations are analogous. The physical concepts are based on energy and energy exchange. Behavior with respect to energy is domain independent. It is the same in all engineering disciplines, as can be concluded when comparing the RLC circuit with the damped mass spring system. This leads to identical bond graphs.

2.3.1. Starting points

Before discussing the specific properties of bond graphs and the elementary physical concepts, we first recall the assumptions general for network like descriptions of physical systems, like electrical networks, mechanical or hydraulic diagrams: · The conservation law of energy is applicable. · It is possible to use a lumped approach This implies that it is possible to separate system properties from each other and to denote them distinctly, while the connections between these submodels are ideal. Separate system properties mean physical concepts and the ideal connections represent the energy flow, i.e. the bonds between the submodels. This idealness property of the connections means that in these connections no energy can be generated or dissipated. This is called power continuity. This structure of connections is a conceptual structure, which does not necessary have a size. This concept is called reticulation (Paynter, 1961) or tearing (Kron, 1963). The system's submodels are concepts, idealised descriptions of physical phenomena, which are recognised as the dominating behaviour in components (i.e. real–life, tangible system parts). This implies that a model of a concrete part is not necessary only one concept, but can consist of a set of interconnected concepts.

2.3.2. Bonds and Ports

The contact point of a submodel where an ideal connection will be connected to is called a power port or port for short. The connection between two submodels is called a power bond or bond; it is drawn as a single line (Figure 2.2). This bond denotes an ideal energy flow between the two connected submodels. The energy entering the bond on one side immediately leaves the bond at the other side (power continuity).

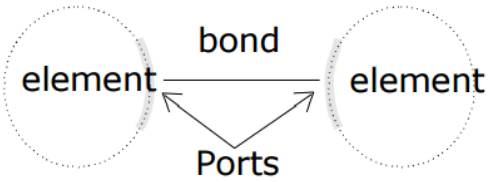

Figure 2.2. The energy flow between 2 submodels represented by a bond

The energy flow along a bond has the physical dimension of power, being the product of two variables. In each physical domain, there is such a combination of variables, for which a physical interpretation is useful. In electrical networks, the two variables are voltage and current. In mechanical systems, the variable pairs are force and velocity for translation and torque and angular velocity for rotation. In hydraulics, it is pressure and volume flow. For thermodynamic systems, temperature and entropy flow are used. These pairs of variables are called power variables. In order to understand the connection as established by a bond, this bond can be interpreted in two different ways, namely:

1. As an interaction of energy. The connected subsystems form a load to each other by their energy exchange. A power bond embodies a connection where a physical quantity is exchanged.

2. As a bilateral signal flow. The connection is interpreted as two signals, an effort and flow, flowing in opposite direction, thus determining the computational direction of the bond variables. With respect to one of the connected submodels, the effort is the input and the flow the output, while for the other submodel input and output are of course established by the flow and effort respectively.

These two ways of conceiving a bond is essential in bond graph modelling. Modelling is started by indicating the physical structure of the system. The bonds are first interpreted as interactions of energy, then the bonds are endowed with the computational direction, interpreting the bonds as bilateral signal flows. During modelling, it need not be decided yet what the computational direction of the bond variables is. Not that, determining the computational direction during modelling restricts submodel reuse. It is however necessary to derive the mathematical model (set of differential equations) from the graph. The process of determining the computational direction of the bond variables is called causal analysis. The result is indicated in the graph by the so-called causal stroke, indicating the direction of the effort, and is called the causality of the bond (Figure 2.3).

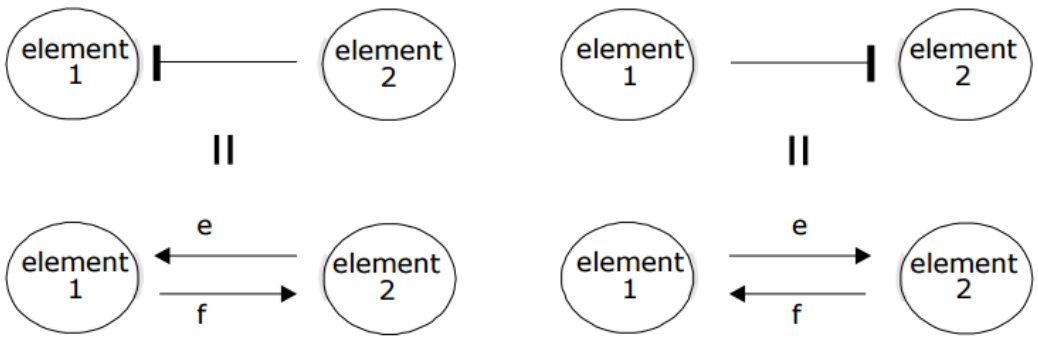

Figure 2.3 Determine the signal direction of the effort and flow (We do not use the power direction at the bonds, so it is not shown here).

The nature of the constitutive equations lay demands on the causality of the connected bonds. Bond graph elements are drawn as letter combinations (mnemonic codes) indicating the type of element. The bond graph elements are the following:

- C storage element for a q-type variable, e.g. capacitor (stores charge), spring (stores displacement).
- I storage element for a p-type variable, e.g. inductor (stores flux linkage), mass (stores momentum).
- R resistor dissipating free energy, e.g. electric resistor, mechanical friction.
- Se and Sf sources, e.g. electric mains (voltage source), gravity (force source), pump (flow source).
- TF transformer, e.g. an electric transformer, toothed wheels, lever.
- GY gyrator, e.g. electromotor, centrifugal pump.
- 0– and 1–junctions, for ideal connecting two or more submodels.

2.3.3. Storage elements

Storage elements store all kinds of free energy. As indicated above, there are two types of storage elements: C–elements and I–elements. The q–type and p–type variables are conserved quantities and are the result of an accumulation (or integration) process. They are the state variables of the system. In C–elements, like a capacitor or spring, the conserved quantity, q, is stored by accumulating the net flow, f, to the storage element. This results in the differential equation which is called a balance equation, and forms a part of the constitutive equations of the storage element. In the other part of the constitutive equations, the state variable, q, is related to the effort e = e(q) This relation depends on the specific shape of the particular storage element. In Figure 2.4, examples of C–elements are given together with the equivalent block diagram. The equations for a linear capacitor and linear spring are:

$$\dot{q} = i, \qquad u = \frac{1}{C} q \tag{2.1}$$

$$\dot{x} = v, \qquad F = kx = \frac{1}{C} x \tag{2.2}$$

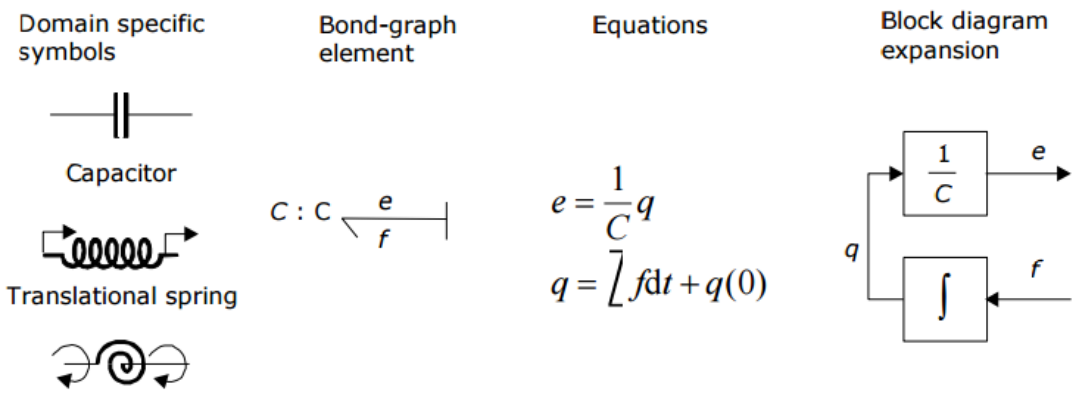

Figure 2.4. Examples of C elements

For a capacitor, C is the capacitance and for a spring, K [N/m] is the stiffness and C [m/N] the compliance. For all other domains, a C–element can be defined.

The effort variable is equal when two C–storage elements connected in parallel with a resistor in between are in equilibrium. Therefore, the domain–independent property of an effort is determination of equilibrium.

In I–elements, like a inductor or mass, the conserved quantity, p, is stored by accumulating the net effort, e, to the storage element. The resulting differential equation is:

$$\dot{p} = e \tag{2.3}$$

In Figure 2.5, examples of I–elements are given together with the equivalent block diagram. The equations for a linear inductor and linear mass are:

$$\dot{\lambda} = i, \qquad i = \frac{1}{L}\lambda \tag{2.4}$$

$$\dot{p} = F, \qquad v = \frac{1}{m}p \tag{2.5}$$

For an inductor, L [H] is the inductance and for a mass, m [kg] is the mass. For all other domains, a I– element can be defined. The flow variable is equal when two I–storage elements connected in parallel with a resistor in between, are in equilibrium. Therefore, at I–elements, the domain–independent property of the flow is determination of equilibrium. For example, when two bodies, moving freely in space each having a different momentum, are being coupled (collide and stick together), the momentum will divide among the masses such that the velocity of both masses is the same (this is the conservation law of momentum).

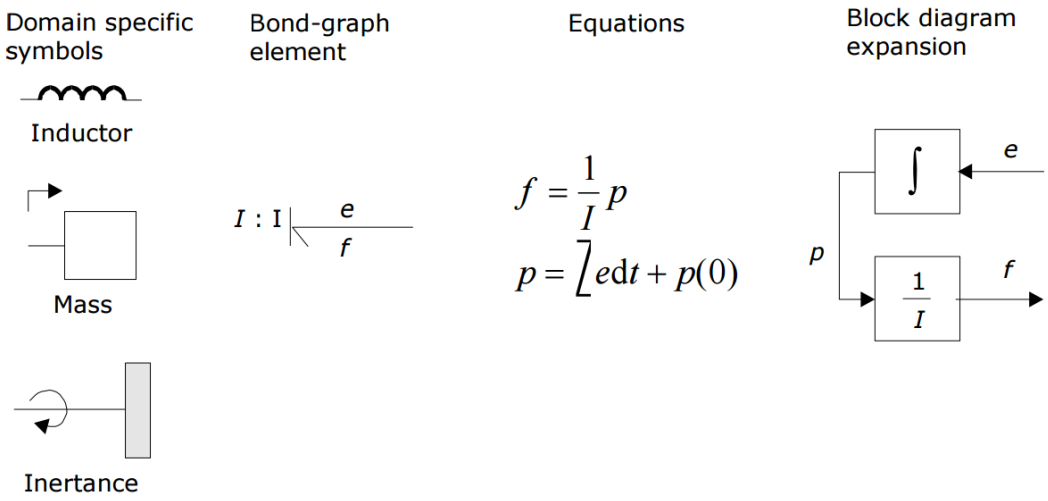

Figure 2.5. Examples of I elements

Note that when at the two types of storage elements, the role of effort and flow are exchanged: the C– element and the I–element are each other's dual form. The block diagrams in Figure 2.4 and 2.5, show the computational direction of the signals involved. They are indeed the expansion of the corresponding causal bond graph. The equations are given in computational form, consistent with the causal bond graph and the block diagram.

2.3.4. Resistors

Resistors, R–elements, dissipate free energy. Examples are dampers, frictions and electric resistors (Figure 2.6). In real-life mechanical components, friction is always present. Energy from an arbitrary domain flows irreversibly to the thermal domain (and heat is produced). This means

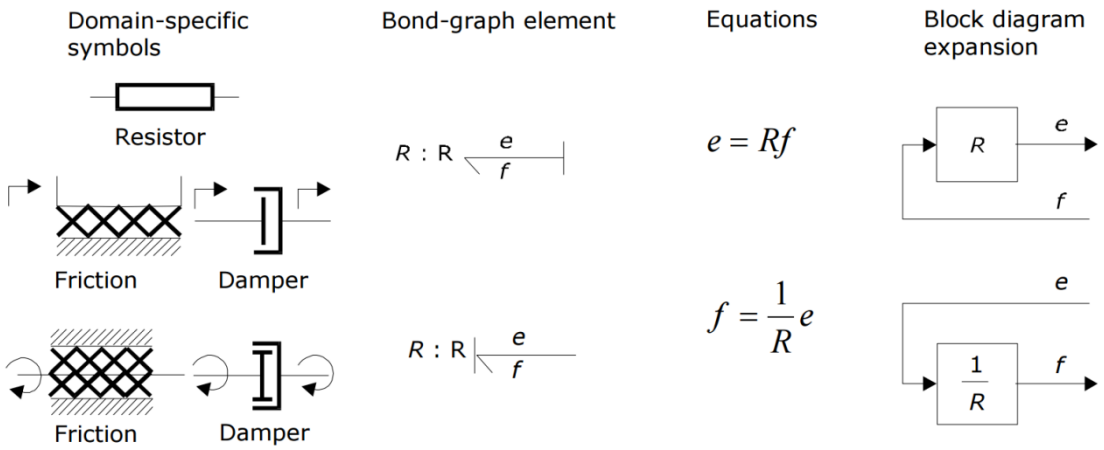

Figure 2.6. Examples of resistors

that the energy flow towards the resistor is always positive. The constitutive equation is an algebraic relation between the effort and flow, and lies principally in the first or third quadrant.

$$e = r(f) \tag{2.6}$$

An electrical resistor is mostly linear (at constant temperature), namely Ohm's law. The electrical resistance value is in [W]. u = Ri Mechanical friction mostly is non-–linear. The resistance function is a combination of dry friction and viscous friction. Dry friction is a constant friction force and viscous friction is the linear term. Sometimes, also stiktion is involved, a tearing–loose force only applicable when starting a movement. All these forms of friction can be modelled with the R–element. The viscous friction has as formula (R in [Ns/m]:

If the resistance value can be controlled by an external signal, the resistor is a modulated resistor, with mnemonic MR. An example is a hydraulic tap: the position of the tap is controlled from the outside, and it determines the value of the resistance parameter. If the thermal domain is modelled explicitly, the production of thermal energy should explicitly be indicated. Since the dissipator irreversibly produces thermal energy, the thermal port is drawn as a kind of source of thermal energy. The R becomes an RS.

2.3.5. Sources

Sources represent the interaction of a system with its environment. Examples are external forces, voltage and current sources, ideal motors, etc. (Figure 2.7). Depending on the type of the imposed variable, these elements are drawn as Se or Sf, source elements are used to give a variable a fixed value, for example, in case of a point in a mechanical system with a fixed position, a Sf with value 0 is used (fixed position means velocity zero). When a system part needs to be excited, often a known signal form is needed, which can be modeled by a modulated source driven by some signal form. An example is shown in Figure 2.8.

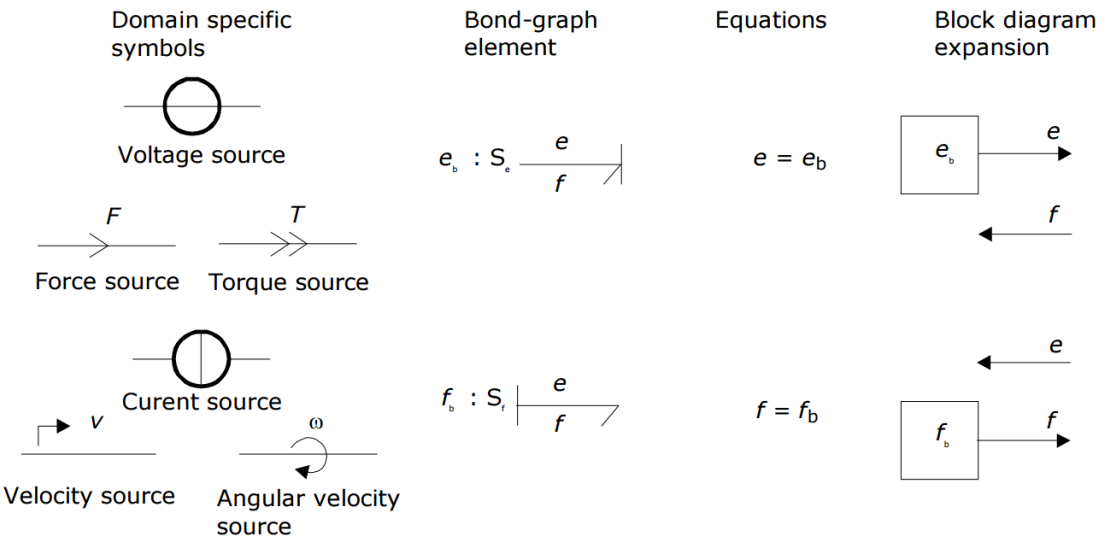

Figure 2.7. Examples of sources

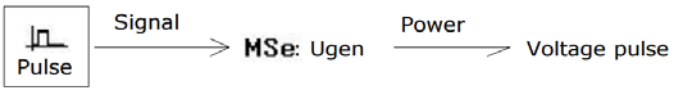

Figure 2.8. Example of a modulated voltage source

2.3.6. Transformers and Gyrators

An ideal transformer is represented by TF and is power continuous (i.e. no power is stored or dissipated). The transformation can within the same domain (toothed wheel, lever) or between different domains (electromotor, winch), see Figure 2.9. The equations are:

$$e_1 = ne_2 \tag{2.7}$$

$$f_2 = nf_1 \tag{2.8}$$

Efforts are transduced to efforts and flows to flows. The parameter n is the transformer ratio. Due to the power continuity, only one dimensionless parameter, n, is needed to describe both the effort transduction and the flow transduction. The parameter n is unambiguously defined as follows: e1 and f1 belong to the bond pointing towards the TF. This way of defining the transformation ratio is standard in leading publications (Karnopp and Rosenberg, 1990; Thoma, 1989; Breedveld, 1985; Cellier, 1991). If n is not constant, the transformer is a modulated transformer, a MTF. The transformer ratio now becomes an input signal to the MTF.

Efforts are transduced to efforts and flows to flows. The parameter n is the transformer ratio. Due to the power continuity, only one dimensionless parameter, n, is needed to describe both the effort transduction and the flow transduction. The parameter n is unambiguously defined as follows: e1 and f1 belong to the bond pointing towards the TF. This way of defining the transformation ratio is standard in leading publications (Karnopp and Rosenberg, 1990; Thoma, 1989; Breedveld, 1985; Cellier, 1991). If n is not constant, the transformer is a modulated transformer, a MTF. The transformer ratio now becomes an input signal to the MTF.

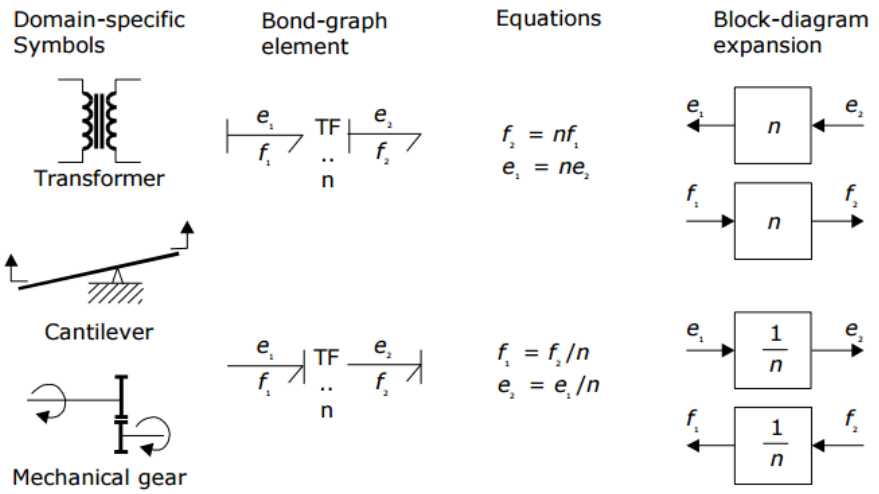

Figure 2.9. Examples of transformers

An ideal gyrator is represented by GY, and is also power continuous (i.e. no power is stored or is dissipated. Examples are an electromotor, a pump and a turbine. Real–life realisations of gyrators are mostly transducers representing a domain–transformation (Figure 2.10). The equations are:

$$e_1 = nf_2 \tag{2.9}$$

$$e_2 = nf_1 \tag{2.10}$$

The parameter r is the gyrator ratio, and due to the power continuity, only one parameter to describe both equations. No further definition is needed since the equations are symmetric (it does not matter which bond points inwards, only that one bond points towards and the other points form the gyrator). r has a physical dimension, since r is a relation between effort and flow (it has the same dimension as the paramer of the R element). If r is not constant, the gyrator is a modulated gyrator, a MGY.

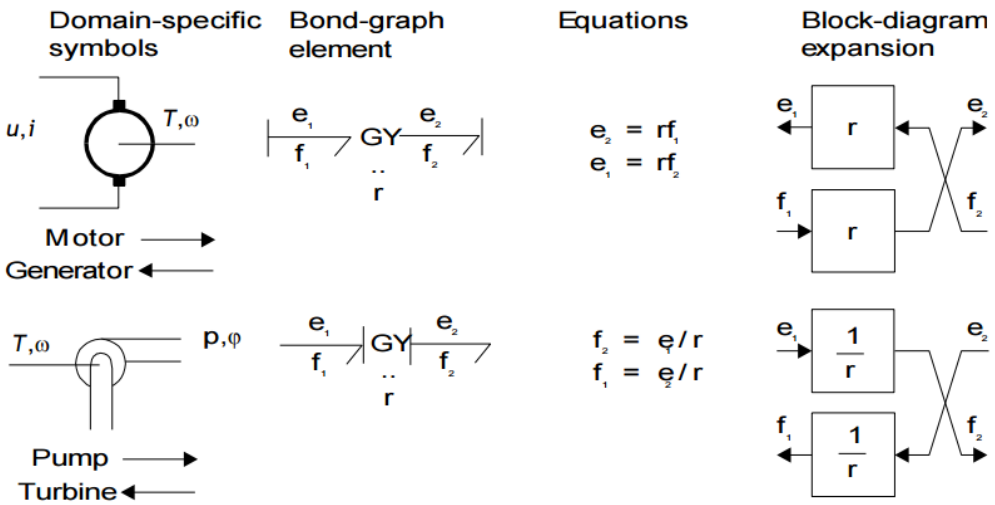

Figure 2.10. Examples of gyrator

2.3.7. Junctions

Junctions couple two or more elements in a power continuous way: there is no energy storage or dissipation in a junction. Examples are a series connection or a parallel connection in an electrical network, a fixed coupling between parts of a mechanical system. Junctions are port–symmetric: the ports can be exchanged in the constitutive equations. Following these properties, it can be proven that there exist only two pairs of junctions: the 1–junction and the 0–junction. The 0–junction represents a node at which all efforts of the connecting bonds are equal (Figure 2.11). An example is a parallel connection in an electrical circuit. Due to the power continuity, the sum of the flows of the connecting bonds is zero, considering the sign. The power direction (i.e. direction of the half arrow) determines the sign of the flows: all inward pointing bonds get a plus and all outward pointing bonds get a minus. This summation is the Kirchhoff current law in electrical networks: all currents connecting to one node sum to zero, considering their signs: all inward currents are positive and all outward currents are negative. We can depict the 0–junction as the representation of an effort variable, and often the 0–junction will be interpreted as such. The 0–junction is more than the (generalized) Kirchhoff current law, namely also the equality of the efforts (like electrical voltages being equal at a parallel connection).

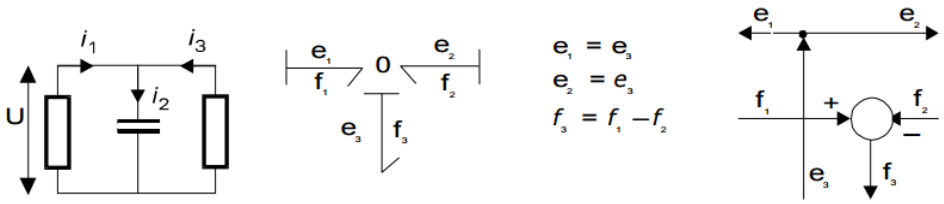

Figure 2.11. Example of a 0-junction

The 1–junction (Figure 2.12) is the dual form of the 0–junction (roles of effort and flow are exchanged). The 1-junction represents a node at which all flows of the connecting bonds are equal. An example is a series connection in an electrical circuit. The efforts sum to zero, as a consequence

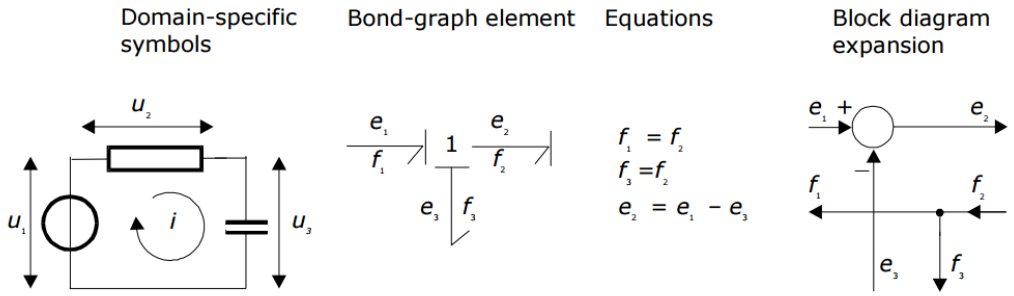

Figure 2.12. Example of a 1-junction

of the power continuity. Again, the power direction (i.e. direction of the half arrow) determines the sign of the efforts: all inward pointing bonds get a plus and all outward pointing bonds get a minus. This summation is the Kirchhoff voltage law in electrical networks: the sum of all voltage differences along one closed loop (a mesh) is zero. In the mechanical domain, the 1–junction represents a force balance (also called the principle of d'Alembert), and is a generalisation of

Newton's third law, action = – reaction). Just as with the 0–junction, the 1–junction is more than these summations, namely the equality of the flows. Therefore, we can depict the 1–junction as the

2.4 . Systematic procedure to derive a bond–graph model

To generate a bond–graph model starting from an ideal–physical model, a systematic method exist, which we will present here as a procedure. This procedure consists roughly of the identification of the domains and basic elements, the generation of the connection structure (called the junction structure), the placement of the elements, and possibly simplifying the graph. The procedure is different for the mechanical domain compared to the other domains. These differences are indicated between parenthesis. The reason is that elements need to be connected to difference variables or across variables. The efforts in the non–mechanical domains and the velocities (flows) in the mechanical domains are the across variables we need. Step 1 and 2 concern the identification of the domains and elements.

- Steps 1 Determine which physical domains exist in the system and identify all basic elements like C, I, R, Se, Sf, TF and GY. Give every element a unique name to distinguish them from each other.
- Steps 2 Indicate in the ideal–physical model per domain a reference effort (reference velocity with positive direction for the mechanical domains). Note that only the references in the mechanical domains have a direction.
- Steps 3 through 6 describe the generation of the connection structure (called the junction structure). 3 Identify all other efforts (mechanical domains: velocities) and give them unique names.
- Steps 4 Draw these efforts (mechanical: velocities), and not the references, graphically by 0–junctions (mechanical: 1–junctions). Keep if possible, the same layout as the IPM.
- Steps 5 Identify all effort differences (mechanical: velocity (= flow) differences) needed to connect the ports of all elements enumerated in step 1 to the junction structure.
- Steps 6 Give these differences a unique name, preferably showing the difference nature. The difference between e_1 and e_2 can be indicated by e_{12}. Construct the effort differences using a 1–junction (mechanical: flow differences with a 0– junction) according to Figure 2.13, and draw them as such in the graph.

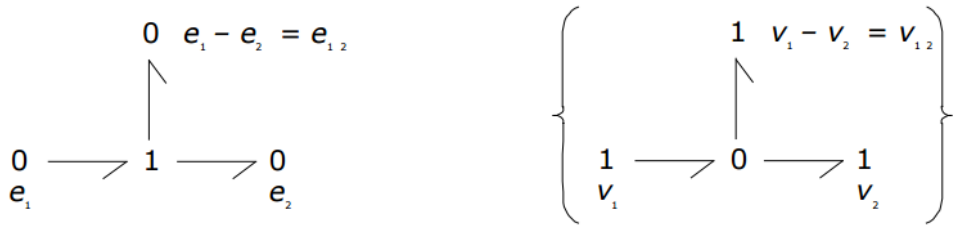

Figure 2.13. Construction of effort differences (velocity differences)

The junction structure is now ready and the elements can be connected.

- Steps 7 Connect the port of all elements found at step 1 with the 0–junctions of the corresponding efforts or effort differences (mechanical: 1–junctions of the corresponding flows or flow differences).

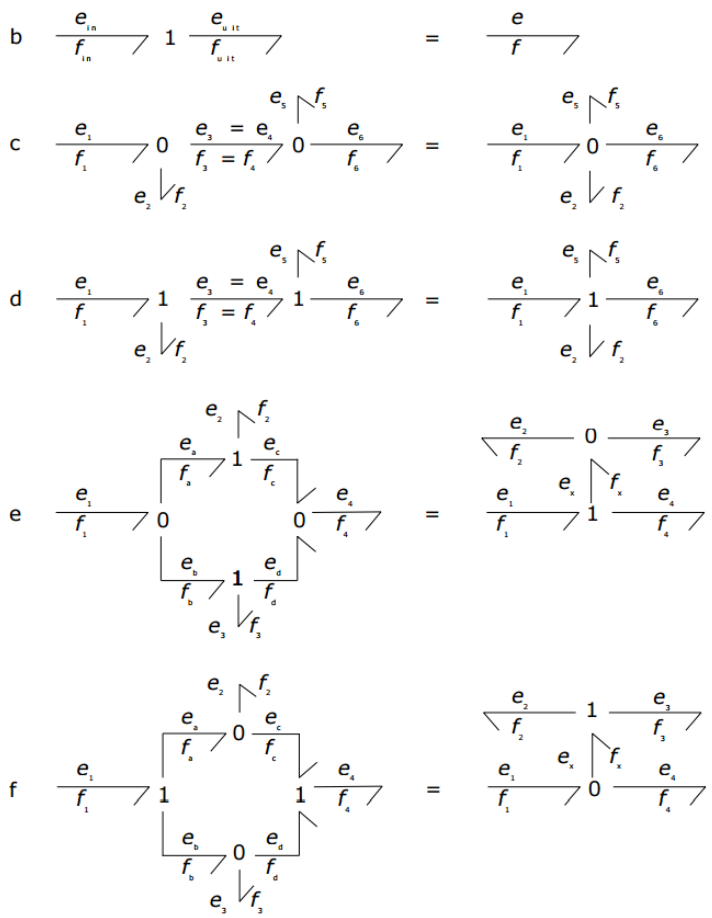

Figure 2.14. Simplification rules for the junction structure. (a, b) Elimination of a junction between bonds. (c, d) Contraction of two the same junctions. (e, f) Two separately constructed identical differences fuse to one difference.

- Steps 8 Simplify the resulting graph by applying the following simplification rules (Figure 2.14):
  - A junction between two bonds can be left out, if the bonds have a 'through' power direction (one bond incoming, the other outgoing).
  - A bond between two the same junctions can be left out, and the junctions can join into one junction.
  - Two separately constructed identical effort or flow differences can join into one effort or flow difference.

2.5 . Conclusion

In this chapter, we have introduced bond graphs to model physical systems in a domain independent way. Only macroscopic systems are treated, thus quantum effects do not play a significant role. Domain indepence has its basics in the fact that physical concepts are analogous for the different physical domains. 6 different elementary concepts exist: storage of energy, dissipation, transduction to other domains, distribution, transport, input or output of energy. Another starting

point is that it is possible to write models as directed graphs: parts are interconnected by bonds, along which exchange of energy occurs. A bond represents the energy flow between the two connected submodels. This energy flow can be described as the product of 2 variables (effort and flow), letting a bond be conceived as a bilateral signal connection. During modelling, the first interpretation is used, while during analysis and equations generation the second interpretation is used. Furthermore, we presented a method to systematically build a bond graph starting from an ideal physical model. Causal analysis gives, besides the computational direction of the signals at the bonds, also information about the correctness of the model. We presented methods to derive the causality of a bond graph. In addition, procedures to generate equations and block diagrams out of a causal bond graph are presented. This chapter is only an introduction to bond graphs. Sometimes, procedures are just presented, without a deep motivation and possible alternatives. It was also not the incentive to elaborate on physical systems modelling. We did not discuss multiple connections (arrays of bonds written as one multibond) and multiport elements (to describe transducers), neither different causal analysis algorithms. Those different causality algorithms give slightly different sets of DAEs especially when applied to certain classes of models (for instance multibody systems with kinematic loops).

References

[1]. Margolis D. 2011. Bond Graph Modelling of Engineering Systems: Theory, Applications and Software Support.

[2]. Merzouki R., Samantaray A.K.,Pathak P.M. and Bouamama B.O. 2013. Intelligent Mechatronic Systems: Modeling, Control and Diagnosis.

[3]. Paynter H.M. 1961. Analysis and Design of Engineering Systems (M.I.T. Press, Cambridge). rm optimization algorithm. ISA Transactions, 51: 641–48.

[4]. Karnopp D.C., Margolis D.L., Rosenberg R.C. 2000. System Dynamics: Modeling and Simulation of Mechatronic Systems (Wiley, New York).

[5]. Bakka T., Reza K.H. 2013. Bond graph modeling and simulation of wind turbine systems, J MechSciTechnol; 27(6): 1843–52.

Chapter 3. Mechatronic Modeling and Control of a Nonlinear Variable-Speed Variable-Pitch Wind Turbine Using the Bond Graph Approach

3.1 . Introduction

Wind turbines can be classified into four categories [1], namely: Fixed-Speed Fixed-Pitch (FSFP), Fixed-Speed Variable-Pitch (FSVP), Variable-Speed Fixed-Pitch (VSFP) and Variable-Speed Variable-Pitch (VSVP). Compared to Variable-Speed (VS), Fixed-Speed (FS) are easy to construct and operate, but VS have the advantages of improved energy capture, reduction in transient load and better power conditioning [2]. Advanced control plays an important role in the performance of large wind turbines. This allows better use of resources of the turbine, increasing the lifetime of mechanical and electrical components, and earning higher returns. The controllers presented in this chapter are designed for VSVP wind turbines operating at high wind speeds. The primary objectives of the controllers can be arranged in the following topics: Maximization of energy capture taking into account the safe operation restrictions such as rated power, rated speed and cut-out wind speed on the one hand, and preventing the WECS from excessive dynamic mechanical loads on the other hand. This general goal encompasses transient loads alleviation, high frequency loads mitigation and resonance avoidance, finally keeping the rotor power at design limits when the wind speed is above its rated value. Two control inputs are available: the generator torque and the blade pitch angle. Wind turbine controllers' objectives depend on the operation area [3, 4]. VSVP wind turbine operation can be divided into four operating regions (Figure. 1):

- Region I: Below cut-in wind speed.
- Region II: Between cut-in wind speed and rated wind speed.
- Region III: Between rated wind speed and cut-out wind speed.
- Region IV: Upper than cut-out wind speed.

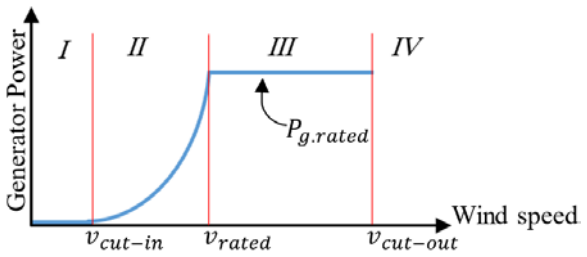

Figure 3.1. Operating regions of the wind turbine

In region I, wind turbines do not run because power available in the wind is low compared to losses in the turbine system. Region II is an operational mode where it is desirable that the turbine captures as much power as possible from the wind. This is due to the fact that wind energy extraction rates are low and the structural loads are relatively small.

The generator torque provides the control input to vary the rotor speed, while the blade pitch is held constant. Region III is encountered when the wind speeds are high enough: then the turbine must limit the fraction of the captured wind power such that safe electrical and mechanical loads are not exceeded. If wind speeds exceed the region III (region IV), the system will undergo a forced stop of the machine, protecting it from excessively high aerodynamic loads. In practice, the passage from region II to region III is somewhat unusual. In fact, the electromagnetic torque in region II controls the rotor speed, and in region III it is the power that should be controlled by the blade pitch control.

Many works have proposed controllers to work around an operating point using control of the generator torque to keep the turbine at a condition of maximum power point tracking, e.g., [5]. Some previously published works suggested pitch control methods to limit the rotor speed at high wind speeds, e.g., [6]. In [7] a combination of proportional integral (PI) and SMC is used to adjust the turbine rotor speed for extracting maximum power without estimating the wind speed. In [8] a PI-based torque control is used to control the Wind Turbine, where optimal gains are achieved by particle swarm optimization and fuzzy logic theory, [9] discussed the multivariable control strategy by combining the nonlinear state feedback control for region II with linear control for region III. Finally, the results are compared with the existing control strategies such as PID and LQG. Wind Turbine control using adaptive radial basic Neuron Network used for both pitch and torque controllers is addressed in [10]. Active disturbance rejection based pitch control for variable speed Wind Turbine is presented in [11]. Relatively few works suggest control strategies based on varying operating conditions for wind turbines and their dynamics and using a unified approach in modeling and control of the wind turbine. The principal aim of this chapter is to show same benefits of the Bond Graph in modeling and control of the wind turbine. In this framework, a wind turbine mechatronic model is developed. The main components of the system are modeled using the Bond-Graph Approach (BGA). The control law is derived by combining a torque control strategy with a pitch control using the inverse model of the Bond Graph. A compression with a PID controller is carried out to validate the proposed control model. The implementation of the complete model and its control system has been conducted by means of the 20-Sim simulation program.

This chapter is organized as follows. Section 2 discusses the modeling of the Wind Turbine using the BGA. Problem formulation and control objectives are discussed in Section 3. The proposed controllers or all the regions are discussed in Section 4. Section 5 discusses the validation of the results using the 20-Sim simulator. Finally in Section 6 a conclusion is drawn from the obtained results, which show that the proposed bond graph model control is working fine for controlling the WT at below- and above- rated wind speeds.

3.2 . System modeling of the wind turbine by using the Bond graph Approach (BGA)

The wind turbine studied in this work is a 5-MW horizontal axis variable speed variable pitch wind turbine. The specifications of this turbine are described in [12] and some of its

parameters are shown in Appendix A. The mechatronic model of the wind energy conversion systems (WECS) can be stated, and the main components of a WECS will be presented using the bond graph approach (BGA). Our primary objective is to show some of the benefits of the BGA in contributing to a model of wind turbine and presenting a nonlinear model of a wind turbine in a unified framework, containing aerodynamic system, drive train, tower, generator and pitching system.

A mechatronics model, of the entire WECS, can be structured as several interconnected subsystem models as shown in Figure 3.2.

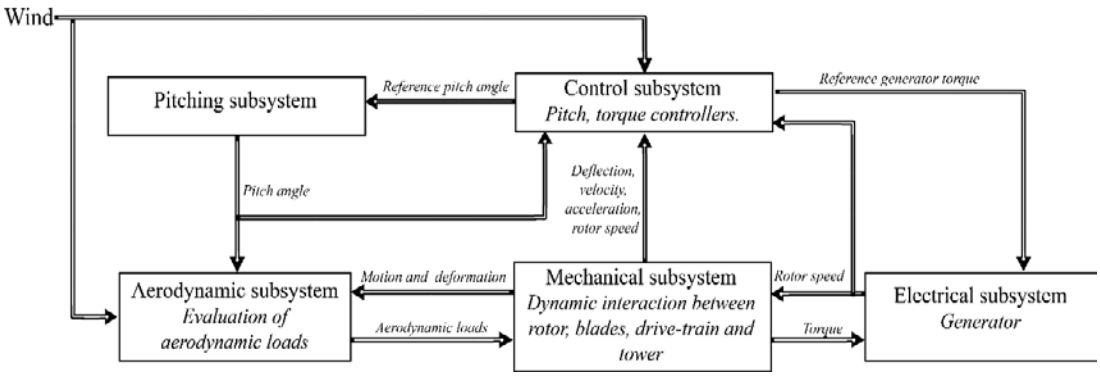

Figure 3.2. Subsystem-level block diagram of a WECS

The aerodynamic subsystem describes the transformation of the wind speed field into forces on the blades that generate the rotational motion. The mechanical subsystem can be divided into two functional blocks, i.e., the drive-train and the support structure. The drive-train transfers the aerodynamic torque on the blades to the generator shaft. It encompasses the rotor, the transmission and the mechanical parts of the generator. The structure is made up of the tower. The electrical subsystem describes the conversion of mechanical power at the generator shaft into electricity. Finally, the actuator subsystem models the pitch servo behavior. In order to analyze the system in the same reference frame, the BGA [Chapter 02, 13, 14] is used.

3.2.1. Aerodynamics Bond Graph Model

The wind turbine rotor transforms the absorbed kinetic energy of the air into mechanical power. The power in the wind is proportional to the cube of the wind speed and can be described as [17]:

$$P_{wind} = \frac{1}{2}\rho\pi R^2 v^3 \tag{3.1}$$

where ρ is air density, R is rotor radius of the wind turbine blade, and v is wind speed. A wind turbine can only extract part of the power from the wind. The ratio of the power $C_p(\beta,\lambda)$ extracted from the wind is a nonlinear function of the blade pitch angle β and the tip-Speed Ratio λ. Therefore, the mechanical power of the wind turbine extracted from the wind can be expressed as [17]:

$$P_{mech} = \frac{1}{2}\rho\pi R^2 v^3 C_p(\beta,\lambda) \tag{3.2}$$

with:

$$\lambda = \frac{R\omega_r}{v} \tag{3.3}$$

where ω_r is the turbine rotor's speed. From (2.3) we can find the aerodynamic torque and the thrust force acting on the tower:

$$T_a = \frac{1}{2}\rho\pi R^2 v^3 C_q(\beta,\lambda) \tag{3.4}$$

$$F_T = \frac{1}{2}\rho\pi R^2 v^2 C_T(\beta,\lambda) \tag{3.5}$$

where $C_q(\beta,\lambda)$ is the torque coefficient given as: $Cq(\beta,\lambda) = \frac{C_p(\beta,\lambda)}{\lambda}$ and $CT(\beta,\lambda)$ is the thrust force coefficient. A generic equation is used to model $C_p(\beta,\lambda)$ and $C_T(\beta,\lambda)$. These equations are based on the modeling turbine characteristics of [18]. The power coefficient used in the calculation of the torque is given in (3.6). A plot of the $C_p(\beta,\lambda)$ curve is shown in Figure 3.3; the plot is made with different pitch angle and tip-speed ratio. Similar formulas can be found regarding the thrust force coefficient $C_T(\beta,\lambda)$. In our calculations only a simple relation is used:

$$C_p(\beta,\lambda) = c_1\left(\frac{c_2}{\lambda_i} - c_3\beta - c_4\right)e^{-\frac{c_5}{\lambda_i}} + c_6\lambda \tag{3.6}$$

$$\lambda_i = \frac{1}{\frac{1}{\lambda + 0.08\beta} - \frac{0.035}{\beta^2 + 1}} \tag{3.7}$$

where c_1=0.5179, c_2=116, c_3=0.4, c_4=5, c_5=21 and c_6=0.0068.

In the aerodynamics part, we need to find a way to convert the wind into torque and

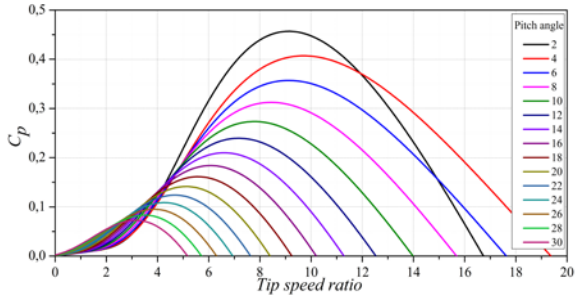

Figure 3.3. Curve of Cp

thrust force, i.e. to transform a flow into efforts. This is done by means of a modulated gyrator MGY. We use the torque and thrust force equations given in (3.4) and (3.5). In this case the transformation is dependent on three varying parameters: the wind speed v, the pitch angle β, and the rotor rotational speed ω_r. Figure 3.4 shows the Bond Graph model of the aerodynamics part.

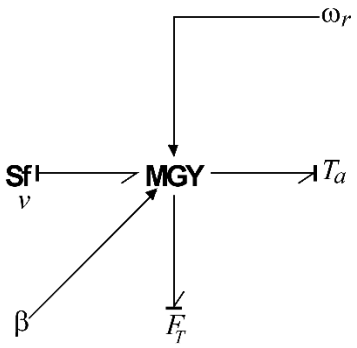

Figure 3.4. Bond graph model of the aerodynamics part

3.2.2. Mechanical subsystem model

The mechanical subsystem includes all mechanical components of the wind turbine system. It can be divided into two flexible structures: the drive train and the tower. In this system, the rotor of the turbine, the transmission elements (gearbox) and the rotor generator make up the drive train. This can be modeled as a multi-body system (MBS) with multiple degrees of freedom. Figure 3.5 shows a sketch of a two-mass drive train model. A more detailed bond graph model is presented in [19]. The Bond Graph representation of the drive train is shown in Figure 3.6. The model consists of two 1-junctions and two 0-junctions. The rightmost 1-junction connected to the rotor inertia J_r and rotor external damping D_r describes the rotor rotational speed ω_r. Since there are dynamics in between the rotor inertia and the generator inertia, they do not have the same speed. This is the reason for the 0-junction in the main and high speed. The 1-junction connected to the R-element (D_{ms}, D_{hs}) and the C-

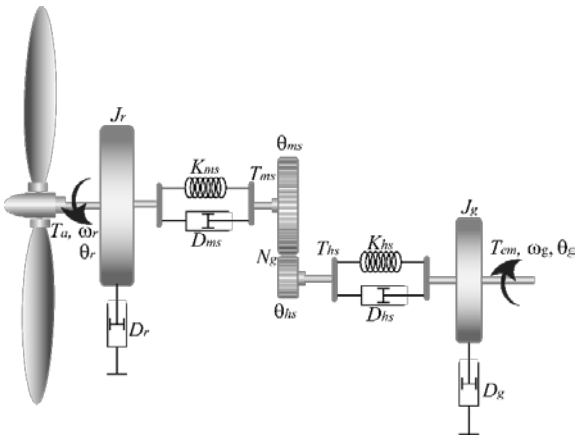

Figure 3.5. Sketch of a two-mass drive train

element (k_{ms}, K_{hs}) describe respectively the damping and stiffness in the main and high-speed shafts. The gearbox is modeled by a simple TF-element where (N_g) is the gearbox ratio. The generator inertia (J_g) and external damping (D_g) are respectively modeled by the I-element and the R-element.

For the tower model, it is assumed that the tower moves only in horizontal direction (Figure 3.7) and does not influence the mechanical system. It only affects its input, i.e. the wind speed. The Bond Graph model of the tower is sketched in Figure 3.8, where m_t is the tower mass, F_t is the thrust force acting on the tower, D_t is the tower damping and K_t is the tower stiffness.

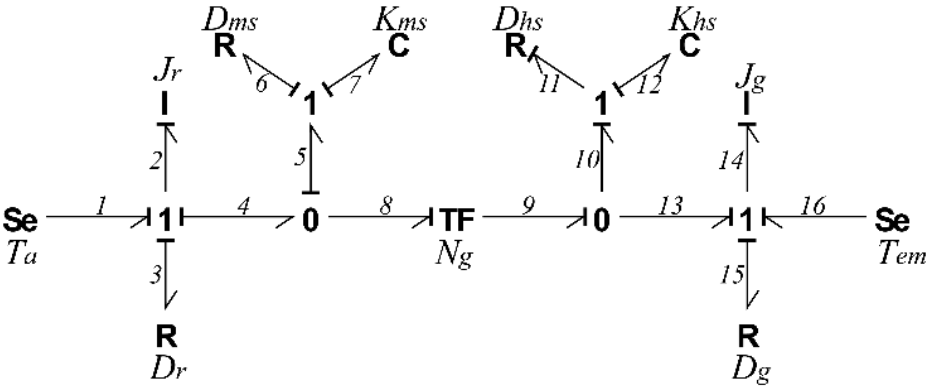

Figure 3.6. Bond graph model of a two-mass drive train

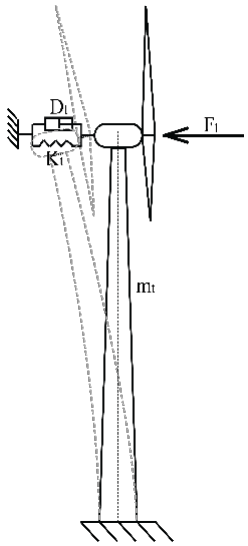

Figure 3.7. Sketch of wind turbine structure

3.2.3. Generator Model

The induction generators are largely the most popular electric machines in WECS industry to convert mechanical power to electric power. In our system, a simple first-order generator model is used for the wind turbine and, accordingly, the generator torque T_{em} can be described as:

$$\dot{T}_{em} = \frac{1}{\tau}(T_{em} - T_{ref}) \tag{3.8}$$

3.2.4. Pitching Subsystem

In WECS, one of the operational problems is the variability and discontinuity of wind. In most cases, wind speed can fluctuate rapidly. Hence, the quality of produced energy becomes an important problem. Several control techniques have been designed to improve the quality of power generated from wind turbines. Pitch control is the most efficient and popular power control method, especially for variable-speed wind turbines. It is a useful method for power regulation above the rated wind speed by changing the pitch angle of the rotor blades. The actuator that drives the blades around their longitudinal axes was extensively modified to make it suitable for controls testing. The original hydraulically actuated pitch system was replaced by a high-speed electromechanical pitch system. The electromechanical system consists of a servo drive electronics box that drives a permanent magnet servo motor. This motor is connected to a gearbox that in turn drives the blade through a pinion and a bull gear system (Figure 3.9). There are many possibilities to model the electric motor with different levels of complexity and accuracy. The detailed method

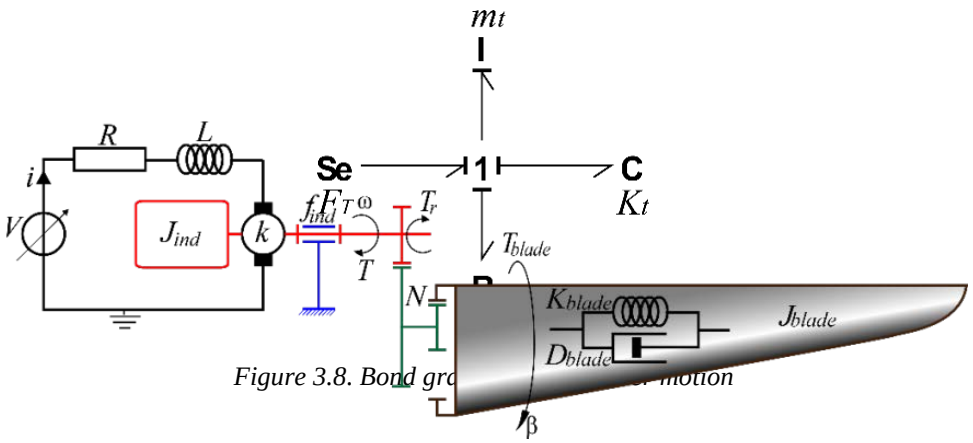

Figure 3.8. Bond gr[illegible] motion

Figure 3.9. Sketch of the pitching system

depends on the motor type. In our model, we use a DC motor for controlling the pitch angle. Figure 3.9 shows also the equivalent circuit of motor in which the armature coil is represented by resistor R and inductor L in series.

The torque generated by a DC motor can be explained as:

$$T = K_T I \tag{3.9},$$

where I is the current through conductor and K_T is the torque constant. The back emfV_b is directly proportional to angular velocity ω of rotation. Thus the back emf is given as:

$$V_b = K_v \omega \tag{3.10}$$

Where K_v is constant back emf.

If we assume there are no losses in the magnetic field, then, for conservative transformation $K_T = K_v = K$ which satisfies $T\omega = V_b I$. Therefore, we can draw the bond graph model of the pitching system as shown in Figure 3.10, where the coil resistance -featuring the rotor losses, is represented by an R-element R and the motor inductance by an I-element L. The electromechanical transformation is modeled as a gyrator K. The mechanical part includes all mechanical components of the pitching system: the rotor of the electric motor is represented by I-element J_{ind}, the bearing damping of the rotor is represented by R-element f_{ind}, and the transmission elements (gearbox) are represented by TF-element N. The dynamic behaviors presented in the blades are represented by R-element D_{blade} and C-element K_{blade}. The rotor blade inertia is represented by I-element J_{blade}.

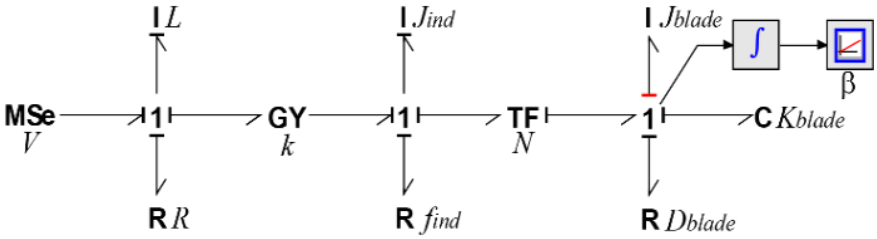

Figure 3.10. Bond graph of the pitching system

From the Figure 10, we can observe an causality problem in the rightmost 1-jonction, this problem can be reserved by coming down the I-element (J_{ind}) and R-element (f_{ind}) next to the elements J_{blade} and D_{blade}. The simplified bond graph is shown in Figure 3.11.

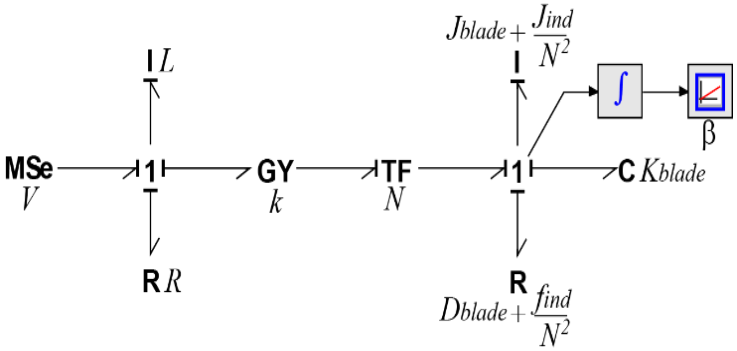

Figure 3.11. Simplified bond graph model of pitching system

3.2.5. Complete System

The individual subsystems presented in the previous sections are combined in a global system as shown in Fig 3.12. The inputs of the aerodynamic subsystem are connected by the wind sources, the hub speed and the pitch angle, the latter representing the primitive of the rotation speed at the pitching subsystem's output. The output torque of the aerodynamic subsystem symbolizes the mechanical subsystem's input applied on the turbine rotor. Mechanical subsystem's output is the mechanical power, which represents the electrical subsystem's input. Pitching subsystem's output is the pitch angle, and its input is the control law.

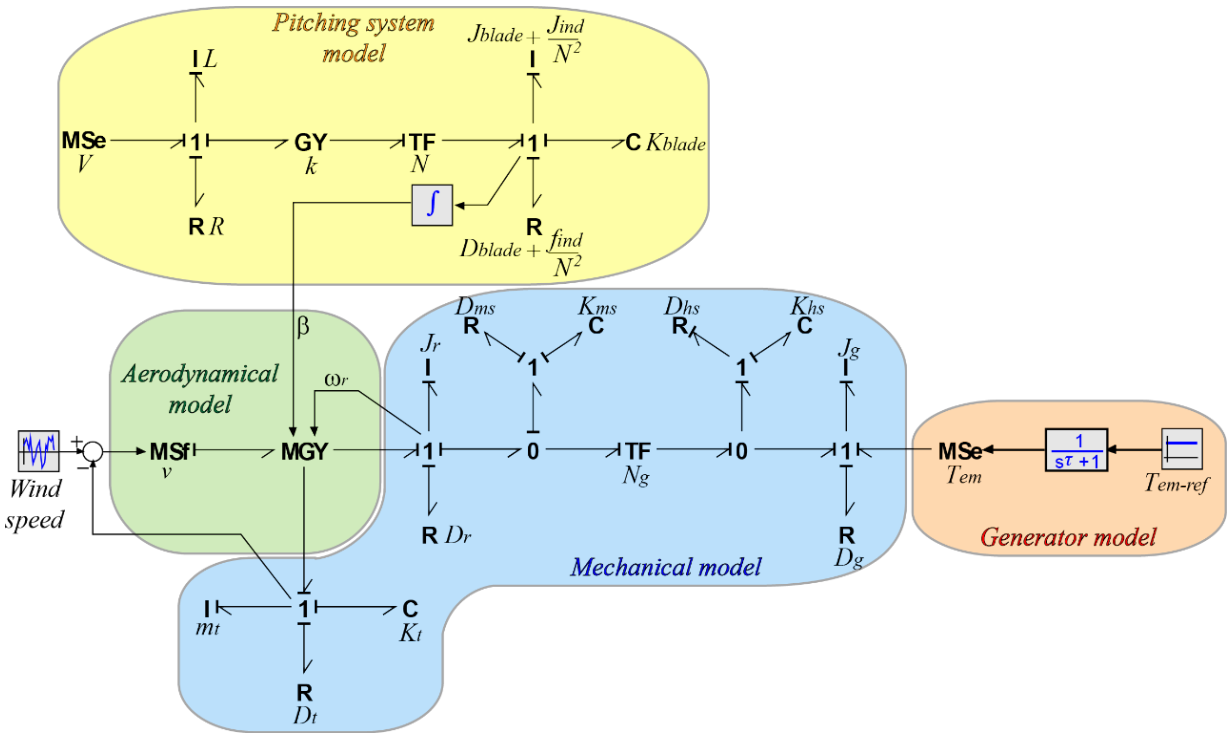

Figure 3.12. Complete System

3.3 . Selection of the Operating Point

Selection of the operating point is critical to preserving aerodynamic stability in the wind turbine system. The rotational speed ω_{ref} operating point and the blade-pitch β_{ref} operating point were selected for each wind speed using the following algorithms.

A wind turbine normally works in different operating modes along the wind speed range. It can be divided into four regions shown in Figure. 1. The wind speeds; considered as the limits of this division, include cut-in wind speed $v_{cut\text{-}in}$, rated wind speed v_{rated} and cut-out wind speed $v_{cut\text{-}out}$[20]. The values of the 5MW wind turbine studied in this paper are presented in appendix A. The control objectives in these regions are substantially different.

Being below cut-in wind speed $v_{cut\text{-}in}$ (region I), the wind turbine power generation is very low and hence not economical. Thus, the control unit shown in Figure. 2 issues the stop

command and the brakes will stop the wind turbine. In this region, the pitch angle is usually set at 90°[20].

In region II, which is called the partial-load region, the wind speed is higher than v_{cut-in}but lower than v_{rated}; the objective is to capture as much energy as possible. In this case, the power coefficient C_p should be set to maximum power coefficient C_{pmax}. This occurs when both the tip-speed ratio λ and the pitch angle β are maintained as close as possible to their optimum values λ_{op} and β_{op}, since $C_{pmax} = C_p(\lambda_{op},\beta_{op})$. In Figure. 3, the maximum C_p value over the entire surface occurs at a pitch angle of 2° and a tip-speed ratio of 9; the rotational speed operating point ω_{op} for each wind speed in this region is:

$$\omega_{op} = \frac{\lambda_{op}}{R} v \tag{3.11}$$

When the generator speed does not exceed the rated generator speed, the reference speed is:

$$\omega_{ref} = \omega_{op} \tag{3.12}$$

Moreover, when the generator speed exceeds the rated generator speed, the reference speed is:

$$\omega_{ref} = \omega_{rated} \tag{3.13}$$

Therefore, the rotational speed is varied in proportion to the wind speed by properly controlling the generator torque. Figure. 3.13 shows the structure of this generator torque control method in wind turbines using the inverse bond graph method.

In region III, which is called the full-load region, the wind speed is higher than vrated but lower than the $v_{cut-out}$. The main control purpose in this region is to keep the generator power P_g around the nominal generator power P_n, by keeping the generator speed ω_g around its rated value $\omega_{g\text{-}rated}$. This is achieved through tuning the pitch angle of the blades. Accordingly, the control unit must send the suitable pitch angle reference β_{ref} to set the pitch angle of the blades [20].

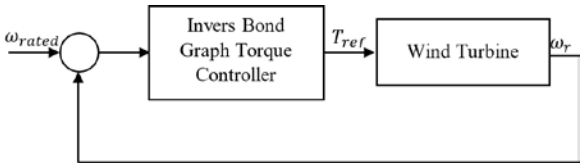

Figure 3.13. Structure of the proposed torque controller

In this region, the optimum tip-speed λ_{op} and the maximum power coefficient C_{pmax} are respectively:

$$\lambda_{op} = \frac{R\omega_{rated}}{v} \tag{3.14}$$

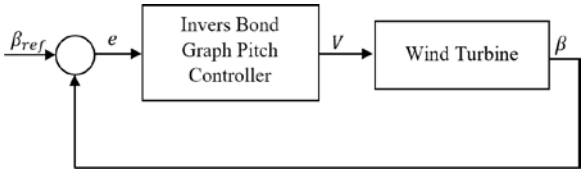

Figure 3.14. Structure of the proposed pitch controller

$$C_{p\max}(\beta_{op},\lambda_{op}) = \frac{P_n}{\frac{1}{2}\rho\pi R^2 v^3} \tag{3.15}$$

Where P_n is the rated turbine power. By using Figure. 3, we can calculate the value of β_{op}, since:

$$\beta_{ref} = \beta_{op} \tag{3.16}$$

Figure. 3.14 shows the structure of the pitch controller in wind turbines using the inverse bond graph method.

The optimal values of λ, C_p, pitch angle β and the reference speed ω_{ref} for each wind speed (Figure. 3.15) for regions II and III can be calculated by using the algorithm presented here.

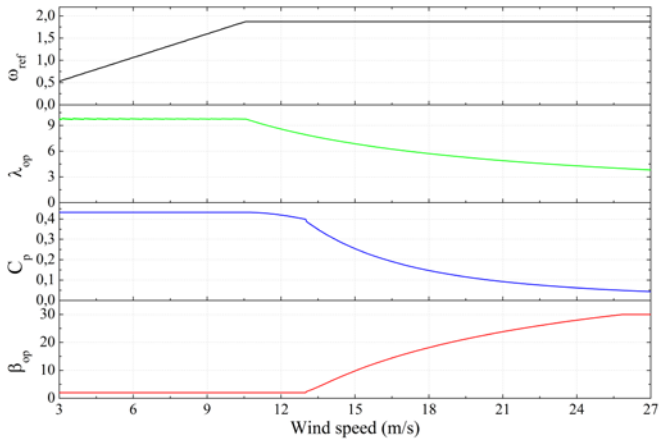

Figure 3.15. Reference parameters

In region IV, where the wind speed is very high (higher than Vcut-out), in order to protect the wind turbine from fatigue damages and mechanical stresses, the wind turbine must be shut down. Thus, like the procedure in region I, the control unit issues the stop command and the brakes will stop the wind turbine. In this case, the pitch angle is usually set at 90°.

The focus of this paper is on full-load region and partial-load region (regions II and III) to design an optimal generator torque and pitch controllers.

3.4 . Torque Control Model

In order to control the rotational speed of the electric machine and obtain the best efficiency and quality power at a wide range of operation, many electric machines equipped with power converters have been proved in industrial applications [21]. For this study, the electric machine is modeled by a first order transfer function, therefore, the electromagnetic torque developed at any instant is:

$$T_{em} = \frac{1}{\tau s + 1} T_{me-ref} \tag{3.17}$$

Where T_{em} is the electromagnetic torque, T_{ref} is the reference torque, and τ is the time constant.

The maximum power extraction techniques allow to determine the speed of the turbine that achieves maximum power generated. For the 1-junction placed between bonds 13, 14, 15 and 16 of the bond graph presented in Figure. 6, we can write:

$$e_{13} + e_{16} = e_{14} + e_{15} \tag{3.18}$$

where $e_{13} = T_{mg}$: which is the mechanical torque from the gearbox, $e_{16} = -T_{em}$, , $e_{14} = J_g(d\omega_g/dt)$, where J_g is the inertia of the generator and ω_g is the generator angular velocity and $e_{15} = D_g\omega_g$, where D_g is the generator external damping.

Since we can write:

$$J_g \frac{d\omega_g}{dt} = T_{mg} - D_g\omega_g + T_{em} \tag{3.19}$$

It can be seen that the mechanical speed is influenced by the action of two torques: the mechanical torque from the gearbox and the electromagnetic torque from the electric machine. The torque control structure presented in this paper adjusts the electromagnetic torque to set the wind turbine speed at its rated speed. In order to control the electromagnetic torque, it is necessary to generate the reference electromagnetic torque. To this aim, a specific algorithm is designed, based on the bicausal bond graph [22] and the performance of the system is compared with a conventional PID controller to validate it.

The inverse model corresponds to a re-organization of the equations where the input and output roles are exchanged: inputs become outputs and vice versa [23]. The inverse model is created by imposing both effort and flow information from the sensor and receiving both at the source. This procedure, where both information can be imposed on a bond, cannot be done through normal causality. This is why, the notion of bicausality[24, 25] is introduced. Bicausality notation splits the causality assignment for the two factors of power, namely effort and flow. By separating the causal strokes, it allows imposing two complementary information at one end of a bond.

In the inverse model, the source element (Se or Sf) is replaced by a source sensor (SeSf) element [23, 24] and the sensor element (De or Df) is replaced by a sensor source (DeDf) element. The difference between the source sensor and the sensor source lies in the causality of the element: the source sensor element receives information of both power variables, whereas the signal source element supplies both. The rule for bicausal 0 (1)-junction is that only one bond can bring effort (flow) information and other bonds can bring the flow (effort) information. This means that at a bicausal junction, there must be one bond bringing in both effort and flow information while there must be another bond taking out both effort and flow information. Thus, at every junction, only two bonds must be bicausalled (not more, not less).

To obtain the inverse model, bicausality is propagated from the original sensor to the original source. In the process, some internal bonds in the model are assigned bicausality such that it is propagated to the receiving source sensor.

The structure of the control in an open loop is designed with the inverse bond graph. The decoupling actions are defined (inverse matrix and disturbance compensation). The open loop structure is then extended to a closed loop control by fixing the dynamics of errors.

In our model, the input variable is the electromagnetic torque Tem and the output variable is the rotor speed ω_r of the turbine. The analysis of the direct bond graph model of Figure. 6 indicates that there is a power line and a causal path between the input variable T_{em} and the output variable ω_r. Therefore, the model is structurally invertible compared to the pair of variables T_{em} and ω_r. The objective of the controller established here is to calculate the electromechanical torque required to set the turbine rotor speed to a reference. For this calculation, it is appropriate to inverse the bond graph model of Figure. 6 relatively to the pair of variables T_{em} and ω_r.

The inverse bond graph model of the system is given in Figure. 16; the sensor (Df) and source (Sf) have been replaced with source sensor (SeSf) element and sensor source (DeDf) element. Note that fixed sources (those which are not control inputs) are retained as they are, e.g., Se: Ta at bond number 1. The SeSf element in bond number 0 imposes both effort and flow information, thereby forcing differential causality in the I-element at bond number 2. Likewise, three more storage elements are forced to assume differential causality. The DeDf element at bond number 16 receives both flow and effort information.

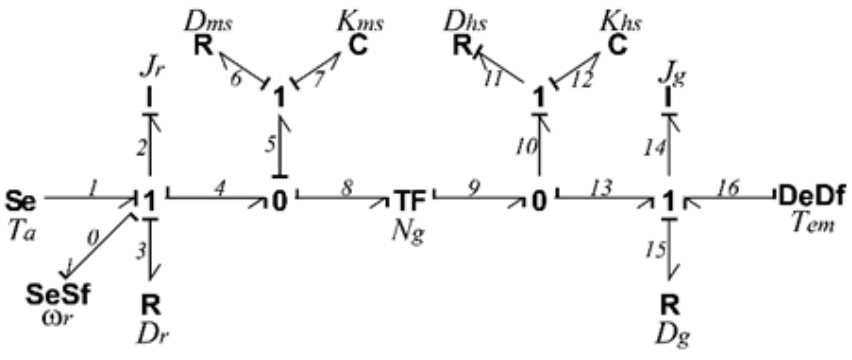

Figure 3.16. Inverse Bond Graph for calculation of the controls laws.

From Figure16, we can write the following from the constitutive relations of the leftmost 1-junction (i.e. 1-junction placed between bonds 0, 1, 2, 3 and 4):

$$\begin{cases} f_0 = f_1 = f_2 = f_3 = f_4 \\ e_4 = e_1 - e_0 - e_2 - e_3 \end{cases} \tag{3.20}$$

where:

$f_0 = \omega_r$, $e_0 = 0$, $e_1 = T_a$, $e_2 = J_r(d\omega_r/dt)$ and $e_3 = D_r\omega_r$. Therefore:

$$\begin{cases} f_4 = \omega_r \\ e_4 = T_a - J_r \dfrac{d\omega_r}{dt} - D_r\omega_r \end{cases} \tag{3.21}$$

To establish the closed loop control law, the dynamics of the error are set in (22) as:

$$\dot{\varepsilon} + k_1\varepsilon = 0 \tag{3.22}$$

Where k_1 represents the controller to be used and $\varepsilon = \omega_{ref} - \omega_r$, is the error. Expression (21) becomes (23) as:

$$\begin{cases} f_4 = \omega_r \\ e_4 = T_a - J_r(\dot{\omega}_{ref} - \dot{\varepsilon}) - D_r\omega_r \end{cases} \tag{3.23}$$

Finally,

$$\begin{cases} f_4 = \omega_r \\ e_4 = T_a - J_r\dot{\omega}_{ref} - J_r k_1(\omega_{ref} - \omega_r) - D_r\omega_r \end{cases} \tag{3.24}$$

For the neighboring 0-junction in Figure 15, we can write:

$$\begin{cases} f_8 = f_4 - f_5 \\ e_4 = e_5 = e_8 \end{cases} \tag{3.25}$$

From the 1-jonction between bonds 5, 6 and 7 we have:

$$\begin{cases} f_5 = f_6 = f_7 \\ e_5 = e_6 + e_7 \end{cases} \tag{3.26}$$

with:

$$\begin{cases} e_6 = D_{ms} f_6 = D_{ms} f_5 \\ e_7 = K_{ms} \int f_7 dt = K_{ms} \int f_5 dt \end{cases} \quad (3.27)$$

Therefore:

$$f_5 = \frac{1}{K_{ms}} (\dot{e}_5 - D_{ms} \dot{f}_5) \quad (3.28)$$

Proceeding in the same way, from the TF-element we can write:

$$\begin{cases} f_9 = N_g f_8 \\ e_9 = \dfrac{e_8}{N_g} \end{cases} \quad (3.29)$$

From the 0-junction placed between bonds 9, 10 and 13, we have:

$$\begin{cases} f_{13} = f_9 - f_{10} \\ e_9 = e_{10} = e_{13} \end{cases} \quad (3.30)$$

where:

$$f_{10} = \frac{1}{K_{ms}} (\dot{e}_{10} - D_{ms} \dot{f}_{10}) \quad (3.31)$$

For the rightmost 1-junction, we can write:

$$\begin{cases} f_{16} = f_{13} \\ e_{16} = -e_{13} + e_{14} + e_{15} \end{cases} \quad (3.32)$$

where:

$e_{16} = -T_{em}$, $e_{14}=J_g(d\omega_g/dt)$, $e_{15}=D_g\omega_g$.

Finally:

$$\begin{cases} f_{16} = f_{13} \\ -T_{em} = -e_9 + J_g \dot{\omega}_g + D_g \omega_g \end{cases} \quad (3.33)$$

To generate the reference electromechanical torque the generator model must be inversed as:

$$T_{em-ref} = \tau \dot{T}_{em} + T_{em} \quad (3.34)$$

The controller block diagram derived from these equations is shown in Figure 17. It is important to notice that the structure of the control law contains a feed-forward control with a derivative action. Figure 17 shows that the proposed gain is a PI controller; the estimate values are considered in the control law.

In the block diagram model, the desired output is the input. The output of the block diagram model is the reference electromagnetic torque. The block diagram contains four derivative (d./dt) blocks. It was simulated for the numerical parameters given in Appendix A.

3.5 . Pitch Controller

For the above rated wind speed the generator power is fixed to its rated value that is, maximum value of the control input. In this condition, a linear pitch control is introduced. The blade pitch angle is adjusted to maintain the generated power constant in its rated value. The form of the blades and, more generally, the turbine characteristics play a key role in this power control.

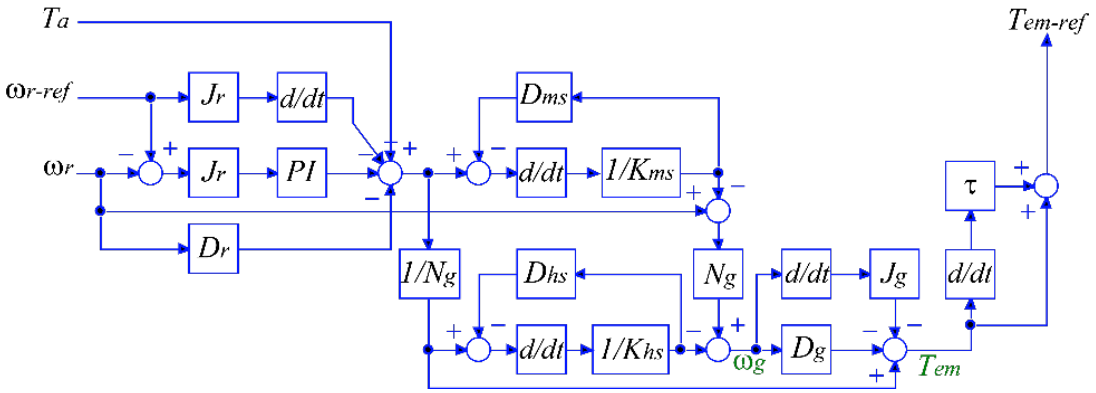

Figure 3.15. Torque control law block diagram

The non-linear model of the turbine makes complex to design an analytical model of this controller. Moreover, very large differences (due to elasticity) may appear a turbine to another. That is why it is more practical to use an experimental characteristic of the blade pitch angle measured for a different wind speed. The inverse control characteristic can give directly for different wind speed the corresponding blade pitch angle; this is achieved by using the algorithm given in section 3 and the controller should provide suitable motors voltage in its output. This is obtained by using the inverse bond graph model of the pitching system.

The analysis of the bond graph model of Figure 11 indicates that there is a power line and a causal path between the input variable V and the output variable β. Therefore, the model is structurally invertible.

The inverse bond graph model of the pitching system is given in Figure 18, as previously mentioned, the sensor (D_f) and source (S_f) have been replaced with source sensor

(S_eS_f) elements. The S_eS_f element in bond number 10 imposes both effort and flow information; the D_eD_f element at bond number 1 receives both flow and effort information.

As previously defined in the torque controller, we can derive the equations from the inverse bond graph of the Figure 3.18.

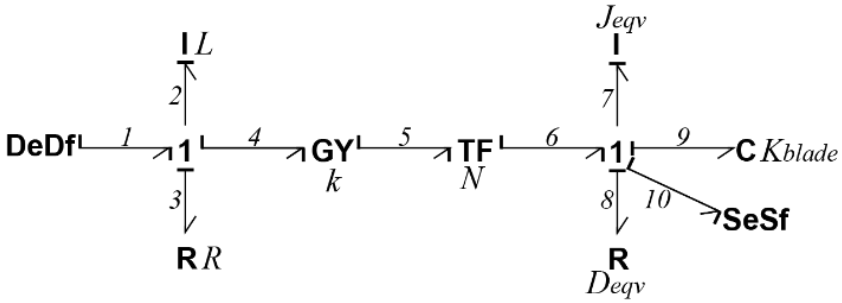

Figure 3.16. Inverse bond graph for calculation of the control law of the pitch system

From Figure 3.18, we can write the following from the constitutive relations of the rightmost 1-junction (i.e. 1-junction placed between bonds 6, 7, 8, 9, and 10):

$$\begin{cases} f_6 = f_7 = f_8 = f_9 = f_{10} \\ e_6 = e_7 + e_8 + e_9 + e_{10} \end{cases} \tag{3.35}$$

Where

$f_{10} = d\beta/dt$, $e_{10} = 0$, $e_9 = K_{blade}\beta$, $e_8 = D_{eqv}(d\beta/dt)$ and $e_7 = J_{eqv}(d^2\beta/dt^2)$.

Therefore:

$$\begin{cases} f_6 = \dot{\beta} \\ e_6 = J_{eqv}\ddot{\beta} + D_{eqv}\dot{\beta} + K_{blade}\beta \end{cases} \tag{3.36}$$

To establish the closed loop control law of the pitch angle the dynamics of the error are set as (the controlled variable is a generalized displacement):

$$\begin{cases} \varepsilon = \beta_{ref} - \beta \\ \ddot{\varepsilon} + k_2\dot{\varepsilon} + k_3\varepsilon = 0 \end{cases} \tag{3.37}$$

Where k_2 and k_3 represent the controllers to be used. Expression (36) becomes (38) :

$$\begin{cases} f_6 = \dot{\beta} \\ e_6 = J_{eqv}(\ddot{\beta}_{ref} + k_2(\dot{\beta}_{ref} - \dot{\beta}) + k_3(\beta_{ref} - \beta)) \\ + D_{eqv}\dot{\beta} + K_{blade}\beta \end{cases} \tag{3.38}$$

From the TF-element and GY-element we can write:

$$\begin{cases} f_5 = \dfrac{f_6}{N} \\ e_5 = N e_6 \end{cases} \tag{3.39}$$

$$\begin{cases} f_4 = \dfrac{e_5}{k} \\ e_4 = k e_5 \end{cases} \tag{3.40}$$

Finally, for the leftmost 1-junction, we can write:

$$\begin{cases} f_1 = f_2 = f_3 = f_4 = i(t) \\ e_1 = V(t) = e_2 + e_3 + e_4 = L\dfrac{di(t)}{dt} + Ri(t) + e_4 \end{cases} \tag{3.41}$$

We can derive a block diagram model from the bicausalled bond graph model to control the pitch angle, which is shown in Figure 19. The proposed gains (k_2 and k_3) are PI controllers; the estimate values are considered in the control law.

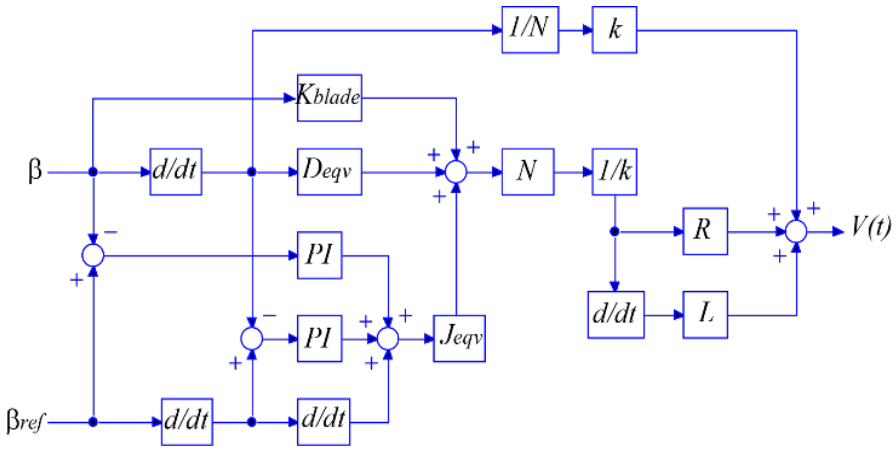

Figure 3.17. Pitch control law block diagram

The Bond Graph representation of the complete system is shown in Figure 3.20. The inputs to the systems are pitch angle, reference parameters and wind speed. It can be seen that the wind turbine control system basically contains two control loops, one is the pitch control loop and the other is the torque control loop. These two control loops operate simultaneously, but only one of them is dominant depending on the operation region shown in Figure 1. When the wind speed is below rated speed, the torque control loop is used to regulate the turbine speed to capture maximal wind power. When the wind speed exceeds rated speed, the pitch control loop is used to provide adequate pitch angle to regulate power at its rated value.

3.6 . Simulation and Discussion

In order to verify the effectiveness and the robustness of the proposed control law, a simulation is carried out by using different turbulent winds to drive the wind turbine, and a comparison between the proposed controller and the conventional PI controller is done by considering these wind profiles. The PI parameters are generated using Ziegler and Nichols methods [26].

Firstly, we consider the wind profile as shown in Figure 21, secondly, we use a turbulent wind with mean speed 12.5m/s and finally, the performance of the control system is tested during a turbulent wind with mean speed 18m/s.

The wind speed profile as shown in Figure 21 changes in step of every 20sec starting from 6m/s to 16m/s. This shows that both the above and below rated wind speeds are included in the wind profile. For below rated wind speed, the torque control comes into action with constant pitch angle, and for above rated wind speed, the pitch control comes into action with rated power.

Figure 22 shows the generator speed for the proposed method (inverse bond graph (IBG)) and PID controller for below and above rated wind speeds. Both controllers achieve the nominal value of the generator speed at 80sec. The corresponding wind speed is around 11m/s which can be seen from Figure 21. As the wind speed approaches the rated speed, the WT generator speed reaches the nominal value, that is, 112.35rad/s.Figs. 23 and 24 show respectively the electrical power and the power coefficient comparison for IBG and PID controllers for the transition period. In region 2 IBG is able to extract more power than PID. Figure 25 shows the generator torque comparison in region 2 for IBM and PID. It can be observed that IBM produces more generated torque compared to PID in region II. As the generator speed remains constant from 80sec onwards it is obvious that IBM captures more power compared to PID. Figure 26 shows the pitch angle comparison for PID and IBG; pitch variation is found to be more for PID compared to IBG. Therefore, the pitch actuator needs more control action for PID. Figure 27 shows the tower displacement comparison for PID and IBG. It can be observed that tower displacement in IBG is less than PID controller.

In order to create the appropriate conditions of comparing the two methods, the wind speed profile shown in Figure 28 with 12m/s average wind speed is used.

As is shown in Figure 29, the turbine rotor speed remains around its rated value 112.35rad/s. Figure 3.30 shows the generator torque. In order to increase generator power, generator torque, generator speed or both must be increased. Figs. 3.29 and 3.30 show that the generator speed and torque in the proposed method are higher in comparison with the conventional PID. Wind turbine power, shown in Figure 3.31, reaches its rated value of 5MW. Figs. 31 and 32 demonstrate that the proposed method is able to capture more electrical power in comparison with the other controller. From Figure 33, we find that the pitch system can track turbulent wind around cut-in speed. Therefore, according to the simulation results, the proposed method has a more effective performance in the generator

torque control and pitch control in comparison with the conventional PID method; the tower displacement in IBG is less than PID controller as shown in Figure 34.

The control system performance is also tested during a turbulent wind with mean speed 18m/s, as shown in Figure 35. Turbine rotor speed, generator torque, power, power coefficient, pitch angle and tower displacement are shown in Figs. 36 through 41 respectively. We can see that even for highly turbulent wind, all key turbine variables behave excellently.

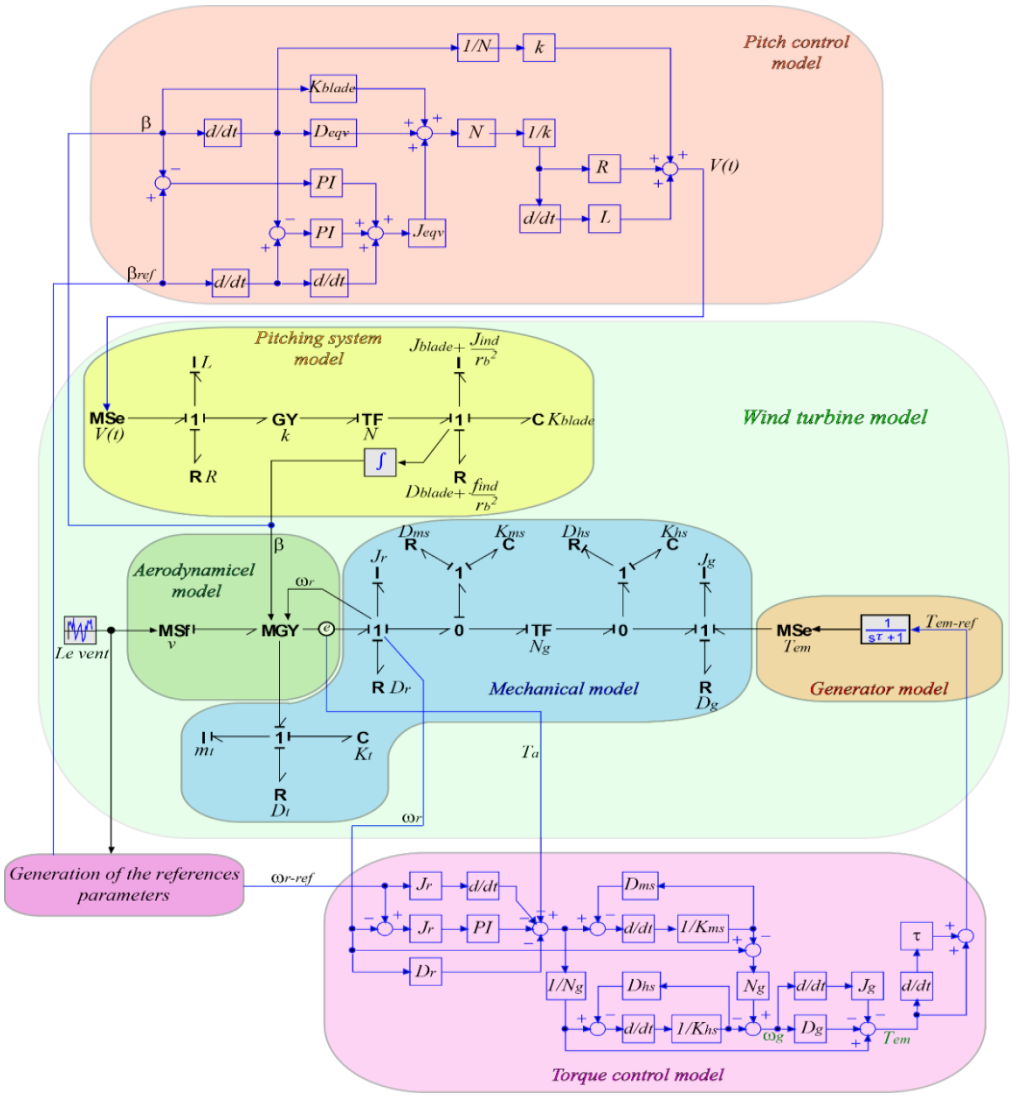

Figure 3.18. The Bond graph model and its control system of the wind turbine

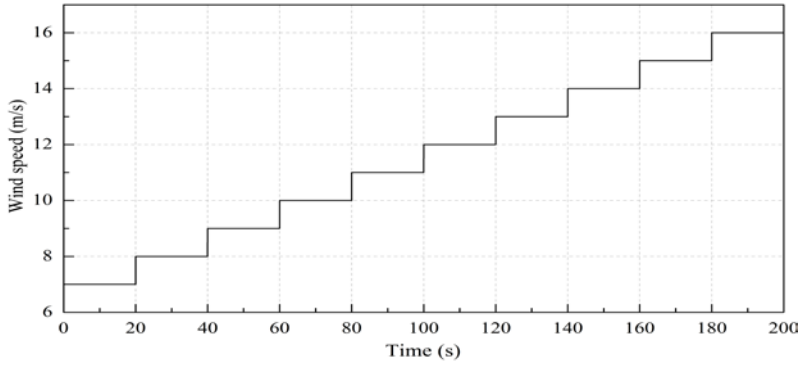

Figure 3.19. Wind speed profile

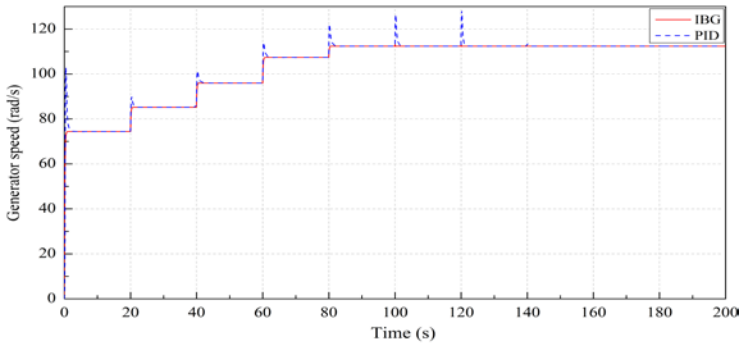

Figure 3.21. Generator speed

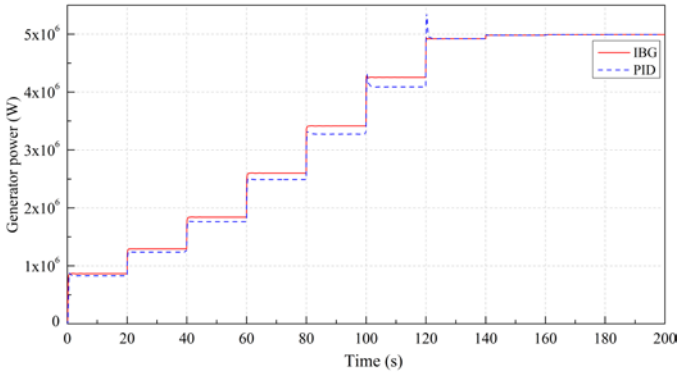

Figure 3.20. Generator power

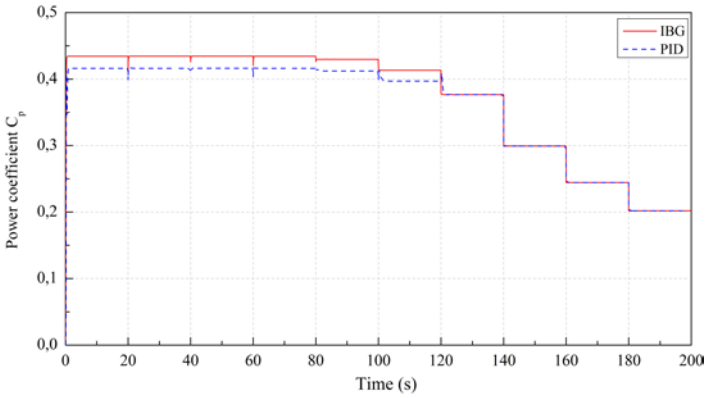

Figure 3.19. Power coefficient

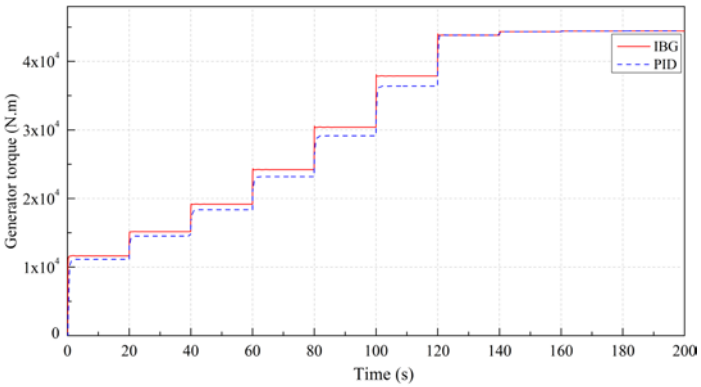

Figure 3.18. Generator torque

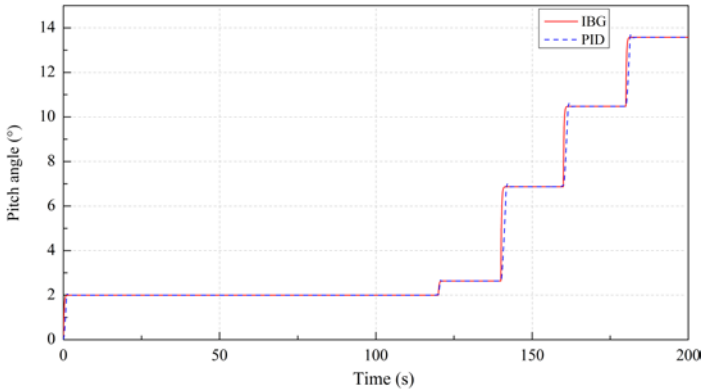

Figure 3.23. Pitch angle

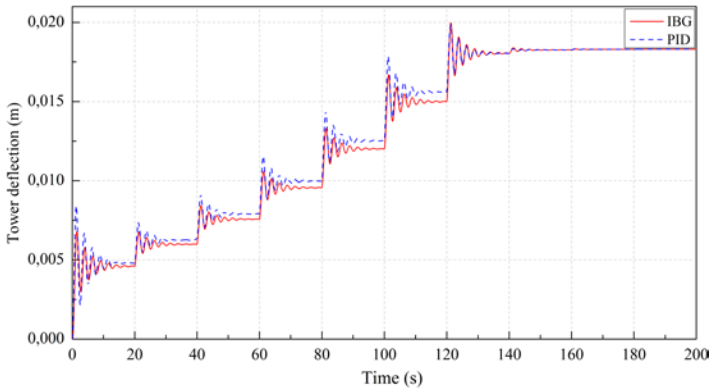

Figure 3.22. Tower displacement

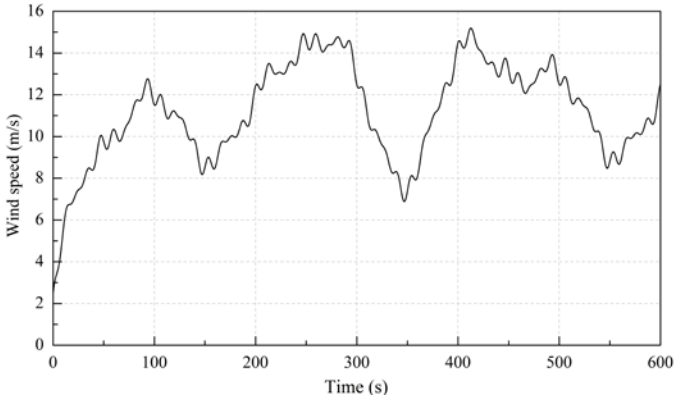

Figure 3.26. Wind speed profile (12m/s)

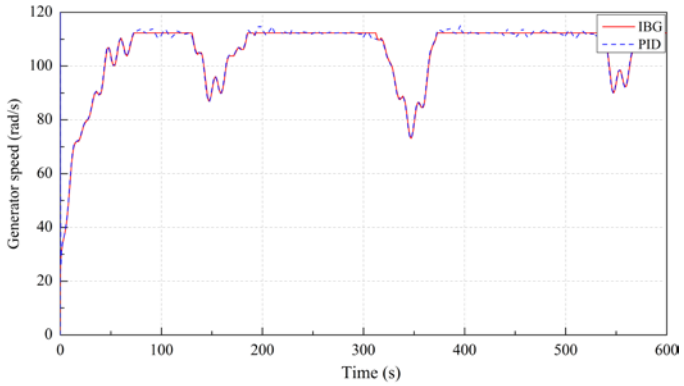

Figure 3.27. Generator speed (12m/s)

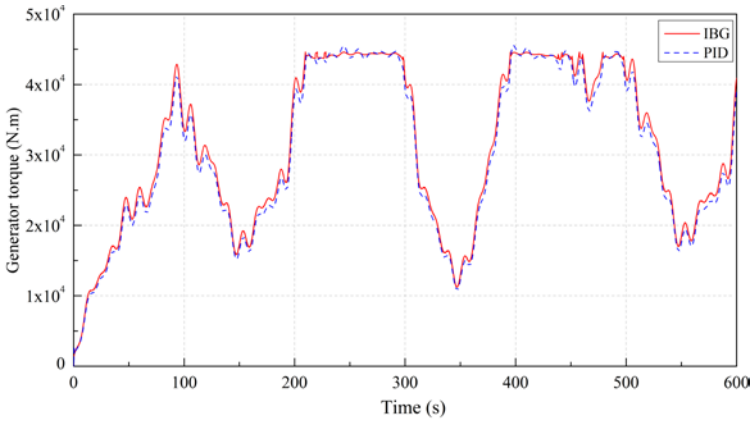

Figure 3.28. Generator torque (12 m/s)

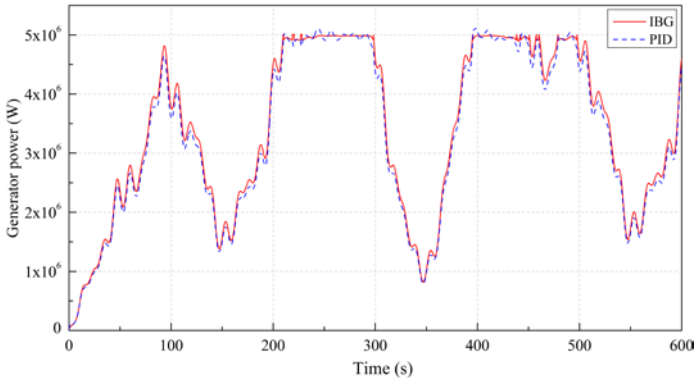

Figure 3.29. Generator power (12m/s)

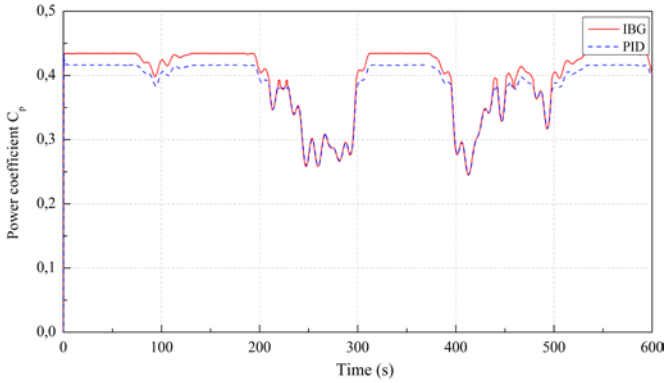

Figure 3.30. Power coefficient (12 m/s)

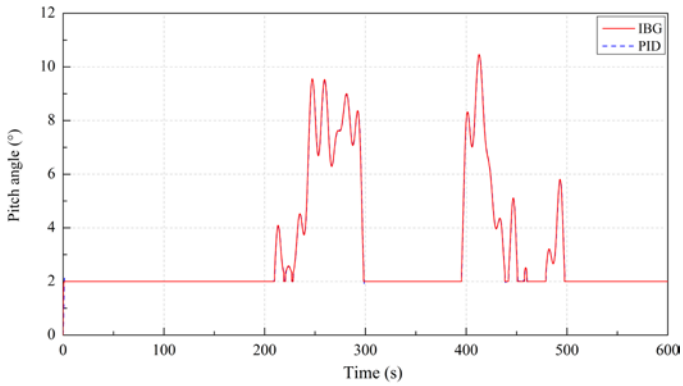

Figure 3.31. Pitch angle (12 m/s)

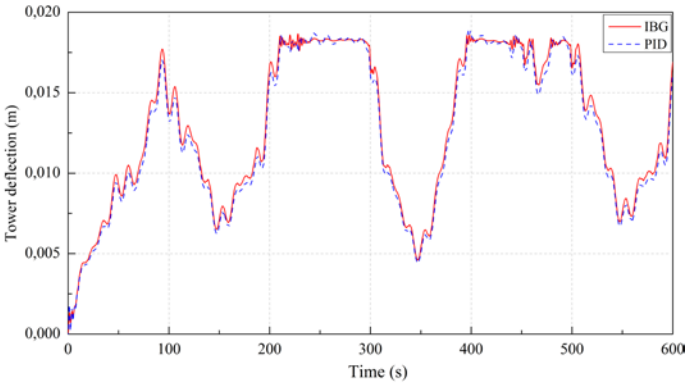

Figure 3.32. Tower displacement (12 m/s)

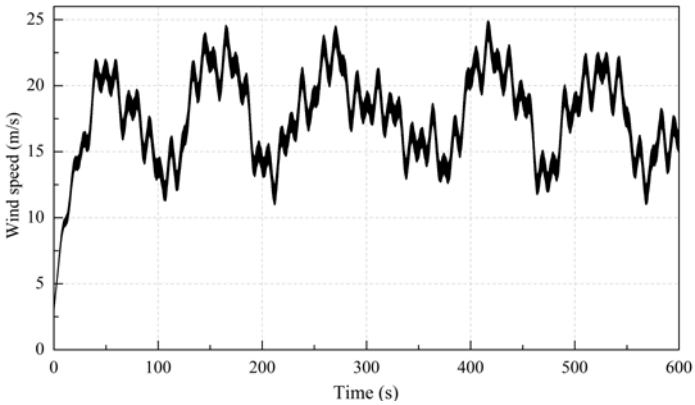

Figure 3.33. Wind speed profile (18 m/s)

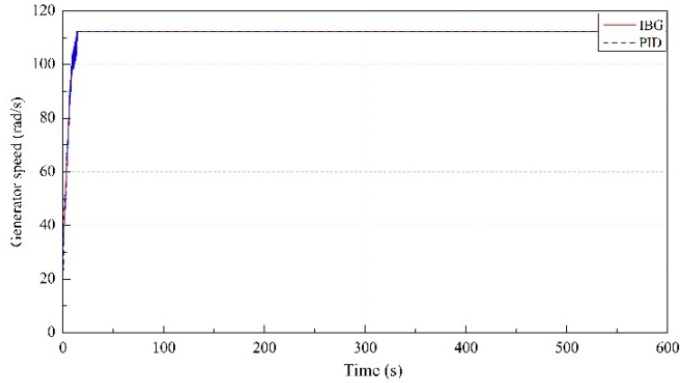

Figure 3.34. Generator speed (18 m/s)

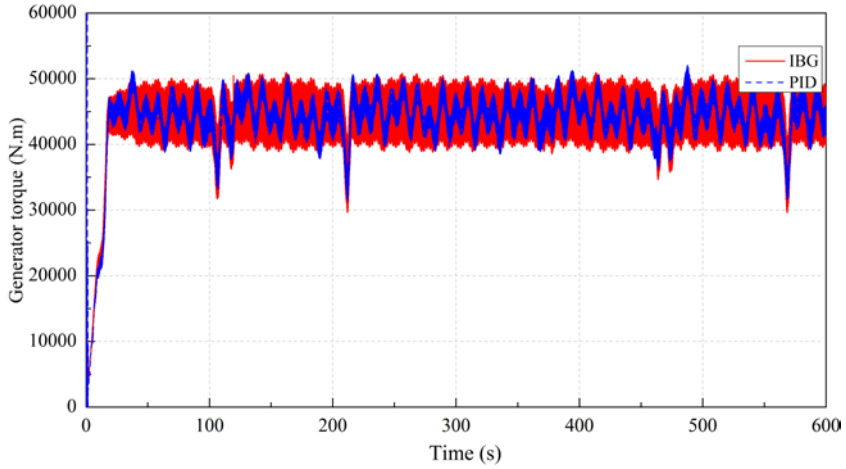

Figure 3.35. Generator torque (18 m/s)

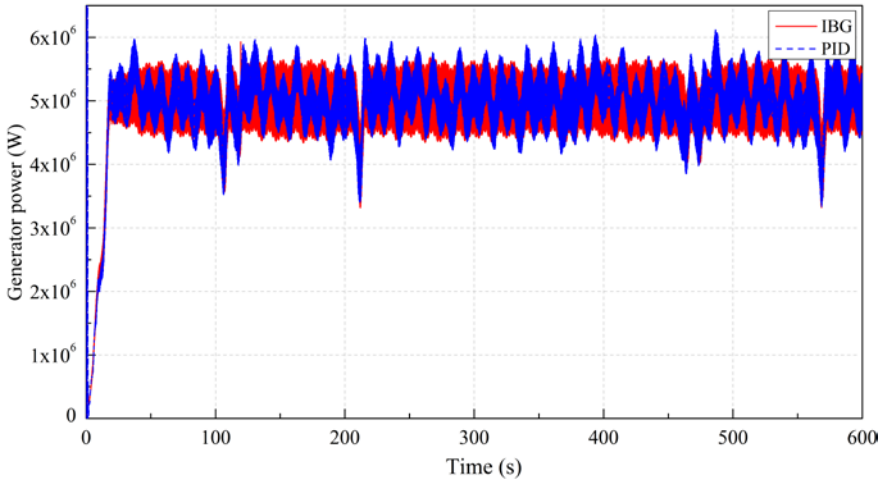

Figure 3.36. Generator power (18 m/s)

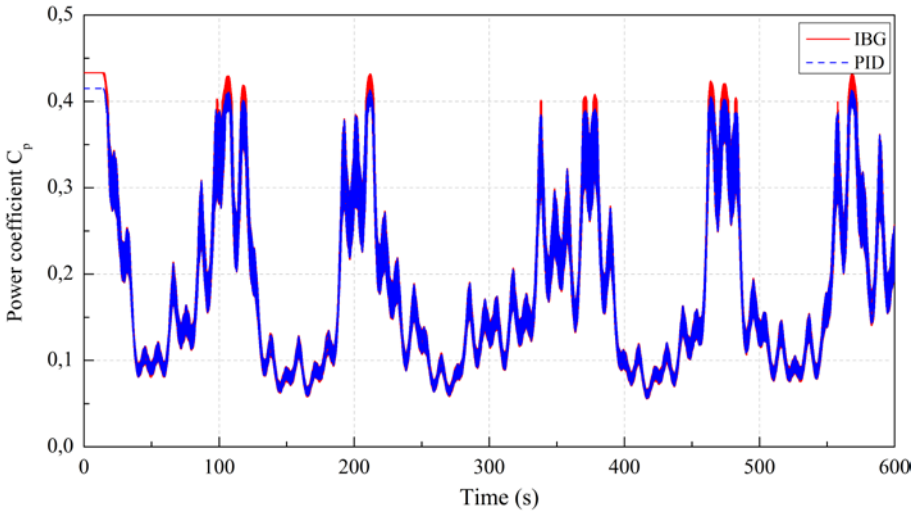

Figure 3.37. Power coefficient (18 m/s)

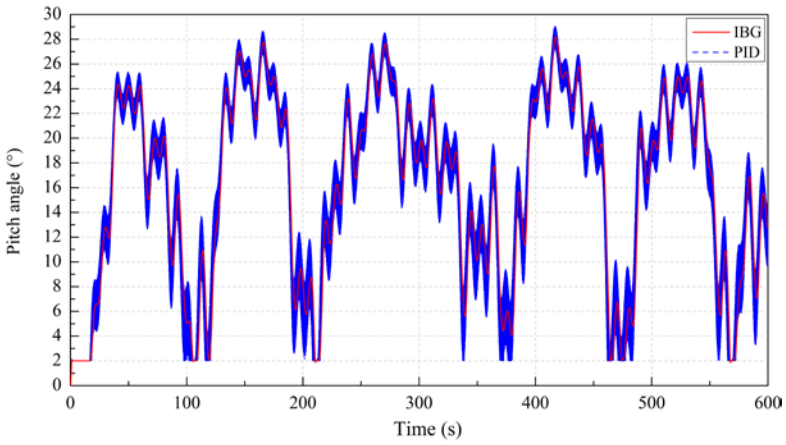

Figure 3.38. Pitch angle (18 m/s)

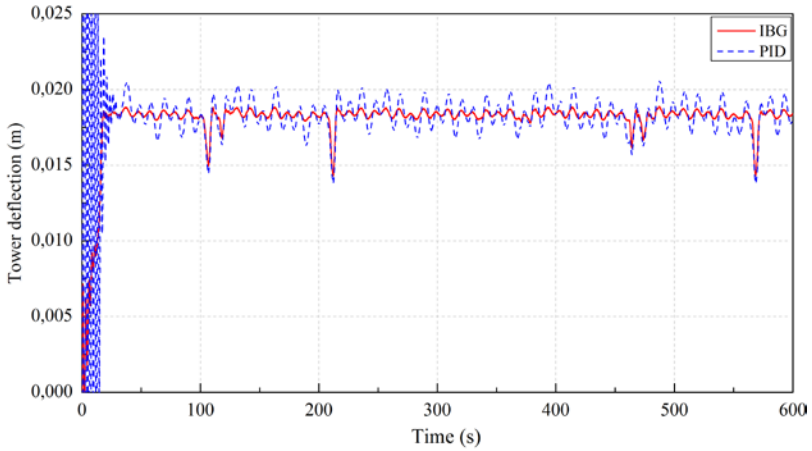

Figure 3.39. Tower displacement (18 m/s)

From the three simulations, it can be concluded that, for arbitrary turbulent wind profile, the proposed control can cope well with wind variation; all key variables can meet the requirements of the wind turbine system. At the end of this simulation, we find that compared with conventional PID strategies, IBG can provide more effective performance in the wind turbine power production. Controllers designed in this paper were tested by using the 20-sim program.

3.7 . Conclusion

In this chapter, a mechatronic model of a wind turbine generating system using the Bond Graph Approach is proposed to analyze and control power and speed of a variable speed variable pitch wind turbine. The proposed controllers used the bond graph model of a wind turbine in order to formulate the Inverse Bond Graph(IBG) model control. The control laws were intuitively obtained by considering this model. The work introduced an effective control strategy applied on a 5MW wind turbine, including both generator torque and pitch angle control at different regions of operation: maximum power (region II) and rated power (region III). The control strategy was designed for a wide range of wind conditions. The main aim is to capture the maximum power in region II and regulated power and generator speed at its rated values in region III, with reduced oscillation on the tower at values below rated speed. A

comparison with PID controller is done. From the simulation the IBG controller can achieve the maximum and quality power in all the regions of wind speed. The simulation results show that the introduced controller has more performance that is more favorable in all the regions of wind speed than the conventional PID controller. All turbine variables, including pitch angle, turbine rotor speed, and power output, behave excellently.

It is suggested in future research work to test the proposed control law by considering a detailed model of the induction machine using the bond Graph Approach, and the control law will be synthetized from the Inverse Bond Graph model by considering the induction generator in its natural reference frame.

Appendix A: The Considered Wind Turbine's Parameters

Parameters	**Values**
Rated turbine power	P_n=5MW
Rotor radius	R=55m
Air density	ρ=1.225 kg/m3
Cut-in wind speed	v_{cut-in}=3m/s
Cut-out wind speed	$v_{cut-out}$=25m/s
Rated wind speed	v_{rated}=12m/s
Rated generator speed	ω_{rated}=112rad/s
Rated generator torque	T_{rated}=43KNm
Drive train	
Rotor inertia	J_r=5.9145.105Kg.m2
Rotor bearing	D_r=1000N.m.s/rad
Main speed shaft stiffness	K_{ms}=8.7354.108N.m/rad
Main speed shaft damping	D_{ms}=6.3478.105N.m.s/rad
Gearbox ratio	N=60:1
High speed shaft stiffness	K_{hs}=108N.m/rad
High speed shaft damping	D_{hs}=1.33.103N.m.s/rad
Generator inertia	J_g=18.7kg.m2
Generator friction coefficient	D_g=0.1N.m.s/rad
Pitch system	
Motor Resistance	R=3.9Ω
Motor inductance	L=4.10-3H
emf constant	k=0.4
Rotor inertia of the motor	Jind=10-3Kg.m2
Rotor bearing of the motor	find=0.01N.m.s/rad
Gearbox ratio	N=0.016
Blade inertia	Jblade=800Kg.m2
Blade dampind	Dblade=2.3.105N.m.s/rad
Blade stiffness	Kblade=1.7.107N.m/rad

References

[1]. Fernando D. Bianchi, Hernán De Battista and Ricardo J. Mantz. 2007. Wind Turbine Control S ystems: Principles, Modelling and Gain Scheduling Design.

[2]. Burton T, Sharpe D, Jenkins N, Bossanyi E. 2001. Wind energy handbook. New York: Wiley Publications.

[3]. YaxingRen, LiuyingLi, JosephBrindley, LinJiang. 2016. Nonlinear PI control for variable pitch wind turbine. Control Engineering Practice, 50: 84–94.

[4]. Richie Gao, ZhiweiGao. 2016. Pitch control for wind turbine systems using optimization, estimation, and compensation, Renewable Energy, 91: 501-15.

[5]. Qiao W., Zhou W.,Aller J. M., and Harley R. G. 2008. Wind speed estimation based sensorless control for a wind turbine driving a DFIG, IEEE Trans. Power Electron, 23(3): 1156–59.

[6]. Yilmaz A. S. and Ozer Z. 2009. Pitch angle control in wind turbine above the rated wind speed by multilayer perception and radial basis function neural networks, IEEE Exp. Syst, 36(6): 9767–75.

[7]. Liao M., Dong L., Jin L.,and Wang S. 2009. Study on rotational speed feedback torque control for wind turbine generator system, in Proceedings of the International Conference on Energy and Environment Technology (ICEET ’09), 853–56.

[8]. Sheikhan M., Shahnazi R., and NooshadYousefi A. 2013. An optimal fuzzy PI controller to capture the maximum power for variablespeed wind turbines, Neural Computing and Applications, 23(5): 1359–68.

[9]. Boukhezzar B., Lupu L., Siguerdidjane H., and Hand M. 2007. Multivariable control strategy for variable speed, variable pitch wind turbines, Renewable Energy, 32(8): 1273–87.

[10]. Jafarnejadsani H., Pieper J., and Ehlers J. 2013. Adaptive control of a variable-speed variable-pitch wind turbine using radial-basis function neural network, IEEE Transactions on Control Systems Technolog y, 21(6): 2264–72.

[11]. Zhang W.and Xu H. 2011.Active disturbance rejection based pitch control of variable speed wind turbine, in Procee dings of the 30th Chinese Control Conference, 5094–98.

[12]. Jonkman J, Butterfield S, Musial W, Scott G. 2009. Definition of a 5-MW reference wind turbine for offshore system development. Technical report. Golden, Colorado. USA: National Renewable Energy Laboratory (NREL)

[13]. Margolis D. 2011. Bond Graph Modelling of Engineering Systems: Theory, Applications and Software Support.

[14]. Merzouki R., Samantaray A.K.,Pathak P.M. and Bouamama B.O. 2013. Intelligent Mechatronic Systems: Modeling, Control and Diagnosis.

[15]. Paynter H.M. 1961. Analysis and Design of Engineering Systems (M.I.T. Press, Cambridge). rm optimization algorithm. ISA Transactions, 51: 641–48.

[16]. Karnopp D.C., Margolis D.L., Rosenberg R.C. 2000. System Dynamics: Modeling and Simulation of Mechatronic Systems (Wiley, New York).

[17]. Bakka T., Reza K.H. 2013. Bond graph modeling and simulation of wind turbine systems, J MechSciTechnol; 27(6): 1843–52.

[18]. Heier, S. 1998. Grid Integration of Wind Energy Conversion Systems. Wiley, New York.

[19]. Khaouch Z. et al. Mechatronic modeling of a 750kW fixed-speed wind energy conversion system using the Bond Graph Approach .ISA Transactions (2016) http://dx.doi.org/10.1016/j.isatra.2016.07.009i

[20]. PoultagonI., Shahnazi R., Sheikhan M. 2012. RBF neural network based PI pitch controller for a class of 5-MW wind turbines using particle swarm optimization algorithm. ISA Transactions 51 (2012) 641–648.
[21]. Villanueva I., Ponce P., Monina A. 2015. Interval Type 2 Fuzzy Logic Controller for Rotor Voltage of a Doubly-Fed Induction Generator and Pitch Angle of Wind Turbine Blades. IFAC-PapersOnLine, 48(3): 2195–202.
[22]. Gawthrop P.J. 1995.Bicausal bond graph, in: Proceeding of the International Conference on Bond Graph Modeling and Simulation ICBGM'95, vol. 27.
[23]. Gawthrop P.J. 2000. Physical interpretation of inverse dynamics using bicausal bond graphs. J. Frankl. Inst., 337(6): 743–69.
[24]. Ngwompo R.F., Scavarda S. 1999.Dimensioning problems in system design using bicausal bond graphs. Simul. Pract. Theory7, 577–587.
[25]. Ngwompo R.F., Scavarda S., Thomasset D. 2001. Physical model-based inversion in control systems design using bond graph representation—part 2: applications. Proc. IMechE Part I J. Syst. Control Eng, 215: 105–12.
[26]. Zigeler J.G., Nichols N.B. 1942 Optimization Setting for Automatic Controller, Trans. ASME, Vol. 64, pp. 756-769.

Chapter 4. Mechatronic Modelling of a 750 KW Fixed-Speed Wind Energy Conversion System Using the Bond Graph Approach

4.1 . Introduction

Wind turbine is a complex mechatronic system, in which different technical areas are involved (mechanics, aeronautics, electrical, among others). There is no doubt that a mechatronic approach is essential in the field of wind turbine design. This approach implies that a mechanic, aerodynamic, electric subsystems and eventually their control subsystem should be designed as an integrated system. This integration is important for a more accurate evaluation of the extreme loads and the fatigue life, and this might reduce the failure rate in the design stage. However, the aerodynamic, mechanical and electrical models should be usable for detailed control system design, which will be necessary as the design goes deeper. Indeed, linear simplified models, (a simple aerodynamic, mechanical or elective models), are not sufficient to take into account the necessary coupling effects among the components.

For the combined analysis of the aerodynamic, structural and control generating systems, or the mechanical, control and aerodynamic subsystems many works either use a very simple mechanical model with a detailed electrical model, or a complicated mechanical model with a simple control system model [3,4]. Hence, the interactions and the dynamics coupling cannot be accurately predicted. In [5] four different models of wind turbines are introduced. On one hand, two static models – the “simple static model” and the “static mechatronic model”, represent two different instances of a simplified behavior. On the other hand, two dynamic models – the “mechanical model” and the “dynamic mechatronic model”, describe the dynamic behavior of a wind turbine in more details.

In [6] a control-generator-structure coupled with analysis in wind turbines using a monolithic modeling and simulation is proposed. The integrated system models were developed on Samcef for Wind Turbines (S4WT) through a nonlinear finite element method (FEM) formalism. Another contribution [7, 8] reviews recent research of technical issues on the development of wind farms. These contributions highlight the importance of having a mechatronic model of the wind turbine, but the models lack some detail. In order to analyze the system in the same reference frame, there are several methods and tools for the modeling and the simulation of physical systems and their controllers, with parameters directly related to physical components. Moreover, it is desired that these (sub-) models should be reusable. Common Block-Diagram- (CBD) or Equation-Based Simulation (EBS) packages do not easily support these features. The Energy-Based Approach (EBA) for modeling physical systems allows the construction of reusable and easily extendable models.

In this chapter, a fixed speed wind turbine mechatronic model has been developed. The main components of the system are modeled in detail using the Bond-Graph Approach (BGA). The implementation of the complete model has been carried out by means of the 20-Sim simulation program (a demo version is freely available on the Internet). Parameters of a 750 kW-power wind turbine were taken from NACA 4415 profile [9]. Verification of results is reported. Conclusions of the conducted research investigation are drawn.

4.2 . Mechatronic Modelling of the Wind Energy Conversion Systems

In the next sections, the mechatronic modelling of the main components of a WECS will be presented. Our first aim is to show the complete wind turbine in a unified framework. The WECS is organized into four main areas, namely the aerodynamic, mechanical, electrical, and pitch servo subsystems. The main components of a WECS are rotor, transmission system and power generator unit. The rotor comprises the blades where the aerodynamic conversion takes place, the hub that links the blades to the transmission and the pitch servos, which are located inside the hub that rotates the blades around their longitudinal axes. The transmission system transmits the mechanical power from the rotor to the electric machine. It comprises the low- and high-speed shafts, the gearbox and the brakes. The gearbox increases the rotor speed to values more suitable for driving the generator, typically from 20-50 rpm to 1000-1500 rpm. The electric generator is the device that converts mechanical power into electricity. Its electric terminals are connected to the utility network. In the case of variable-speed WECS, an electronic converter is used as interface between the AC grid and the stator or rotor windings.

A mechatronic model, that takes into consideration the dynamic behavior of the entire WECS, can be structured as several interconnected subsystem models as shown in Figure 3.2. The aerodynamic subsystem describes the transformation of the three-dimensional wind speed field into forces on the blades that generate the rotational motion. The mechanical subsystem can be divided into two functional blocks, i.e., the drive-train and the support structure. The drive-train transfers the aerodynamic torque on the blades to the generator shaft. It encompasses the rotor, the transmission and the mechanical parts of the generator. The structure is made up of the tower and the blades. The electrical subsystem describes the conversion of mechanical power at the generator shaft into electricity. Finally, the actuator

Subsystem-level block diagram of a WECS

In order to analyze the system in the same reference frame, the Bond-Graph Approach (BGA) [10, 11] is used.

4.2.1. Mechanical Subsystem

A horizontal-axis wind turbine is a complex mechanical system that consists of interacting devices with some degree of flexibility. Like any flexible structures, such system exhibits many vibration modes. Some oscillatory movements inherent to these modes are illustrated in Fig. 4.1 [12]. The existence of these vibration modes demands a careful design of the wind turbine and controller.

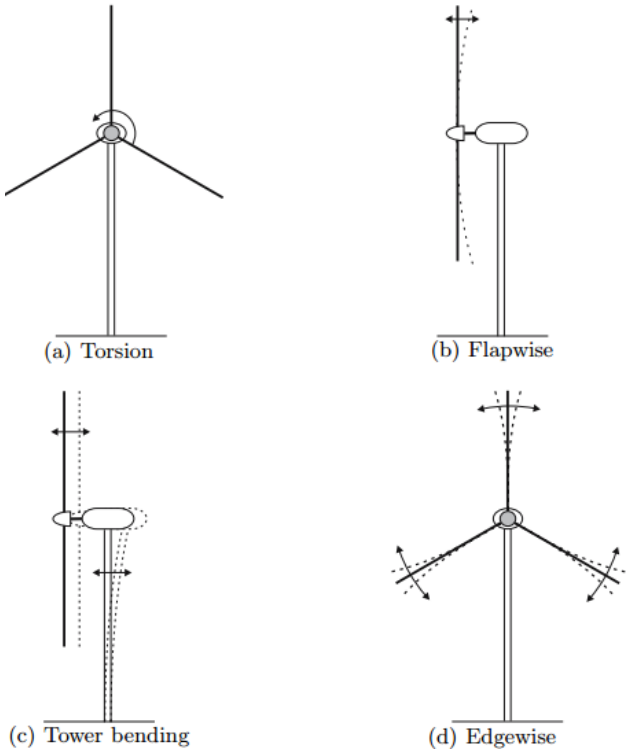

Figure 4.1. Mode shapes for horizontal-axis wind turbines

For the WECS modeling, the most involved part is probably the mechanical subsystem. The complexity arises from the interaction of three flexible structures: the blade, drive train and the tower. Each of these structures is fixed to a reference frame that rotates with respect to the other. This leads to high-order nonlinear dynamic models. Moreover, most of the forces applied to the structures come from a three-dimensional wind field.

The mechanical subsystem model (blade, tower, and gearbox), that takes into account the dynamic behavior of a horizontal-axis wind turbine, can be undertaken by various analysis methods [13, 14]. In this section, a bond graph model of the mechanical subsystem is proposed. It considers the blade and tower as a Rayleigh beam composed of a number of sections submitted to aerodynamic forces, and the gearbox as a multi-body dynamic system. Subsequently, the model can be used to develop pitch control algorithms, which should minimize the vibrations probability and also increase wind turbine lifetime by mastering the loads effects and the costs reduction without sacrificing the aerodynamic output.

Bond graph model of the wind turbine blade

In this section, we study the structural dynamic behavior of the wind blade. A blade bond graph model is developed. It consists of considering the blade as a three-dimensional beam composed of a number of sections Fig. 4.2(a). The sections vary according to NACA 4415 airfoil sections. In [15, 16], only constant sections were used. Many studies on the behavior of the blade dynamic structure were conducted. In [17] a structural model of the wind turbine blade is proposed based upon the Rayleigh beam model. The blade - assumed as a twisted beam, is divided into three components, each of which is subject to the aerodynamic wind forces. Nevertheless the deformation of the axial extension and the pitching moment applied to the center of gravity are taken into consideration. These "gaps" are addressed in this work where they are integrated in our model. The dynamic model of the blade is shown in

Fig. 4.2(b). For each element in the aerodynamic forces, we also add the deformation of the axial extension and the pitching moment blade. Therefore, the blade is modeled as a three-dimensional beam.

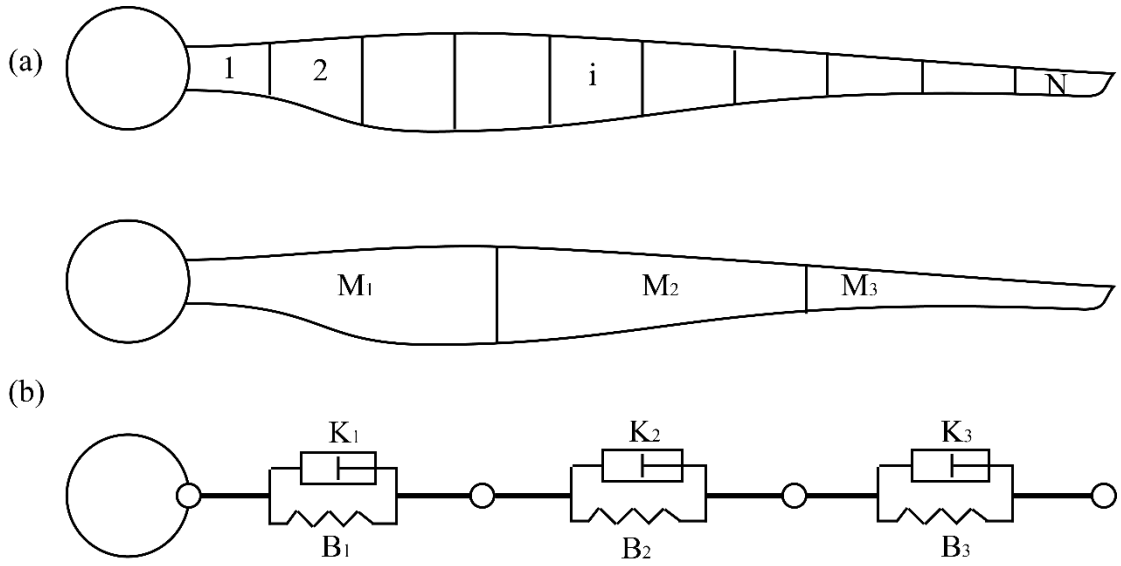

Figure 4.2. Turbine Blade with space reticulation (a), Dynamic model of blade (b)

The stiffness of the beam element relates the generalized Newtonian forces to the generalized displacements at the ends of the element as given by (Eq12), (Eq13) and (Eq14).

$$\begin{bmatrix} F_{yi} \\ M_{zi} \\ F_{yi+1} \\ M_{zi+1} \end{bmatrix} = [K_{fyi}] \begin{bmatrix} y_i \\ \theta_{zi} \\ y_{i+1} \\ \theta_{zi+1} \end{bmatrix} \tag{4.1}$$

$$\begin{bmatrix} F_{zi} \\ M_{yi} \\ F_{zi+1} \\ M_{yi+1} \end{bmatrix} = [Kf_{zi}] \begin{bmatrix} y_i \\ \theta_{yi} \\ y_{i+1} \\ \theta_{yi+1} \end{bmatrix} \tag{4.2}$$

$$\begin{bmatrix} M_{xi} \\ M_{xi+1} \end{bmatrix} = [K_t] \begin{bmatrix} \theta_{xi} \\ \theta_{xi+1} \end{bmatrix} \tag{4.3}$$

Where $[K_{fyi}]$ is the flexural stiffness around y, $[K_{fzi}]$ is the flexural stiffness around z and $[K_t]$ is the flexural stiffness around x, are given by (4.4), (4.5) and (4.6):

$$[K_{fyi}] = \frac{E(I_{zi-1} + I_{zi})}{\left(l_{i-1} + \frac{l_i}{2}\right)^3} \begin{bmatrix} 12 & 6(l_{i-1} + l_i/2) & -12 & 6(l_{i-1} + l_i/2) \\ 6(l_{i-1} + l_i/2) & 4(l_{i-1} + l_i/2)^2 & -6(l_{i-1} + l_i/2) & 2(l_{i-1} + l_i/2)^2 \\ -12 & -6(l_{i-1} + l_i/2) & 12 & -6(l_{i-1} + l_i/2) \\ 6(l_{i-1} + l_i/2) & 2(l_{i-1} + l_i/2)^2 & -6(l_{i-1} + l_i/2) & 4(l_{i-1} + l_i/2)^2 \end{bmatrix} \quad (4.2)$$

$$[K_{fzi}] = \frac{E(I_{yi-1} + I_{yi})}{\left(l_{i-1} + \frac{l_i}{2}\right)^3} \begin{bmatrix} 12 & -6(l_{i-1} + l_i/2) & -12 & -6(l_{i-1} + l_i/2) \\ -6(l_{i-1} + l_i/2) & 4(l_{i-1} + l_i/2)^2 & 6(l_{i-1} + l_i/2) & 2(l_{i-1} + l_i/2)^2 \\ -12 & 6(l_{i-1} + l_i/2) & 12 & 6(l_{i-1} + l_i/2) \\ -6(l_{i-1} + l_i/2) & 2(l_{i-1} + l_i/2)^2 & 6(l_{i-1} + l_i/2) & 4(l_{i-1} + l_i/2)^2 \end{bmatrix} \quad (4.3)$$

$$[K_t] = \frac{GJ}{L} \begin{bmatrix} 1 & -1 \\ -1 & 1 \end{bmatrix} \quad (4.4)$$

Where E is the Young module of the material, G is the Coulomb module, Iy,z the second moments of area about the axis of deflection, J is the second polar moment and L is the length of the finite element, The structural damping matrix is given by $[R_i] = \mu[K_i]$, where the μ factor represents the coefficient of structural damping.

Fig. 4.3 shows the Bond Graph model of the blade. Fig. 4.3(a) represents the axial extension deformation of the blade, Fig. 4.3(b) the tangential extension deformation and Fig. 4.3(c) the torsional deformation of blade. For Fig. 4.3(a) and Fig. 4.3(b), two motions are shown: rotation at the top and translation at the bottom of the figure. In Fig. 4.3(c) the model is represented by one rotation motion. For each model, the displacements and rotations at the center of gravity of each element are represented by 1-junction. For each element aerodynamic forces are applied, meanings that the effort is imposed. The stiffness and the structural damping matrixes between the centers of gravity of adjacent elements are represented using C-field and R-field elements, respectively.

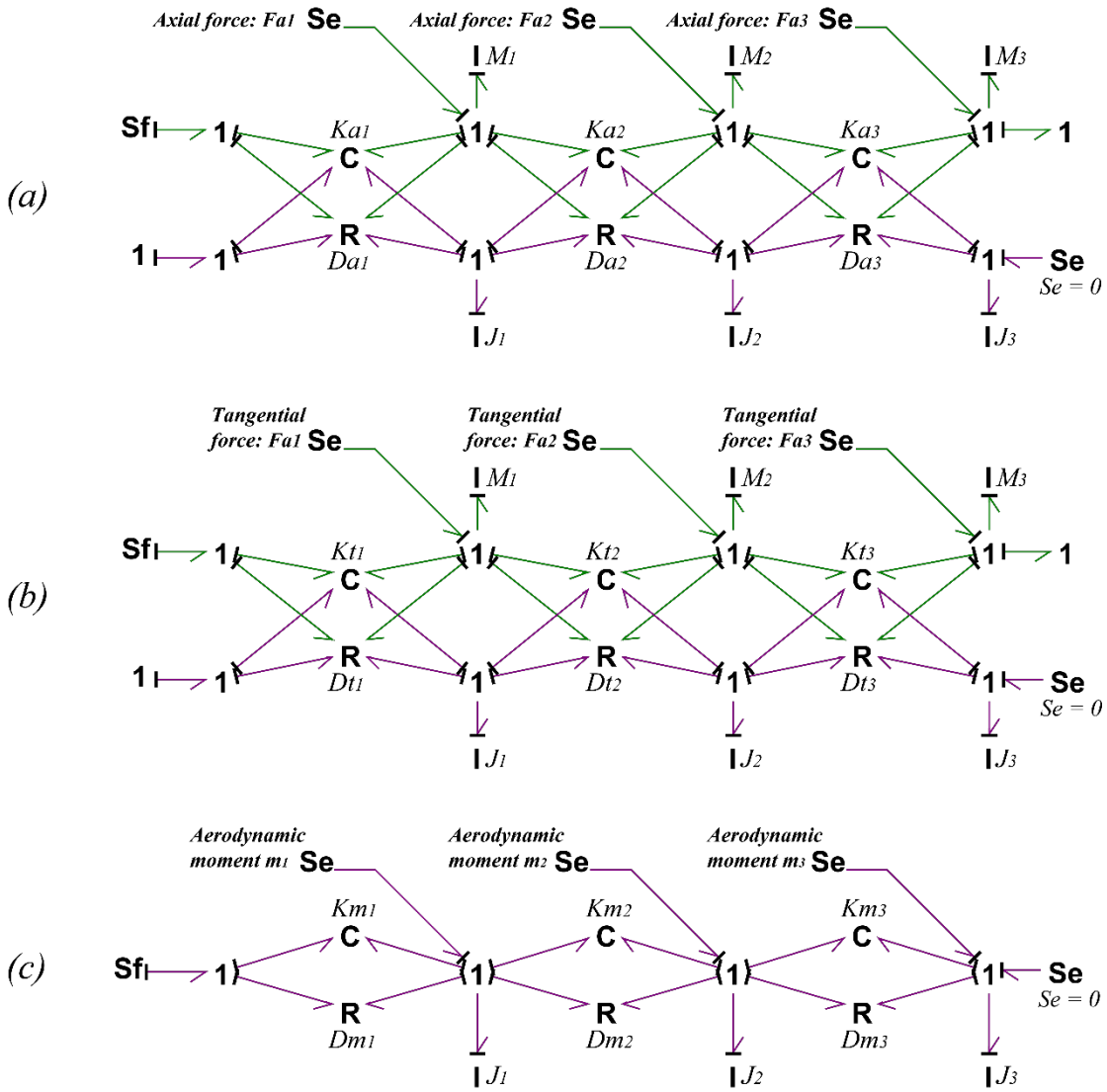

Figure 4.3. Structural bond graph of blade, axial extension (a), tangential extension (b), torsional extension (c)

Boundary conditions of the model for the tangential extension deformation are represented by the S_f and S_e sources. Connection between the blade and the hub must be rigid, i.e. $S_f = 0$, and the blade has only one degree of freedom, so $S_e = 0$. Boundary conditions for the axial extension deformation are represented by the Se source. The blade has only one degree of freedom, then $S_e = 0$. Connection between the blade and the hub as well as between the hub and the tower are assumed to be rigid. Therefore, the movement at the tower top is the same as the movement at the blades bottom. This relationship between the blade and the tower can be modeled by 1-junction. Boundary conditions for the torsional deformation are represented by the Sf source which represents the pitch actuator system's velocity. Dynamic equations and natural frequencies of the blade can be directly obtained from the Bond Graph model.

Three sources of effort, which represent the aerodynamic forces, need to be calculated in the input wind. This process will be treated in the aerodynamic subsystem section. Sub-models, as shown in Fig. 4.4 can represent the model of the blade (Fig. 4.3).

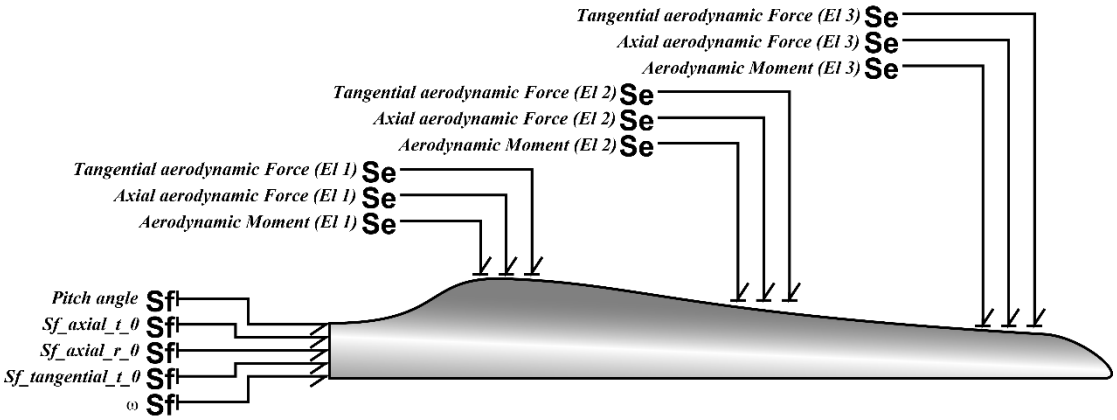

Figure 4.4. Three sections bond graph blade

To check the model validity, a simulation of the torque at the rotor blade is shown in Fig. 4.5. Parameters are available in Appendix A. A constant tangential aerodynamic force is applied at each element's center of gravity (S_e = 100 N). These forces are transformed into a blade rotor torque($T = \sum_{i=1}^{3} F_i r_i$). This simulation shows that the torque in steady state is equal to 3510.25 N.m. Based upon the parameters in appendix A, we have $T = 100 * 3.9 + 100 * 11.7 + 100 * 19.5 = 3510$ N. m. We find the same value of the torque. Therefore, the model works very well. The vibrations presented in the model are due to the dynamic behavior between the mesh stiffness and the momentum of inertias.

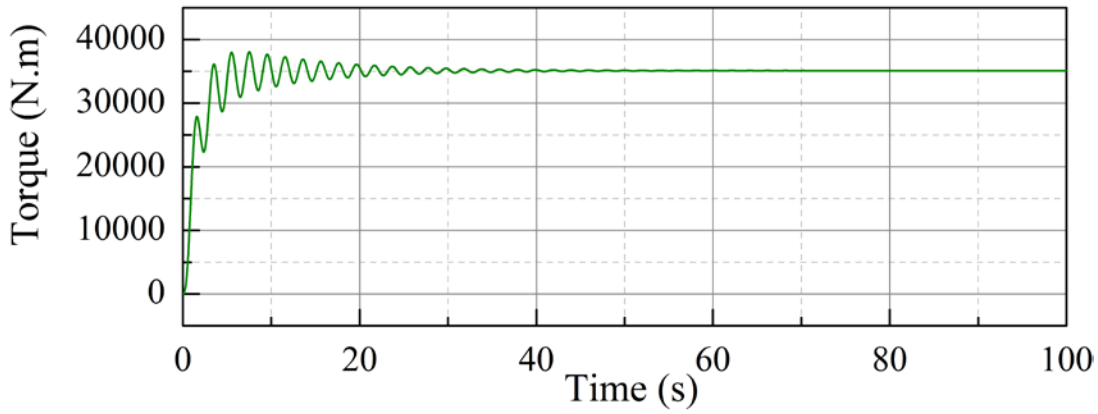

Figure 4.5. Torque simulation of the blade

Bond Graph Model of the Hub

The hub model links the blades tangential model to the transmission, the blades axial model to the tower and the blades pitching moment to the pitch servos system. The latter is located inside the hub and rotates the blades around their longitudinal axes. The Bond Graph model of the hub is shown in Fig. 4.6.

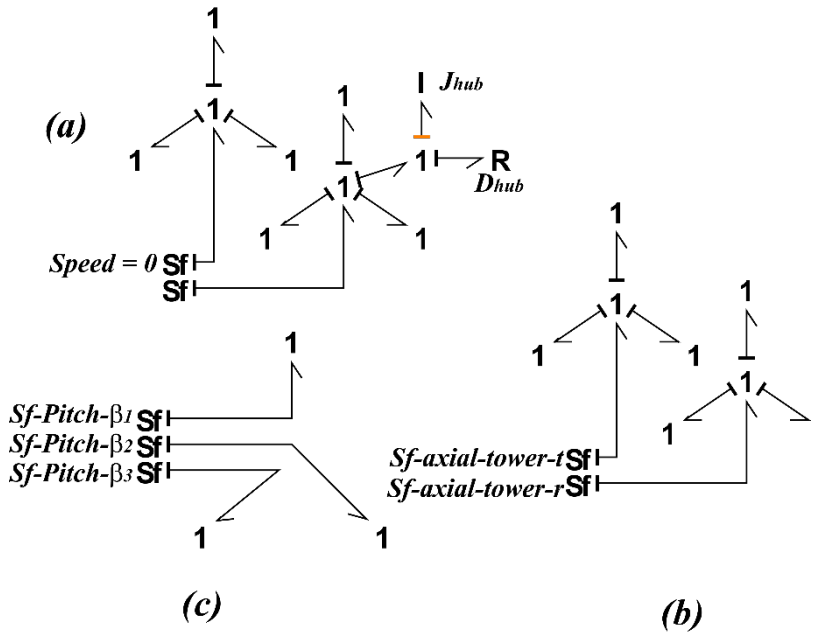

Figure 4.6. Bond graph model of the hub

Fig. 4.6(a) sketches the connection between the tangential model of the blades and the transmission. I-elements and R-elements represent the inertia and main bearing of the hub respectively. Fig. 4.6(b) shows the connection between the axial model of the blades and the tower. Fig. 4.6(c) deals with the connection between the pitching moment model and the pitch servos system. Sub-models, as shown in Fig. 4.7 can represent the model of the hub (Fig. 4.6).

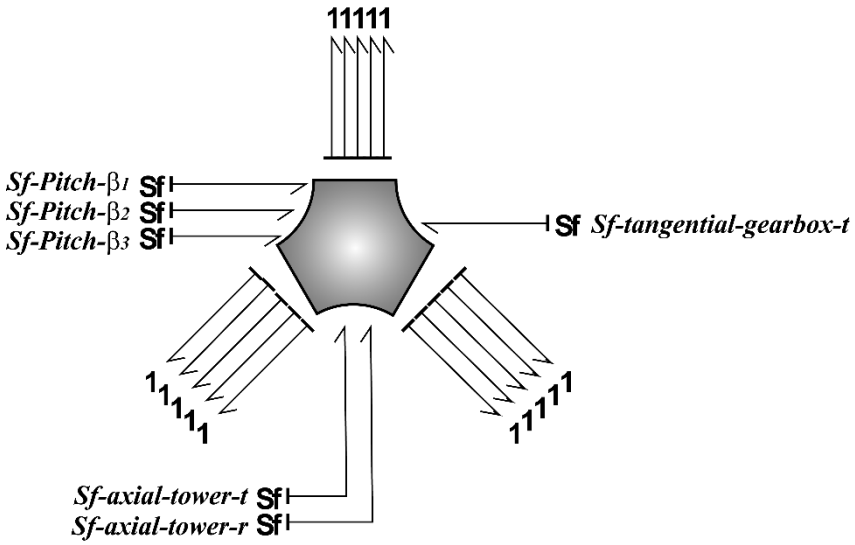

Figure 4.7 Wind Turbine Tower Model.

Bond Graph Model of the tower

Dynamic behavior of a wind turbine tower is subjected to random wind loads - which produces large vibrations that could, on the long run, lead to fatigue and failure is examined [18]. Therefore, the control system should be designed in such a way to minimize the effects of external loads and eliminate vibrations of the flexible tower.

The tower is modeled as a tubular Rayleigh beam with three different sections (Fig. 4.8(b). However, it can be divided into more segments. The wind loads on the rotors are transferred to the tower as bending moments at the tower top. In the right-handed Cartesian coordinate system shown in Fig. 4.8(a), the z-axis is assumed to coincide with the elastic axis, as well as the cross section's center of the thin-walled beam, the y-axis is in the direction of wind. The model is constructed on the assumption that every segment has uniform cross-sectional properties (Fig. 4.8(b), with distributed parameters by the Bond Graph Approach. This model can be used to develop pitch control algorithms, which would minimize the probability of extremely high levels of tower vibrations.

In order to evaluate the structures vibration properties, the wind turbine tower is modeled as an elastic tubular beam with a rigid rotor on the top and a fixed-base on the ground. The dynamic model of the tower is shown in Fig. 4.8(c).

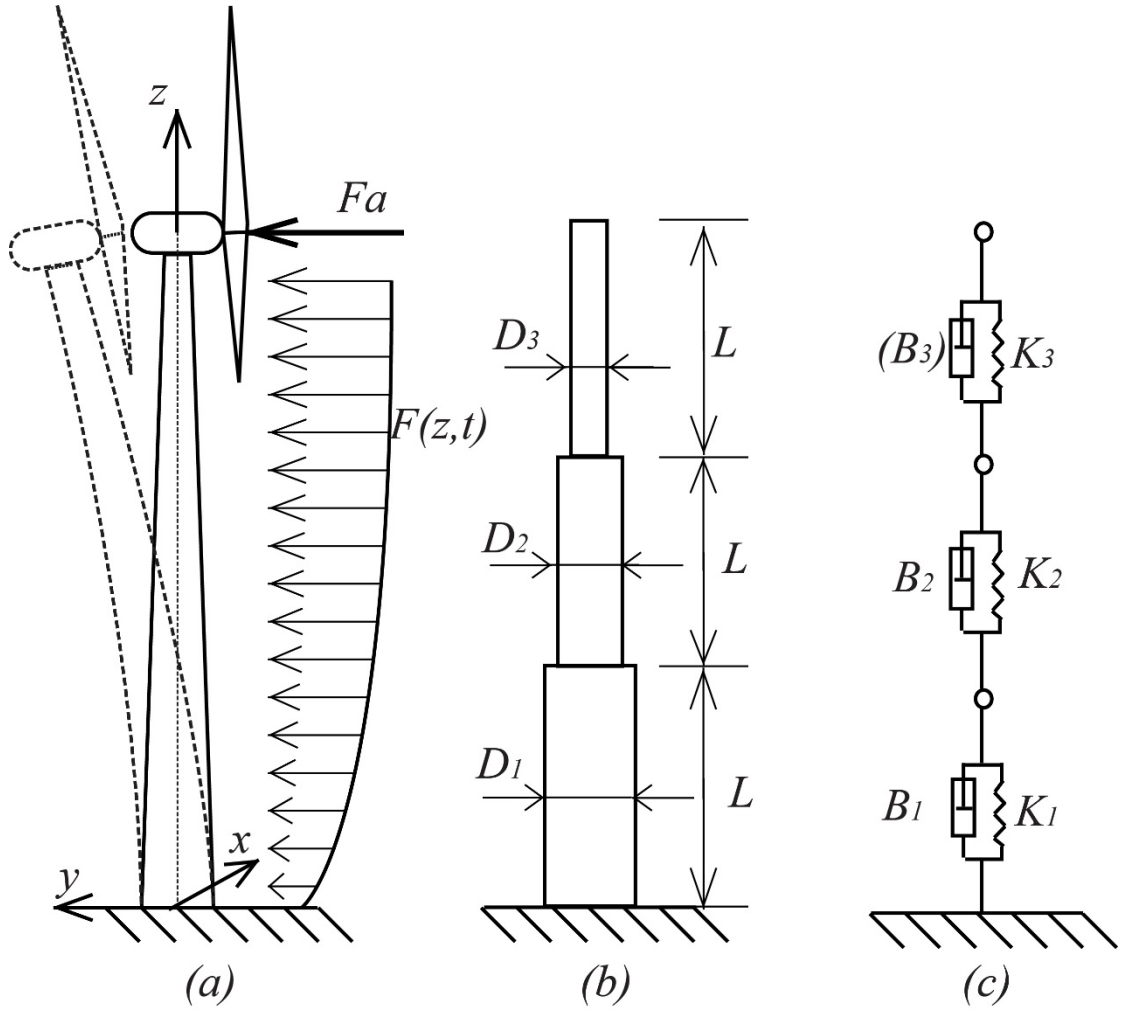

Figure 4.8. Rayleigh beam model of the tower (a), analyzing model of the tower (b), dynamic model of the tower (c)

The stiffness of the beam element relates the generalized Newtonian forces to the generalized displacements at the ends of the element as given by (Eq18):

$$\begin{bmatrix} F_{yi} \\ M_{zi} \\ F_{yi+1} \\ M_{zi+1} \end{bmatrix} = [K_{fyi}] \begin{bmatrix} y_i \\ \theta_{zi} \\ y_{i+1} \\ \theta_{zi+1} \end{bmatrix} \tag{4.5}$$

With

$$[K_{fyi}] = \frac{E(I_{zi-1} + I_{zi})}{\left(l_{i-1} + \frac{l_i}{2}\right)^3} \begin{bmatrix} 12 & 6(l_{i-1} + l_i/2) & -12 & 6(l_{i-1} + l_i/2) \\ 6(l_{i-1} + l_i/2) & 4(l_{i-1} + l_i/2)^2 & -6(l_{i-1} + l_i/2) & 2(l_{i-1} + l_i/2)^2 \\ -12 & -6(l_{i-1} + l_i/2) & 12 & -6(l_{i-1} + l_i/2) \\ 6(l_{i-1} + l_i/2) & 2(l_{i-1} + l_i/2)^2 & -6(l_{i-1} + l_i/2) & 4(l_{i-1} + l_i/2)^2 \end{bmatrix} \tag{4.6}$$

Where E the Young module of the material, and Izi the second moment of area about the axis of deflection. The structural damping matrix is given by: $[R_i] = \mu[K_i]$

where the μ factor represents the structural damping coefficient. The Bond Graph model and sub-model of the tower is shown in Fig. 4.9. We assume tower movement only in horizontal direction.

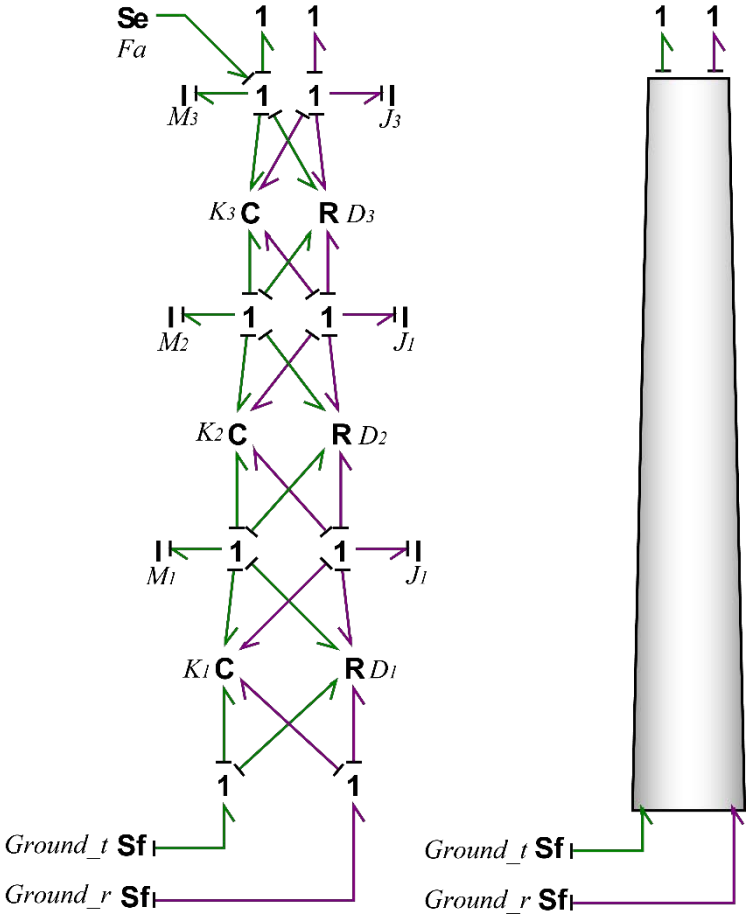

Figure 4.9. Bond graph model of the tower

Boundary conditions of the model are represented by the S_f source. The tower-base is fixed on the ground, i.e. $S_f = 0$. Connection between the tower-top and the hub for the axial deformation is ensured by the 1-junction. It is assumed that the tower movement will influence the wind speed of the aerodynamic subsystem input.

Bond Graph Model of the Wind Turbine Gearbox.

Gearbox is used in the WECSs to increase the angular velocity. It is the most important part of a wind turbine, where most of faults occur. In [17] it is reported that a wind turbine has around 20 years of life span, but normally the gearbox needs to be replaced every 5 years. For this reason, big manufacturing companies of wind turbines intend to use a direct drive wind turbine without a gearbox.

Nowadays, most of the installed wind turbines are equipped with a gearbox. Actually, most of the 270 GW of wind turbine power is installed around the world with this configuration [19]. Based on this context, a model of the gearbox is presented in this paper. In terms of a Bond Graph Approach, The Bond Graph model of a gearbox has been addressed in several works [20; 21]. The gearbox can be considered as a simple model in which the conversion ratio Np/Ng, where Np is the teeth number of pinion and Ng the teeth number of gears) can be introduced directly in a transformer (TFelement of bond graph). However this model does not describe the dynamic behavior of the gearbox. Therefore, a more accurate model needs to be developed. This model will be used in a future work as a base, in order to formulate the law control to compensate any perturbation due to a gearbox default.

Wind turbine's gearbox consists of three stages. The first one is a planetary gear and the two others are parallel gears. The gearbox scheme is shown in Fig. 4.10.

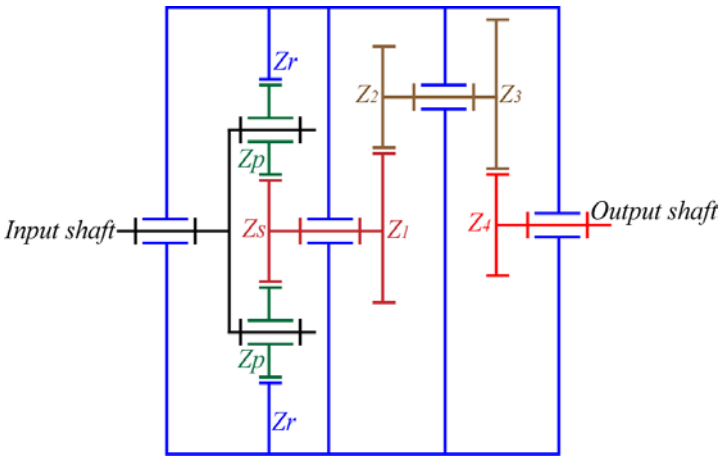

Figure 4.10. Gearbox scheme

In [22] a detailed gearbox Bond Graph model is proposed. The planetary gear model is presented in detail but the parallel stage is modeled by a simple TF element. This resource is taken as a reference to develop the wind turbine gearbox model, to which we add a detailed model of parallel gear stage. Moreover, the dampers of all components of the system are also considered.

For a planetary gear, several identical planet p gears are in mesh with the sun gear and the ring gear r, and the carrier c holds all of the planet gears. Planet gears rotate in two kinematic modes called revolution around the sun gear and autorotation around its own axis.

Power flow into the planetary gear will split or converge. A basic kinematic model of a single planetary gear is shown in Fig. 4.11.

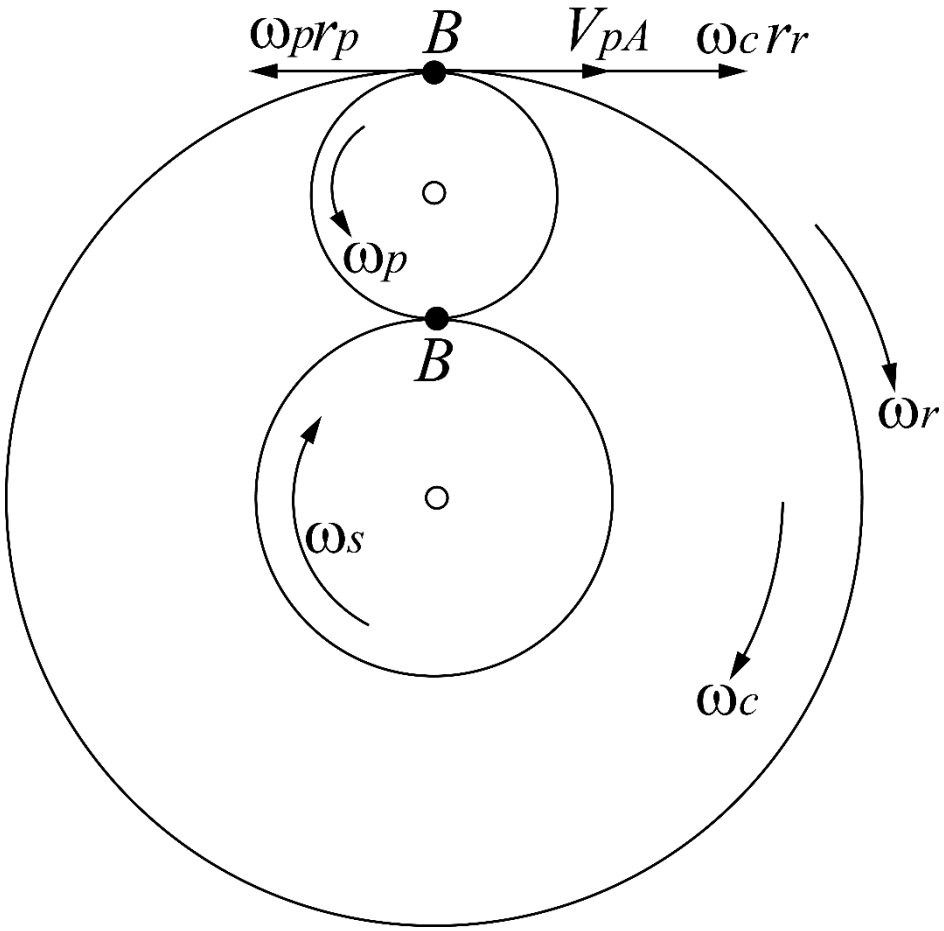

Figure 4.11. Kinematic model of planetary gearbox

According to the kinematic relation of the components shown in Fig. 21, the translation velocities in contact point A and B can be described as follows:

$$V_{pA} = -\omega_p r_p + \omega_c r_r \quad (4.7)$$

$$V_{rA} = \omega_r r_r \quad (4.8)$$

$$V_{pB} = \omega_p r_p + \omega_c r_s \quad (4.9)$$

$$V_{sB} = \omega_s r_s \quad (4.10)$$

Where, ω_j and r_j stand for the rotating velocity and the base circle radius (j = r, s, p) respectively. A is the meshing point of the ring gear and the planet gear, and B is the meshing point of the sun gear and the planet gear. V_{pm} is the velocity of planets in point m along

tangent direction, where m = A, B. Similarly, V_{rA} and V_{sB} are the linear velocities of ring gear in A and sun gear in B.

In a gear system's modeling, the gear mesh interfaces are usually considered as spring-damper systems [23, 24]. The spring stiffness (also called the mesh stiffness), is one of the major sources of gear vibration. The dynamic model of planetary gearbox is shown in Fig. 4.12(a). Fig. 4.12(b) depicts the bond graph model of the gearbox.

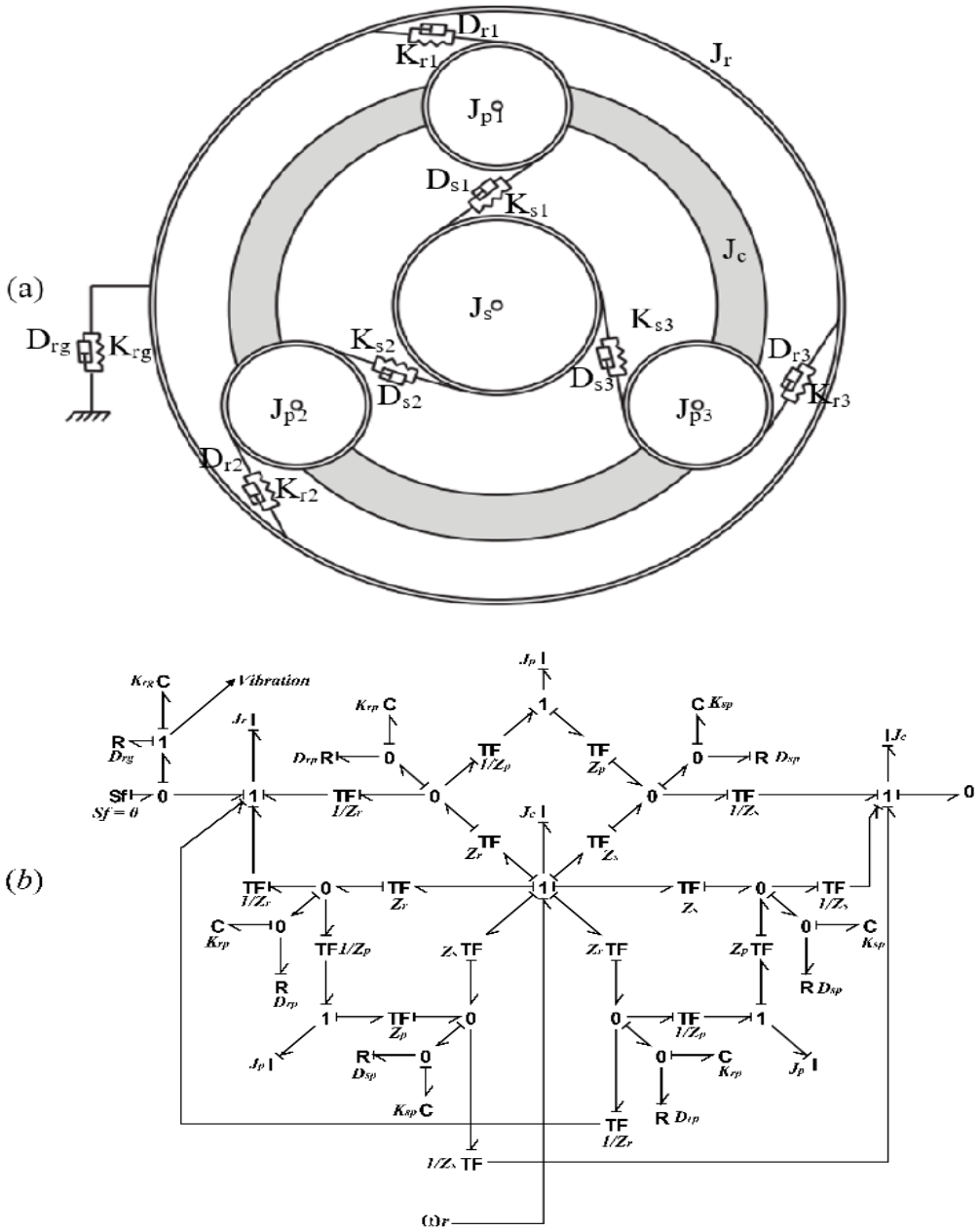

Figure 4.12. Physical model for dynamic meshing problem (a), bond graph model of planetary gearbox (b)

The planet gears represented by momentum of inertia J_{pi} are connected to each other through a common carrier. Therefore, they get the same rotational speed imposed by the carrier. 1-junction represents the rotation speed of the carrier (c), and I-elements J_c denote the rotary inertia of the carrier. These planets are bound to sun and ring gears by the mesh stiffness dumping K_{sp}, B_{sp} and K_{rp}, B_{rp} respectively. J_r is the ring gear's momentum of

inertia. The connection between the ring and the hub is carried out by an elastic joint modeled through a spring-damper. In this joint, the vibration signal of the gear can be obtained. In the model, Z_i (i=p,s,r) represents the teeth number of each gear.

The flow 1-junction represents the angular velocity of planets, carrier, ring and sun gear, respectively. They are related to each other through TF-elements. The zero junctions, between the transformers, represent the effort variable that the planet moves in tangential direction.

The parallel gear stage of the wind turbine gearbox is composed of two stages (Fig. 4.13(a). The dynamic model and the bond graph model are shown in Fig. 4.13(b).

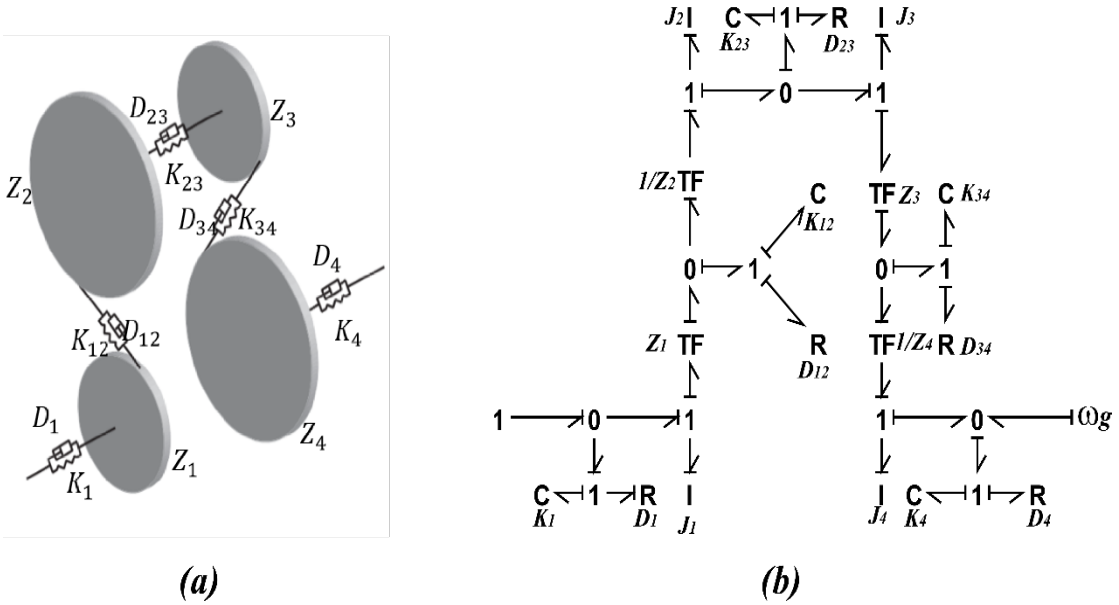

Figure 4.13. Dynamic model of parallel gear (a), Bond graph model of parallel gear (b)

The complete bond graph model of a wind turbine gearbox and its sub-models are depicted in Fig. 4.14.

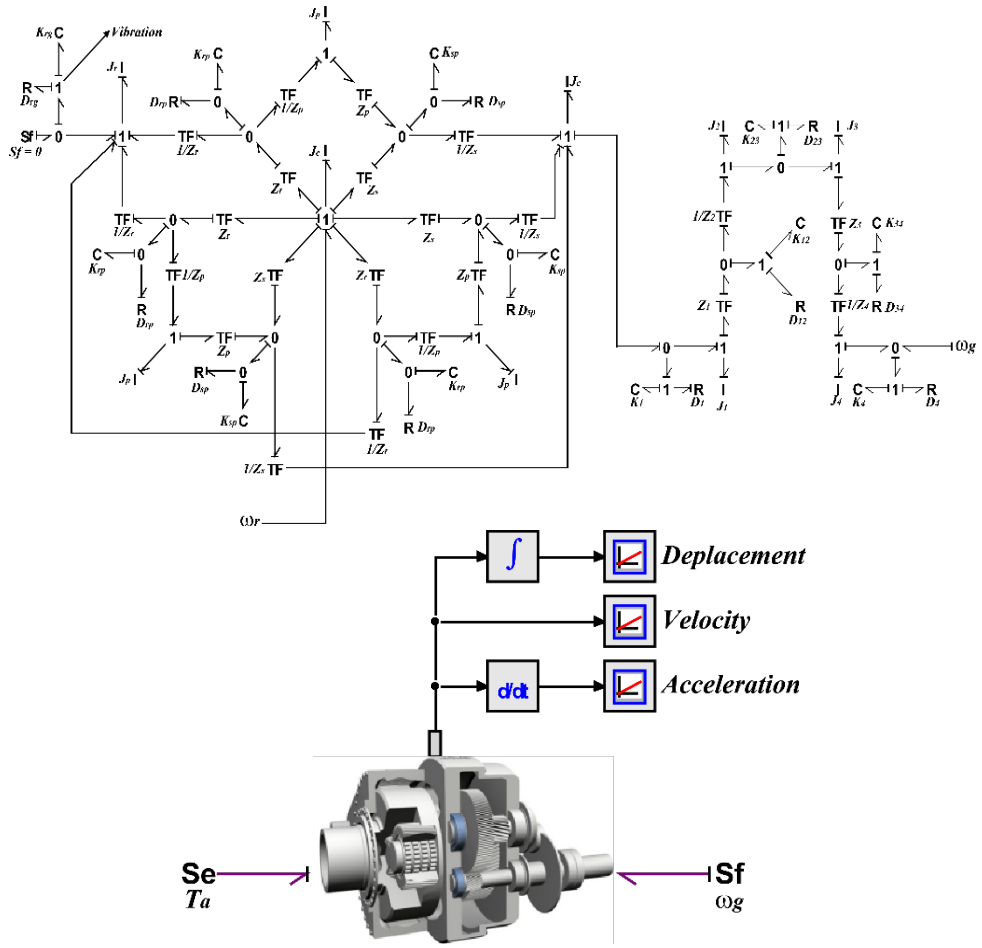

Figure 4.14. Bond graph model and sub-model of a wind turbine gearbox

Fig. 4.15 represents a simulation of the gearbox behaviors. A constant torque is applied at the input of the gearbox (S_e = 60 Nm). This output torque decreases with a ratio of 60. The same outcome is observed in the angular velocity curves. For a constant angular velocity at the gearbox output, the gearbox input is reduced with a ratio of 60. From the teeth number of each gear (Appendix A), we can calculate the gearbox ratio, which is equal to 60. This comes in line with the predictions of the gear's bond graph model.

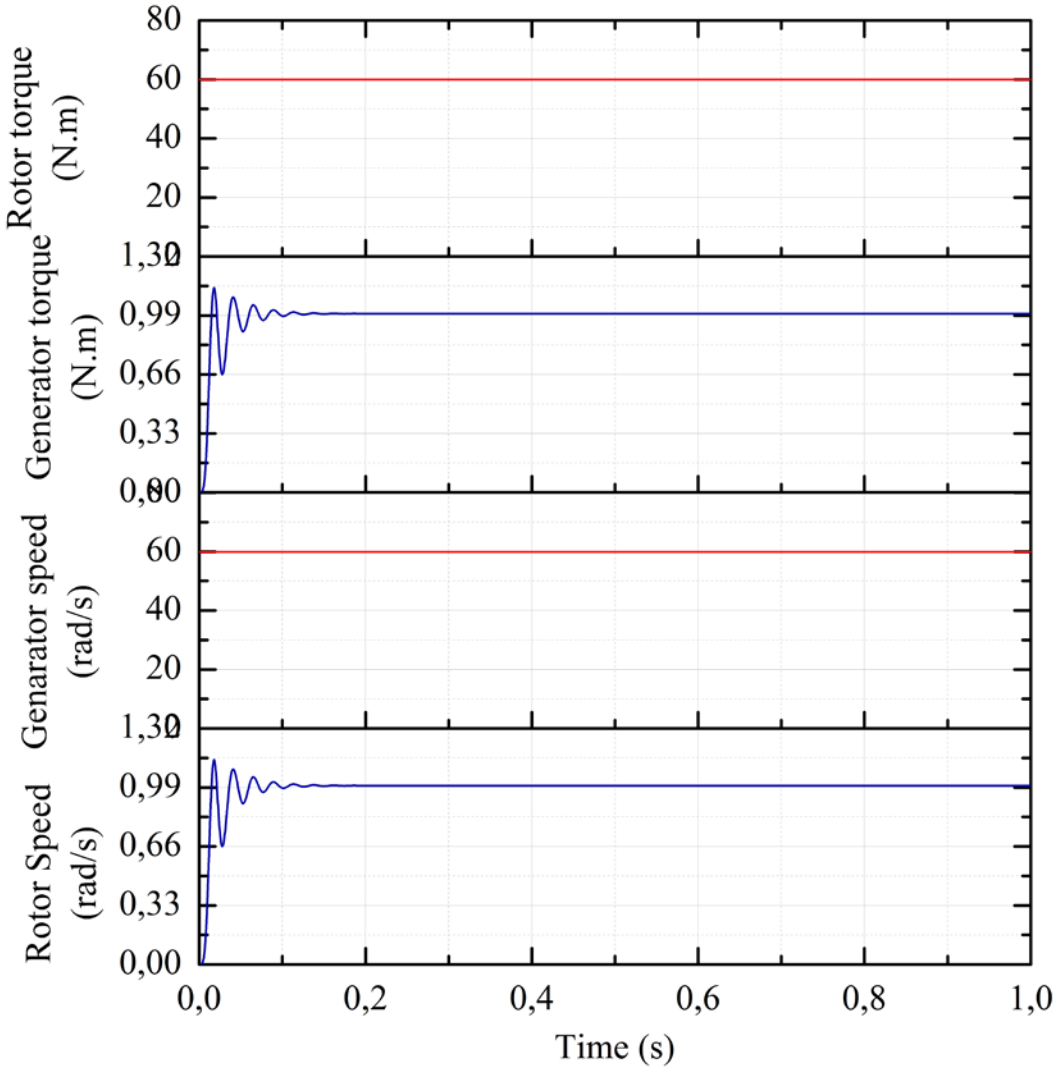

Figure 4.15. Gearbox simulation model

The system undergoes the same vibrations patterns; which are due to the dynamics involved between the mesh stiffness and the momentum of inertias.

The model of the mechanical subsystem of WECS is shown in Fig. 4.16, where all parts of the mechanical subsystems are related by the means of the hub.

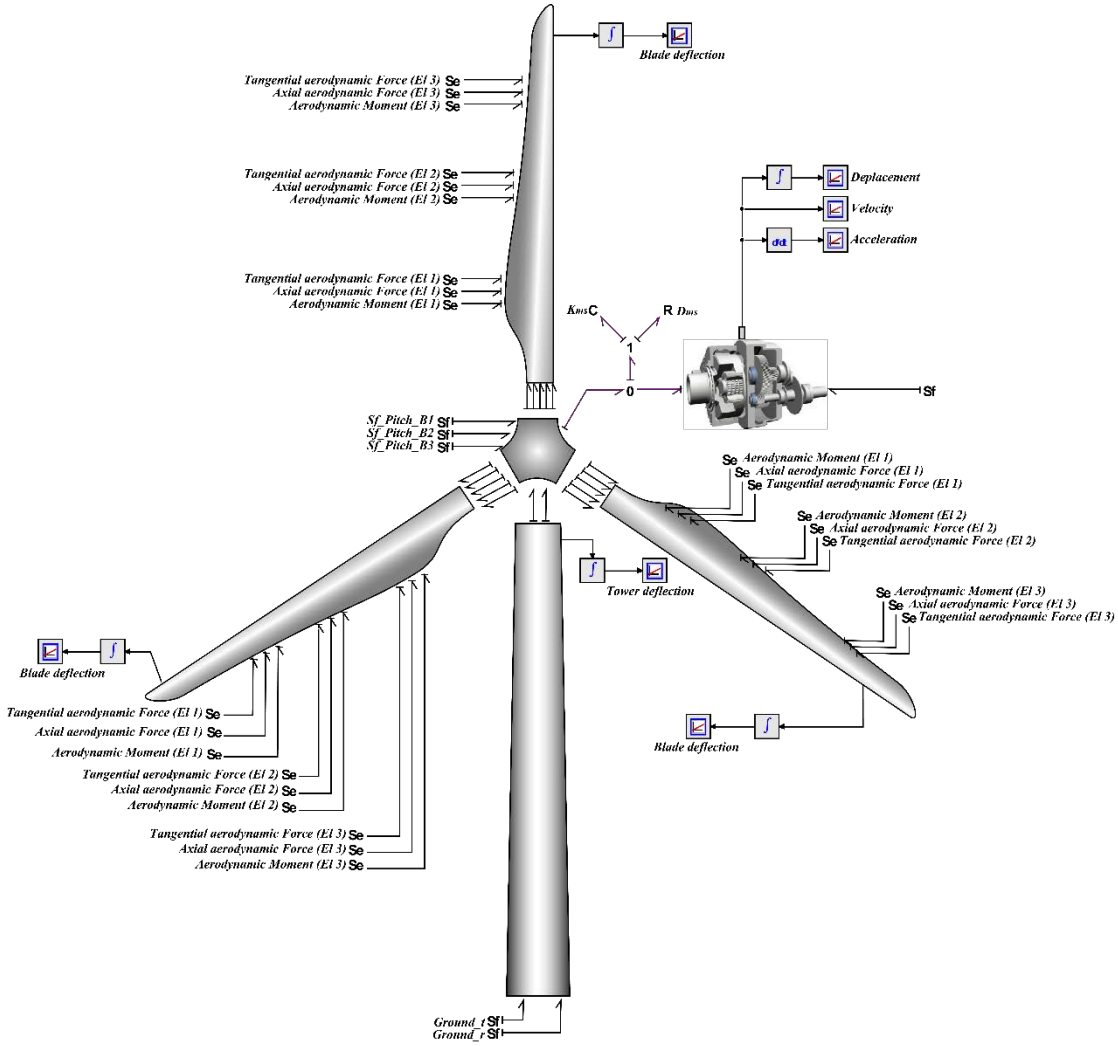

Figure 4.16. The complete model of the mechanical subsystem of WECS

4.2.2. Aerodynamic Subsystem

The aerodynamic subsystem transforms the three-dimensional wind field into lumped forces acting on the rotor blades. As observed in the block diagram of Fig 1, the inputs to the aerodynamic subsystem are the wind speed V, the pitch angle β, the rotational and axial speeds of the rotor Ω_r and the axial displacement of the blades caused by flapping and tower bending $\dot{y}_b$, respectively. Its outputs are the aerodynamic torque T_r (tangential force F_r), the thrust force F_T and the aerodynamic moment.

Wind turbine aerodynamic models are used to relate wind inflow conditions to the loads applied to the turbine. The subsequent analysis develops the most common aerodynamics theory employed in the wind turbine design and analysis environment. It corresponds to the Blade Element Momentum theory (BEM). Extensive literature deals with the BEM theory explanation and presentation [25, 26].

The BEM Theory combines two methods of examining how a wind turbine operates. The first method uses a momentum balance on a rotating annular stream tube passing through a turbine. Axial Thrust dF_T and Tangential Force dF_r -in terms of flow parameters, are:

$$dF_T = 4a(1-a)\rho V^2 \pi r dr \tag{4.11}$$

$$dF_r = 4a'(1-a)\rho V \Omega_r \pi r^2 dr \tag{4.12}$$

Where V represents the wind velocity, ρ the air density, a the axial induction factor, a' the angular induction factor, Ω_r the angular velocity of the blades, and r is the radius of an annular element, having a thickness dr.

The second method is to examine the forces generated by the airfoil lift and drag coefficients at various sections along the blade. Axial Force, Tangential Force and Aerodynamic Moment - in terms of the lift, the drag and the pitching moment coefficients of the airfoil, are as follows:

$$dF_T = \frac{1}{2}\rho \frac{V^2(1-a)^2}{\sin^2\phi}(C_L\cos\phi + C_D\sin\phi)cdr \tag{4.13}$$

$$dF_r = \frac{1}{2}\rho \frac{V^2(1-a)^2}{\sin^2\phi}(C_L\sin\phi - C_D\cos\phi)cdr \tag{4.14}$$

$$dM_x = \frac{1}{2}\rho \frac{V^2(1-a)^2}{\sin^2\phi}[C_m c + y_G(C_L\cos\phi + C_D\sin\phi) - (z_G - z_a)(C_L\sin\phi - C_D\cos\phi)]cdr \tag{4.15}$$

$$\phi = \tan^{-1}\left(\frac{V(1-a)}{\Omega_r r(1+a')}\right) \tag{4.16}$$

Where c is the chord length of the blade element, the wind inflow angle, ϕ is the angle between the local flow direction and the rotor plane (Eq4.19), parameters involved in these expressions are graphically represented in Fig. 4.17(a). (y_G, z_G) are the center of gravity coordinates, z_a: the aerodynamic center's coordinate, as shown in Fig. 4.17(b).

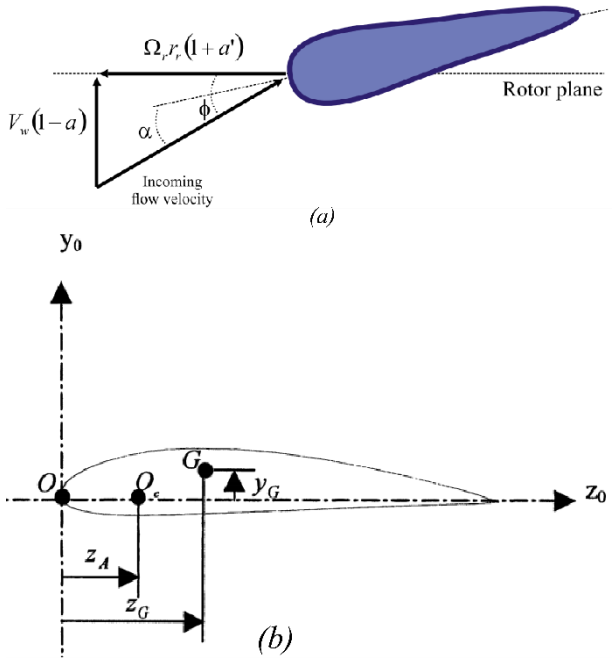

Figure 4.17. Velocities at rotor plane (a), Center of gravity coordinates and the aerodynamic center (b)

C_L, C_D and C_m are lift, drag and pitching moment dimensionless coefficients respectively as functions of the angle of attack (known also as leading angle) α. Lift, Drag and Pitching moment coefficients for a NACA 4415 airfoil are shown in Fig. 4.18. This graph indicates that for low values of incidence angle, the airfoil successfully produces a large amount of lift with little drag.

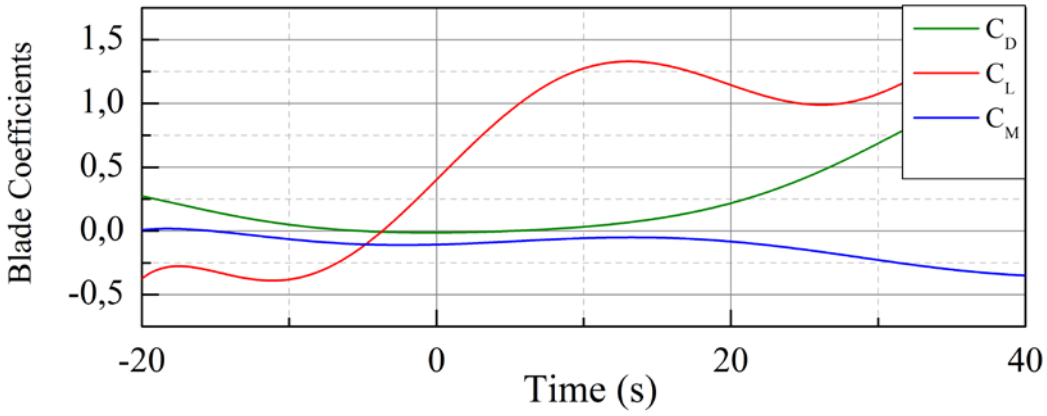

Figure 4.18. Lift, Drag and pitching moment Coefficients for a NACA

Equations (Eq4.25) and (Eq4.27) are used to calculate the axial induction:

$$a = \left(1 + \frac{4\sin^2\phi}{\sigma'(C_L\cos\phi + C_D\sin\phi)}\right)^{-1} \tag{4.17}$$

Equations (4.15) and (4.17) are used to calculate the tangential induction factor:

$$a' = \left(-1 + \frac{4\sin\phi\cos\phi}{\sigma'(C_L\sin\phi - C_D\cos\phi)}\right)^{-1} \tag{4.18}$$

Solution for a given blade cannot be found directly from the equations but an iterative method is required to calculate the axial induction factor, the tangential induction factor, angles of attack and thrust coefficients for each section along the span of the blade. It is composed of the following steps:

Estimate the initial value of the axial induction factor a_i and the tangential induction a'_i relative to the i^{th} blade element.

An efficient technique (among others) is to assume that the inflow angle is small: $\sin\phi_i \approx \phi_i$. The tangential induction a'_i and the drag coefficient C_{Di} are null. The lift coefficient is $C_{Li} = 2\pi\alpha_i$, where the angle of attack is $\alpha_i = \phi_i - \beta_i$, with β_i the sum of the twist angle β_i depending on the position of the center of gravity of the i^{th} section and the pitch angle β which is an input control variable.

After some rearranging, it yields to:

$$a_i = \frac{1}{4}\left(2 + \pi\lambda_{ri}\sigma'_i - \sqrt{4 - 4\pi\lambda_{ri}\sigma'_i + \pi\lambda_{ri}^2\sigma'_i(8\beta_i + \pi\sigma'_i)}\right) \tag{4.19}$$

With: $\lambda_{ri} = \frac{\Omega_r r_i}{V}$ is the local speed ratio and $\sigma'_i = \frac{c_i}{2\pi r_i}$ is the local solidity, calculated using chord values c_i depending on r_i (Appendix A).

Use the initial value of a_i and a'_i to calculate ϕ_i.

$$\phi_i = \tan^{-1}\left(\frac{V(1 - a_i)}{\Omega_r r_i(1 + a'_i)}\right) \tag{4.20}$$

Calculate incidence angle α_i and then C_{Li} and C_{Di} using look-up tables (Fig 20)

$$\alpha_i = \phi_i - \beta_i \tag{4.21}$$

Calculate new values of a_i and a'_i using the following Equations :

$$a_i = \left(1 + \frac{4\sin^2\phi_i}{\sigma'_i(C_{Li}\cos\phi_i + C_{Di}\sin\phi_i)}\right)^{-1} \tag{4.22}$$

$$a'_i = \left(-1 + \frac{4\sin\phi_i\cos\phi_i}{\sigma'_i(C_{Li}\sin\phi_i - C_{Di}\cos\phi_i)}\right)^{-1} \tag{4.23}$$

In this process iterations are carried out until the values of induction factors and inflow angle converge to their final values, and then we can calculate the axial force and the tangential force for each section along the blade by:

$$F_{Ti} = \frac{1}{2}\rho \frac{V^2(1-a_i)^2}{\sin^2\phi_i}(C_{Li}\cos\phi_i + C_{Di}\sin\phi_i)c_i l_i \tag{4.24}$$

$$F_{ri} = \frac{1}{2}\rho \frac{V^2(1-a_i)^2}{\sin^2\phi_i}(C_{Li}\sin\phi_i - C_{Di}\cos\phi_i)c_i l_i \tag{4.25}$$

$$M_{xi} = \frac{1}{2}\rho \frac{V^2(1-a_i)^2}{\sin^2\phi_i}[C_{mi}c_i + y_{Gi}(C_{Li}\cos\phi_i + C_{Di}\sin\phi_i) - (z_{Gi} - z_{ai})(C_{Li}\sin\phi_i - C_{Di}\cos\phi_i)]c_i l_i \tag{4.26}$$

The fundamental aerodynamic theory used by the bond graph model is presented in this work. An MGY-element of bond graph is used to implement equations (Eq4.32) through (Eq4.39), with wind flow (MS_f source) being transformed into aerodynamic forces (S_e source), as shown in Fig. 4.19.

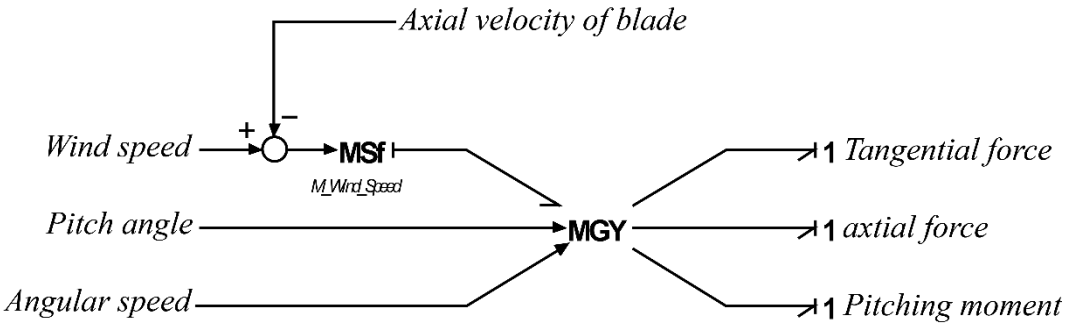

Figure 4.19. Bond graph model of the aerodynamic subsystem

Modulated inputs to MGY elements of Fig. 4.19 are the pitch angle β, the angular velocity Ω_r, and the wind speed V and the axial displacement of the blades caused by flapping and tower bending. In order to simulate the blade model, equations (4.22) through (4.29) are integrated within each MGY element; which means that their traditionally constitutive relation is changed.

The non-dimensional power coefficient C_p represents the fraction of available power in the wind that is extracted by the turbine. It can be rewritten as:

$$C_p = 4a(1-a)^2 \tag{4.27}$$

The theoretical maximum power coefficient from an idealized rotor C_{pmax}, known as Betz limit, can be found by setting the derivative of C_p with respect to a equal to zero, which

leads to : a=1/3 and $5\,C_{pmax} = 0.596$ which corresponds to the maximum possible efficiency for an idealized wind turbine of 59.6%.

Fig. 4.20 shows the values of C_p, the simulation program calculates C_p as:

$$C_p = \frac{F_r * R * \Omega_r}{\frac{1}{2}\rho\pi R^2 V^3} \tag{4.28}$$

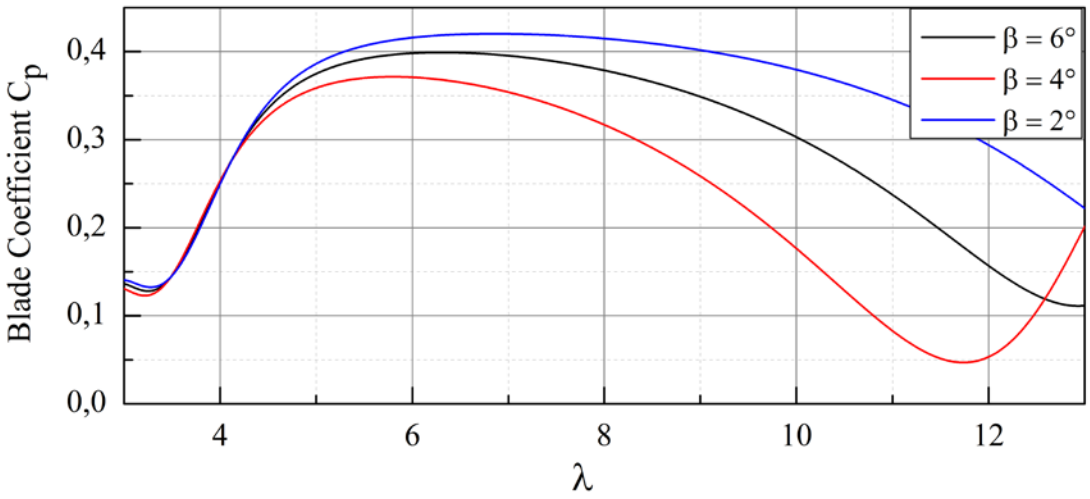

Figure 4.20. Curve of C_p vs λ

From the figure the maximum values of C_p is 0.42, having a tip speed of 7; the theoretical maximum value of C_p is 0.596, known as Betz limit, at around a tip speed of 8. In practical designs, the maximum achievable C_p is below 0.5. The difference to standard values is acceptable and it is better that the value shown in [15] (around 0.33). This simulation confirms that dynamical model of the blade + hub + main bearing adequately performs.

4.2.3. Electrical Subsystem

Energy is basically produced in mechanical form and consumed in electrical form. The Induction generators are largely the most popular electric machines in WECS industry to convert mechanical power to electric power through the medium of magnetics. Thus, a multi-domain energy exchange in an induction machine takes always place. This increases the complexity of modeling an induction machine. Therefore, for an efficient control of the mechanical-magnetic-electric energy, the induction machine has to be accurately modeled [27].

Induction machines have been addressed in many publications. There are two general frameworks models: one using a Park reference frame [28] and the other using the natural reference frame (three sinusoidal waveforms) [29]. An induction machine bond graph model in the natural reference frame is sketched in Fig. 4.21.

Induction machines have been addressed in many publications. There are two general frameworks models: one using a Park reference frame [28] and the other using the natural reference frame (three sinusoidal waveforms) [29]. An induction machine bond graph model

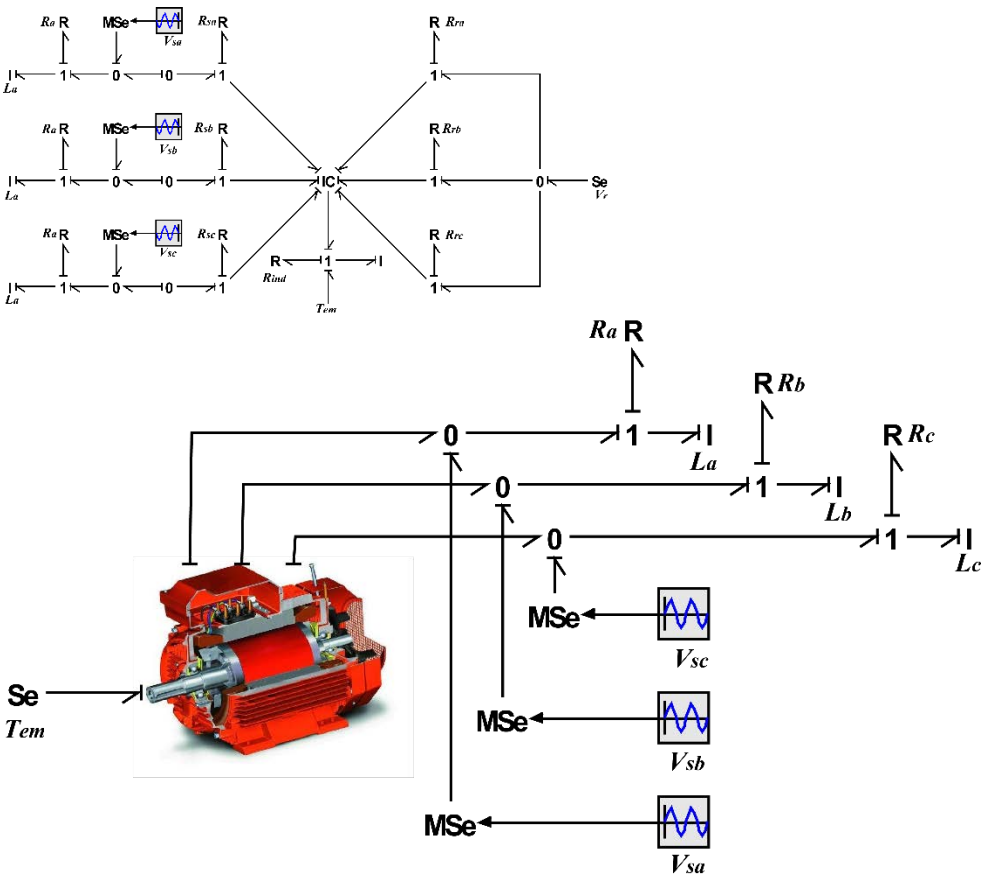

Figure 4.21. Bond graph model and sub-model of the induction machine

in the natural reference frame is sketched in Fig. 4.21.

The assumptions considered for the induction machine model are:

- Magnetic hysteresis and magnetic saturation effects are neglected.
- The stator windings are sine-wave-distributed throughout the air–gap.
- The stator slots cause no appreciable variation of the rotor inductances with respect to the rotor position.

Fig 4.21 model explicitly shows the three phases of stator and rotor. The phase 'a' stator input voltages is represented by a modulated effort source (MS_e= Vsa). Coil resistance translating the losses of phase 'a' is represented by R-field, IS

$$\begin{pmatrix}\phi_{a,b,cs}\\ \phi_{a,b,cr}\end{pmatrix}=\begin{pmatrix}L_S & L_S\\ L_M^T & L_R\end{pmatrix}\begin{pmatrix}i_{a,b,cs}\\ i_{a,b,cr}\end{pmatrix} \tag{4.29}$$

Where,

$$L_S = \begin{pmatrix} L_{IS} + L_{MS} & -\frac{1}{2}L_{MS} & -\frac{1}{2}L_{MS} \\ -\frac{1}{2}L_{MS} & L_{IS} + L_{MS} & -\frac{1}{2}L_{MS} \\ -\frac{1}{2}L_{MS} & -\frac{1}{2}L_{MS} & L_{IS} + L_{MS} \end{pmatrix} \quad (4.30)$$

$$L_R = \begin{pmatrix} L_{IR} + L_{MR} & -\frac{1}{2}L_{MR} & -\frac{1}{2}L_{MR} \\ -\frac{1}{2}L_{MR} & L_{IS} + L_{MR} & -\frac{1}{2}L_{MR} \\ -\frac{1}{2}L_{MR} & -\frac{1}{2}L_{MR} & L_{IR} + L_{MR} \end{pmatrix} \quad (4.31)$$

$$L_M = L_{SR} \begin{pmatrix} \cos(\theta) & \cos(\theta - \frac{2\pi}{3}) & \cos(\theta + \frac{2\pi}{3}) \\ \cos(\theta + \frac{2\pi}{3}) & \cos(\theta) & \cos(\theta - \frac{2\pi}{3}) \\ \cos(\theta - \frac{2\pi}{3}) & \cos(\theta + \frac{2\pi}{3}) & \cos(\theta) \end{pmatrix} \quad (4.32)$$

The IC-port field is used because the equation (4.35) contains sine and cosine relations, which are necessary to calculate the rotor position θ_m(Equation (4.12)). This means that the speed machine is integrated in order to calculate θ_m.

At the shaft level, the developed electromagnetic torque (expression (4.36)) as a function of the stator, rotor currents and the angle between them is represented in the IC-port output. The electromagnetic torque T_e is consumed at the 1-junction by the inertial moment J_{ind}, frictional and mechanical torque T (which, in this case, will be provided by output gearbox stage). The information flow at this junction, which gives the rotor speed value, is transmitted to the Axis Rotor for calculating the instantaneous angle of the rotor windings. Equation (4.37) shows the mechanical part expression.

$$T_e = (i_{sa} \quad i_{sb} \quad i_{sc}) * \frac{d}{d\theta_m}(L_M(\theta_m))_{3\times3} * \begin{pmatrix} i_{ra} \\ i_{rb} \\ i_{rc} \end{pmatrix} * p \quad (4.33)$$

$$J_{ind}\frac{d}{dt}\Omega_m = T_e - T \quad (4.34)$$

A simulation is conducted to check out the model's behavior. In order to allow a direct electrical network connection, an RL element, used as a load, is connected in series between the generator and the three-phase power network. Appendix A contains the complete set of parameters.

Stator currents curves and speed rotor are shown in Fig. 4.22. The goal is to show that the model works as expected. In the next section, it will be connected as a generator having a negative torque.

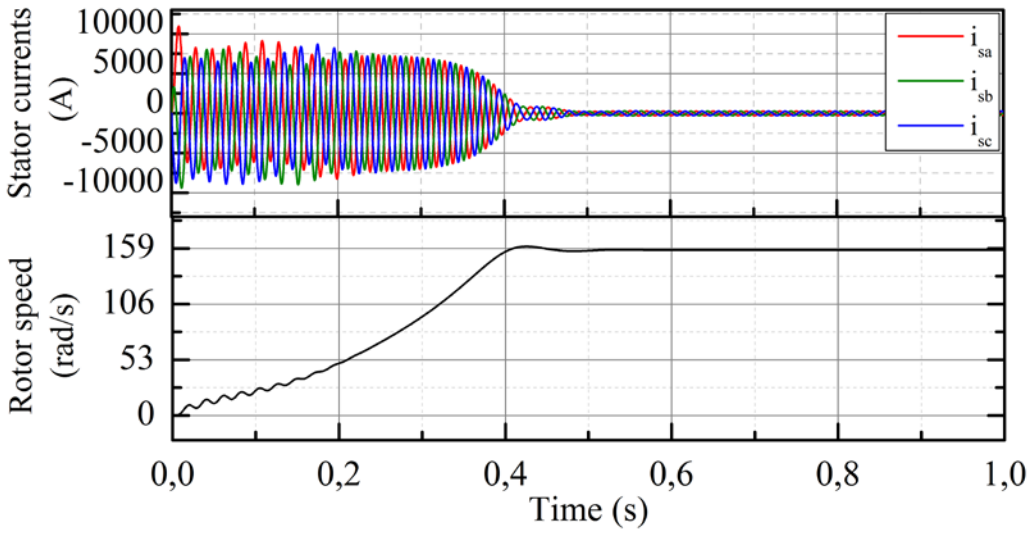

Figure. 4.22. Stator currents forms and speed rotor simulation

4.2.4. Pitching Subsystem

In WECS, one of the operational problems is the variability and discontinuity of wind. In most cases, wind speed can fluctuate rapidly. Hence, quality of produced energy becomes an important problem. Several control techniques have been designed to improve the quality of power generated from wind turbines. Pitch control is the most efficient and popular power control method, especially for variable-speed wind turbines. It is a useful method for power control above the rated wind speed by changing the pitch angle of the rotor blades. The actuator that drives the blades around their longitudinal axes is a hydraulic or electromechanical device. Higher flexibility of these devices enabled the implementation of efficient and reliable model and control strategies for power or speed limitation. The pitch actuator is a nonlinear servo that generally rotates all the blades – or part of them.

Many wind turbines are equipped with controlled electromechanical actuators to adjust the rotor blades. Taking the dynamic characteristics of the pitching system into consideration is crucial, for defining the control strategy and for designing the pitch drive components.

The pitching system of a wind turbine can be divided into four subsystems (Fig. 4.23) [30]. The consideration of the interaction between these systems is essential in order to achieve a correct load calculation for the components of the total system [31].

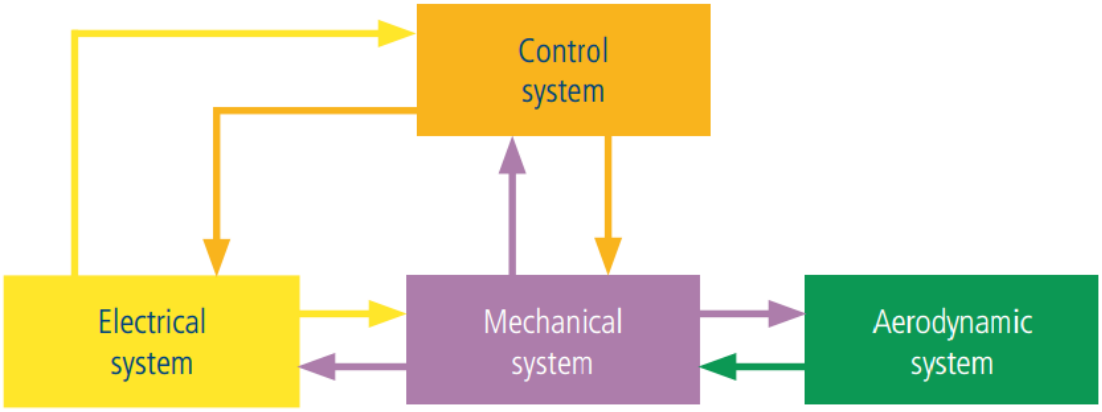

Figure 4.23. Subsystems of the pitching system

The bond graph of the pitching system is depicted in the Fig. 4.24, where the different functional parts of the pitching system are sketched. The mechanical subsystem includes all mechanical components of the pitching system: the inertia of rotor of the electric motor is represented by I-element (J_{rotor}), the friction at the rotor by R-element (B_{rotor}) the transmission elements (gearbox) is represented by TF-element (TF). The rotor blade inertia is represented by I-element (J_{blade}).

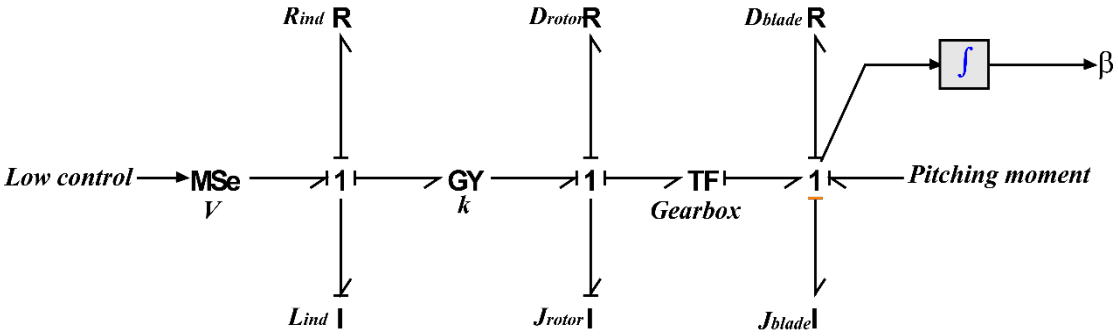

Figure 4.24. Bond graph model of the pitching system

The aerodynamics effort is represented by Se-element that represents the aerodynamic moment applied for each blade elements for which the angle of attack α is calculated by iteration. The used airfoil provides the lift, drag and pitch moment coefficientsC_L, C_D, C_M.. Besides, the pitching moment is determined using equations that were introduced in Aerodynamic Subsystem section.

The electrical subsystem represents the electric motor's behavior. There are many possibilities to model the electric motor with different levels of complexity and accuracy. The detailed method depends on the motor type. In our model, we use a DC motor for controlling the pitch angle. The bond graph model is depicted in the electrical part of Fig. 4.24, where the coil resistance - featuring the rotor losses, is represented by an R-element (Rind) and the motor inductance by an I-element (Lind). Fig. 4.25 shows the bond graph sub-model.

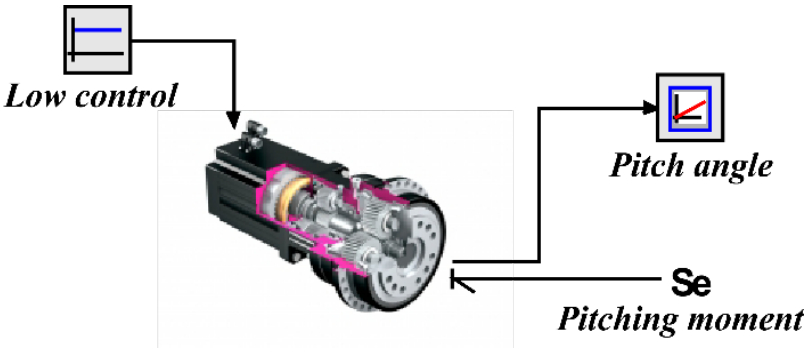

Figure 4.25. Bond graph sub-model of the pitching system

4.2.5. Complete System

The individual subsystems presented in previous sections are combined in a global system as shown in Fig. 4.26. The three inputs of the aerodynamic subsystem are connected by the wind sources, the hub speed and the pitch angle, the latter representing the primitive of the rotation speed at the pitching subsystem's output. The three output forces of the aerodynamic subsystem symbolize the mechanical subsystem's inputs applied on each blade element. Mechanical subsystem's output is the mechanical power, which represents the electrical subsystem's input. The power network connects the output of the electrical subsystem. In order to insure a power exchange, a load is connected between generator and power network. Pitching subsystem's output is connected with the pitching moment model of the mechanical subsystem, and its input is the control law. The different control laws (i.e. pitch, speed and break control.) are not dealt with in this paper. A more detailed model will be presented in a subsequent paper. Actually, some considerations are required to allow the wind turbine to work without pitch control. The assumptions are:

Wind flow never exceeds its nominal values. This allows the wind turbine to operate without pitch control.

A load is connected between the generator and the power network, this yields a power exchange.

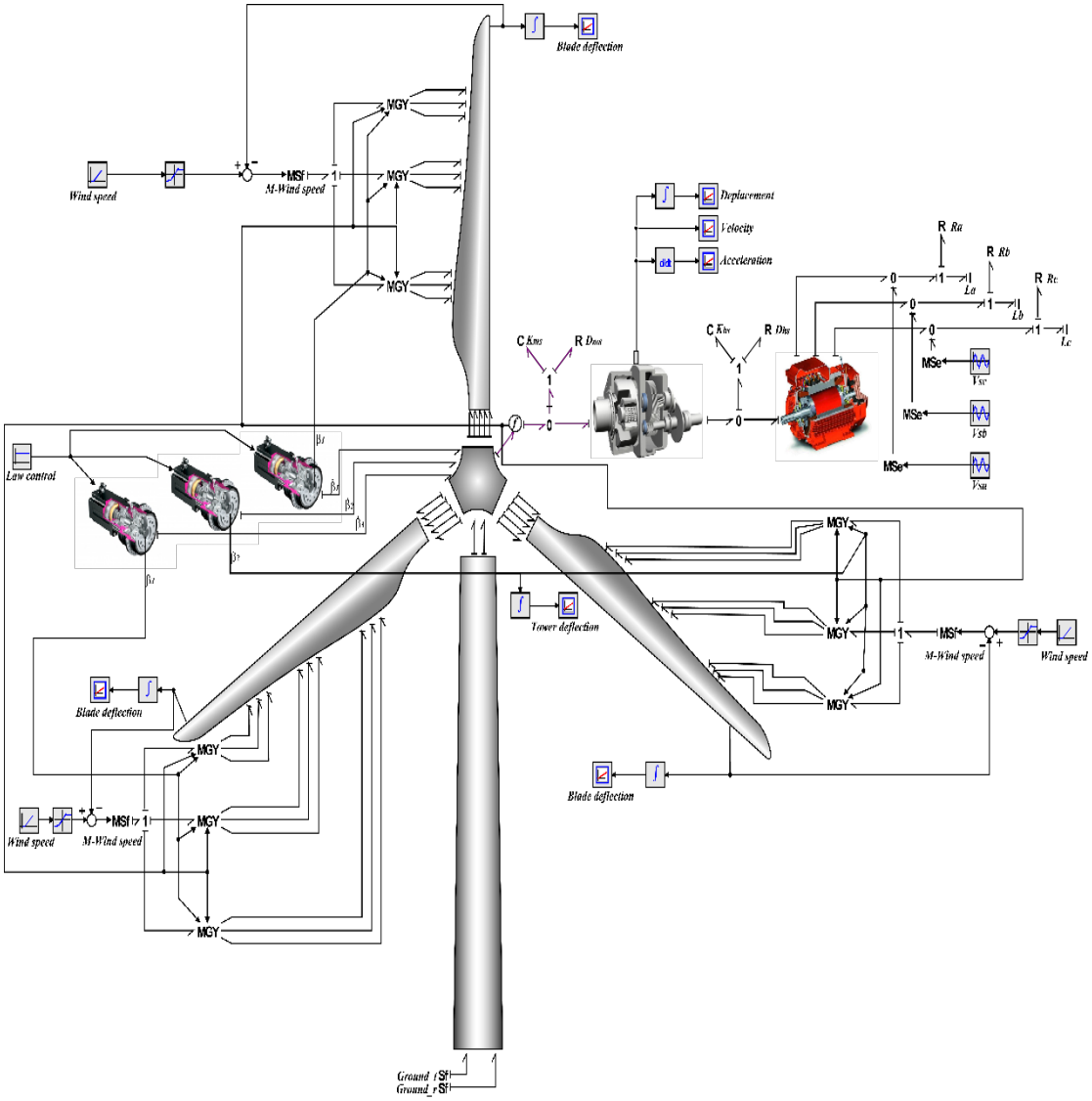

Figure 4.25. Complete Wind turbine model

4.3 . Simulation and discussion.

Besides calculating various parameters of the wind turbine, two different simulations were carried out. A constant and variable wind profile is considered in the time domain in order to analyze the interaction between the different subsystems of the wind turbine. The constant wind simulation scenario is: a constant wind flow of 5 m/s is applied at the simulation start; then, at t=10s, a wind ramp is applied. This wind ramp increases from 5 m/s up to 13 m/s, for t=10s through t= 50 s. This value is maintained until the simulation ends (no control laws are used for the simulation).

The following figures show the simulation scenario of the whole wind turbine conversion system for the constant and variable wind profiles. Fig 4.26 depicts the three aerodynamic forces applied in each one of the blade element's center of gravity, from t=50 s to t=100 s. The tangential aerodynamic forces applied for each elements are: $F_{t1} =$ 1,45 KN; $F_{t2} = 1{,}5$ KN; $F_{t3} = 1{,}2$ KN. And each element's center of gravity position is: $r_1 =$ 3.9 m; $r_2 = 11.7$ m; $r_3 = 19.5$ m. Actually, the rotor torque of the three blades must be: $T_t = 3 * \sum_{i=1}^{3} F_{ti} r_i = 139{,}815$ KNm, which is verified as shown in Fig. 4.27 where the

torque value from t=50 s to t=100 s is: $T_t = 140.067$ KNm. The system undergoes some oscillations in the beginning of the simulation due to the dynamic behaviors of the system in the transient phase. Fig 30 shows also the torque at high shaft, from t=50 s to t=100 s. The high shaft and low torque are respectively: $T_t = 140.067$ KNm, and $T_g = 2.334$ KNm. With these two values, it was proved that a relationship between the high and the low shafts confirms the gearbox's reduction ratio of 60.

A 490 V generator is used as an input of the electrical subsystem. Fig. 4.28 shows the three-phase stator currents.

Wind turbine converts wind power into mechanical power, and into electrical power, and then distributed to the load or to the power network. Fig. 4.29 shows the aerodynamic, mechanical and electrical power in the wind turbine model. The power of the main shaft and the high speed shaft approximately match (740 kW); the generator's active power (733 kW), is close to this value. This difference is due to the lost power in the generator. Fig. 4.30 also shows the conventional values for C_p and λ. Fig. 4.31 sketches the blades, tower deflections, and the gearbox vibration. The maximum deflection of the tower and the blades are respectively 0.2 m and 0.45 m. The latter (whose value is 0.45m) takes into accent the deflection of the tower, because it is assumed that the top of the tower and the bottom of the blade in the axial extension are rigidly connected. Therefore, the actual deflection blade is 0.25 m. (namely 0.45 – 0.2). The vibration amplitude of the gearbox lies between ±0.004 m. These values are acceptable while the proposed wind profile is around its rated value. In the case of the high wind speed, a control system is needed to keep the structure system and the gearbox vibration around its rated values.

The second simulation is carried out using a variable wind speed. Figs. 4.32 through 4.37 show the simulation responses for the generator selected variables. The torque values, C_P, λ and omega are taken to their average values. It is revealed that responses of each stage change with wind speed. In contrast to a constant wind input, currents and power responses also reflect their variability with wind profile. This allows the behavior verification of the proposed model.

This contribution was based on real data for a 750 kW wind turbine. All parameters of the system are reported in appendix A.

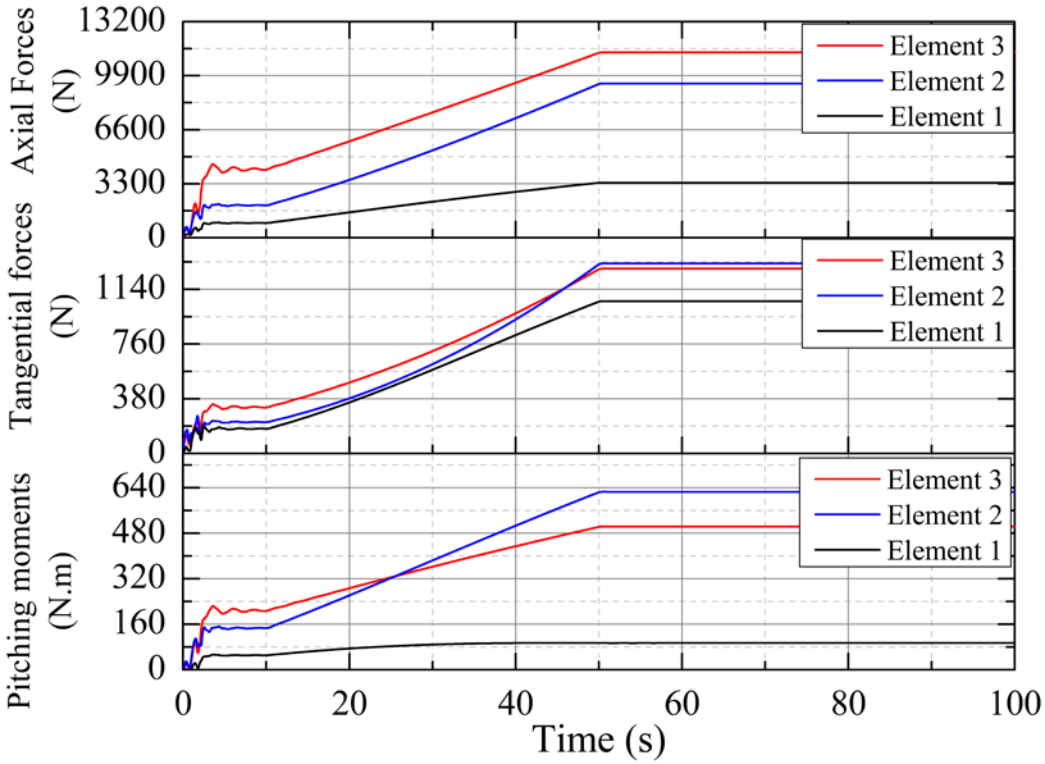

Figure 4.26. Axial and tangential forces and Pitching moment

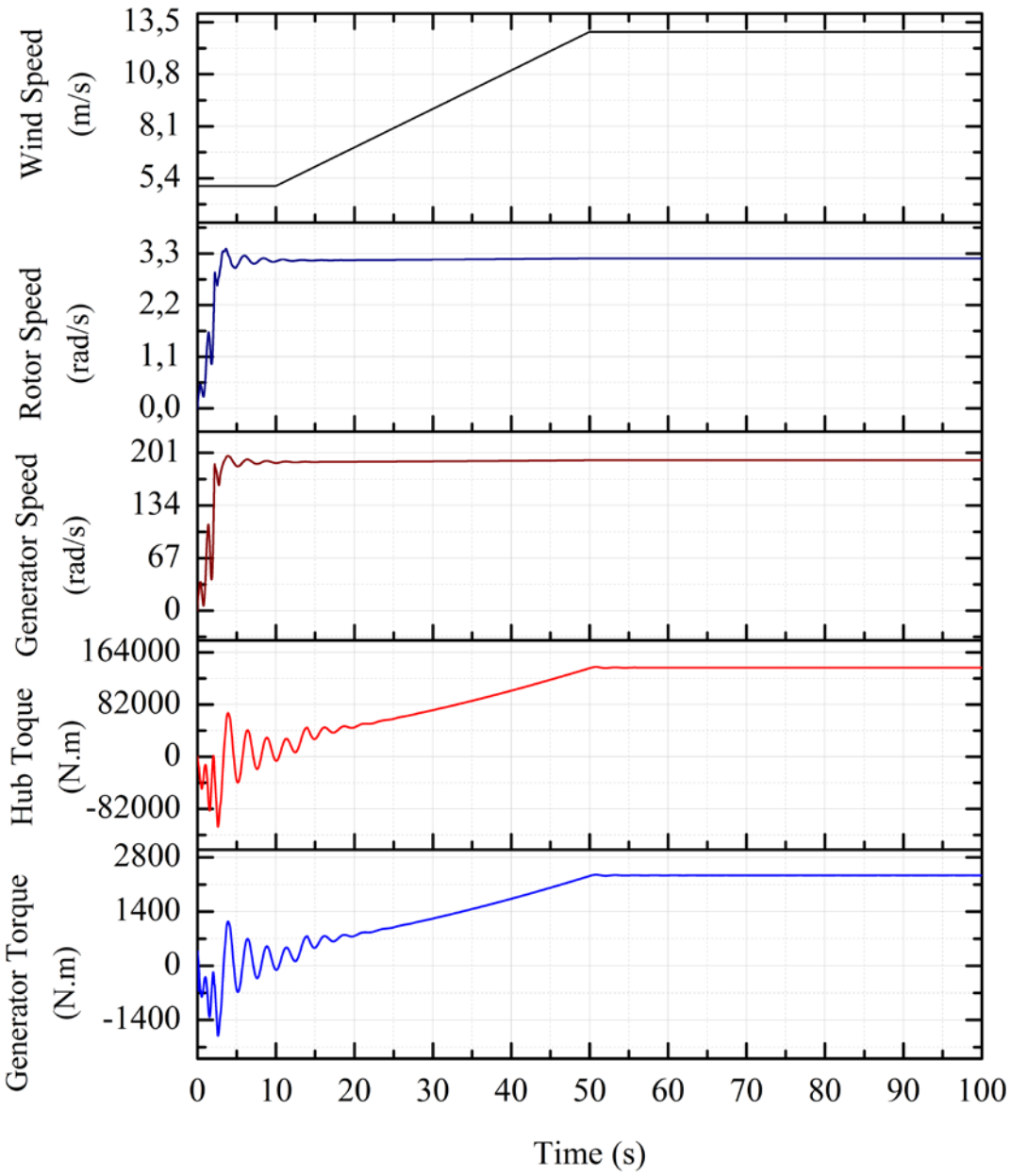

Figure 4.27. Responses for a constant wind

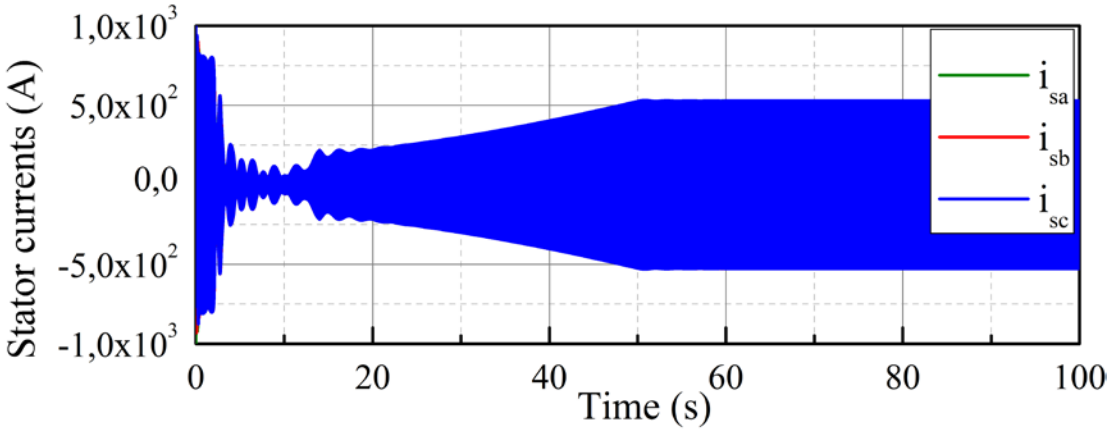

Figure 4.28. Stator currents of generator

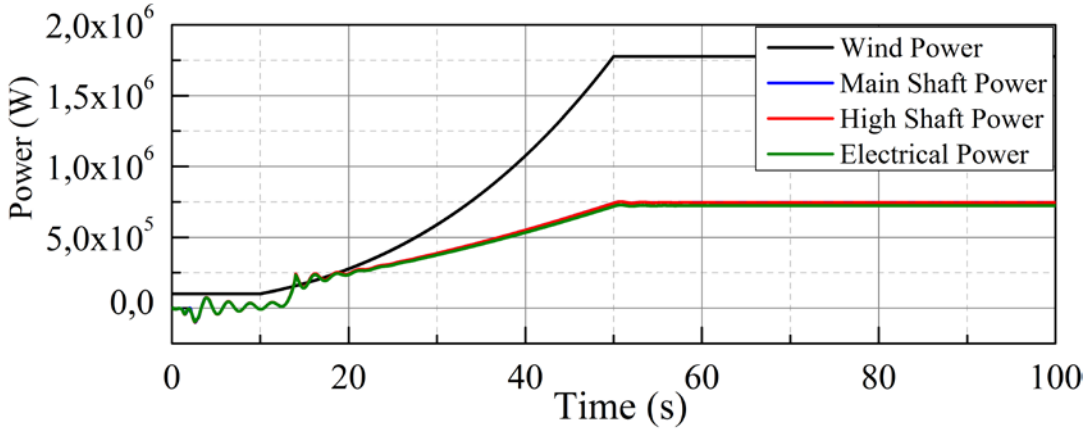

Figure 4.29. Power curves of model

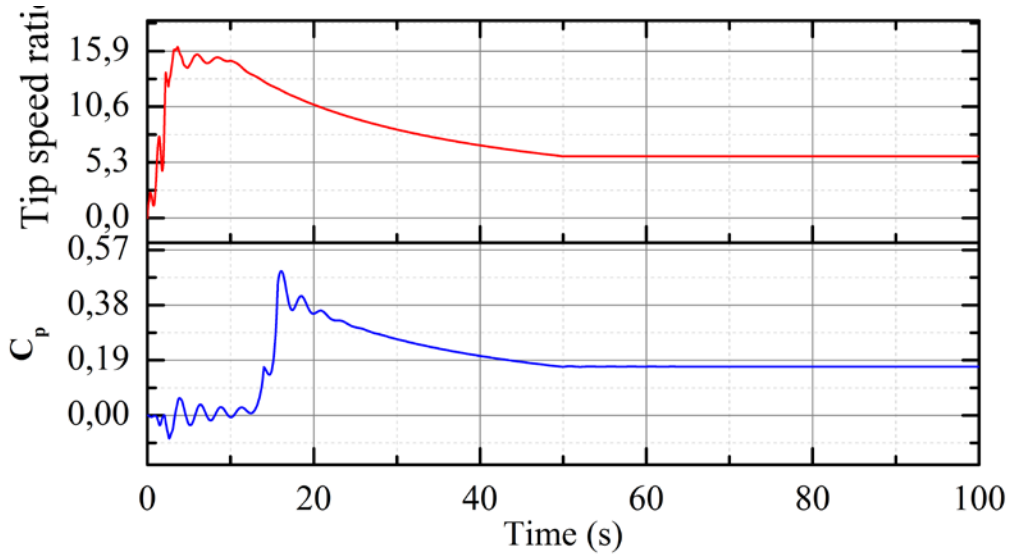

Figure 4.30. Curve C_P and λ

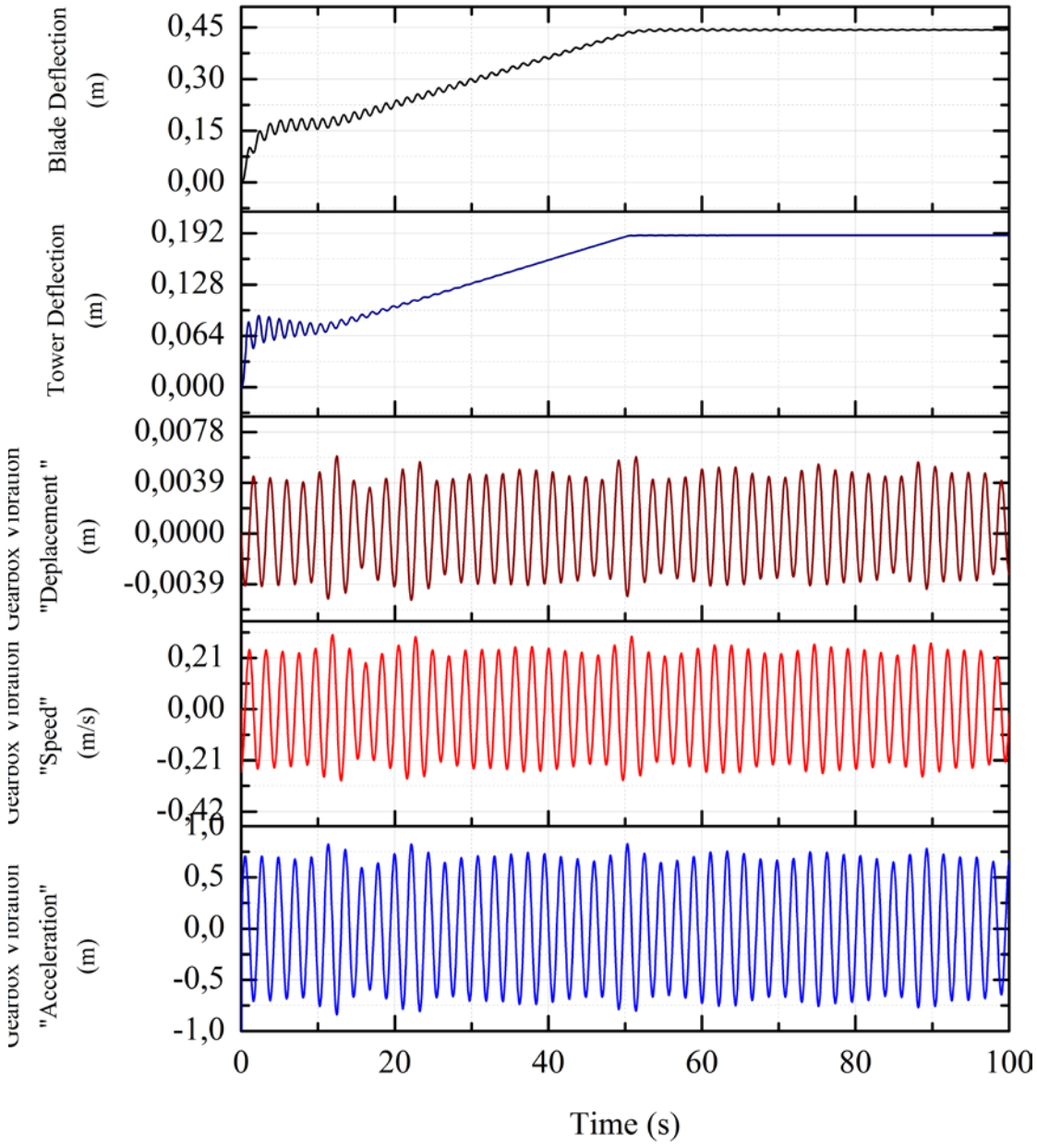

Figure 4.31. Gearbox vibration and Deflection blades and tower

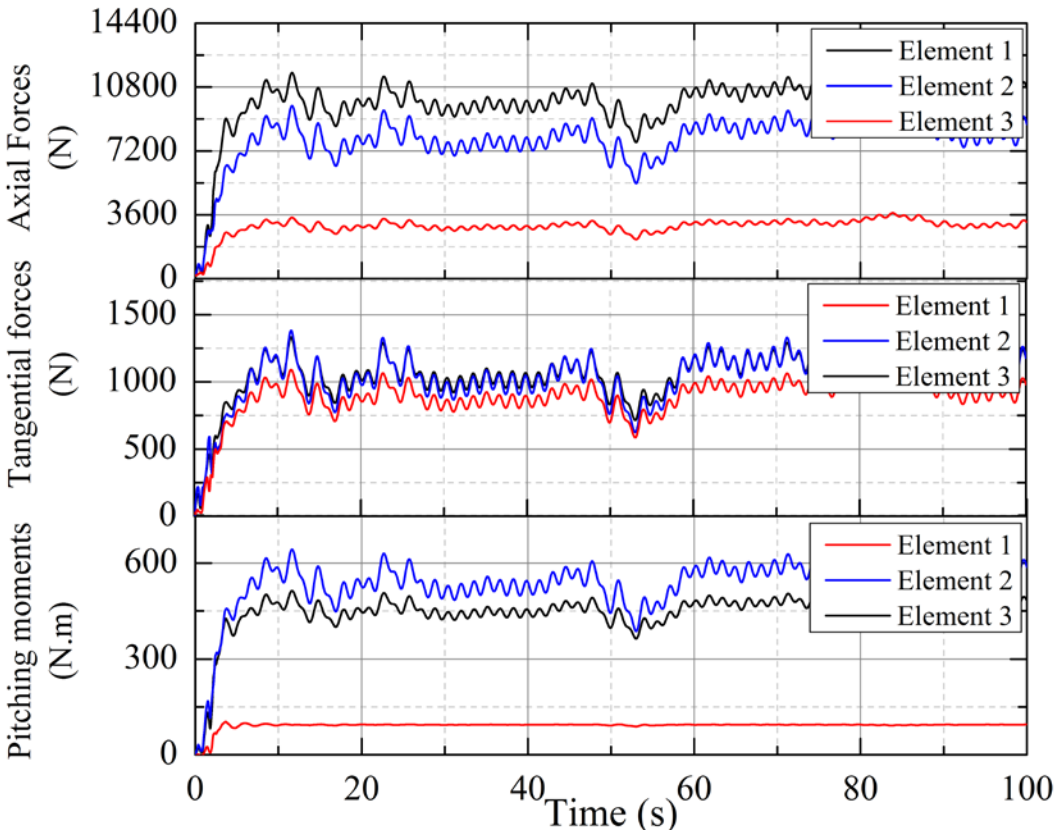

Figure 4.32. Axial Force, Tangential Force and Pitching Moment

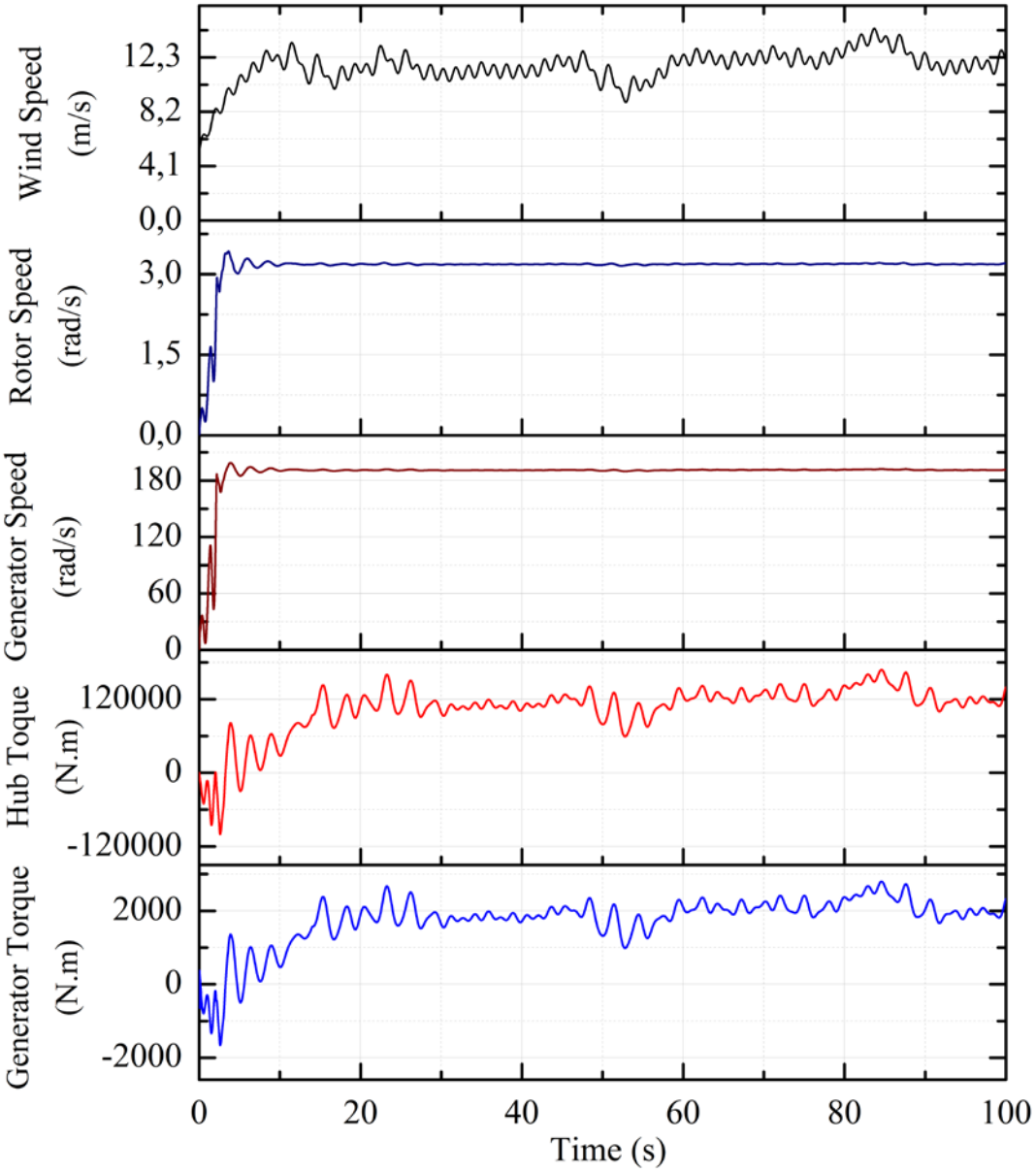

Figure 4.33 Responses for a variable wind

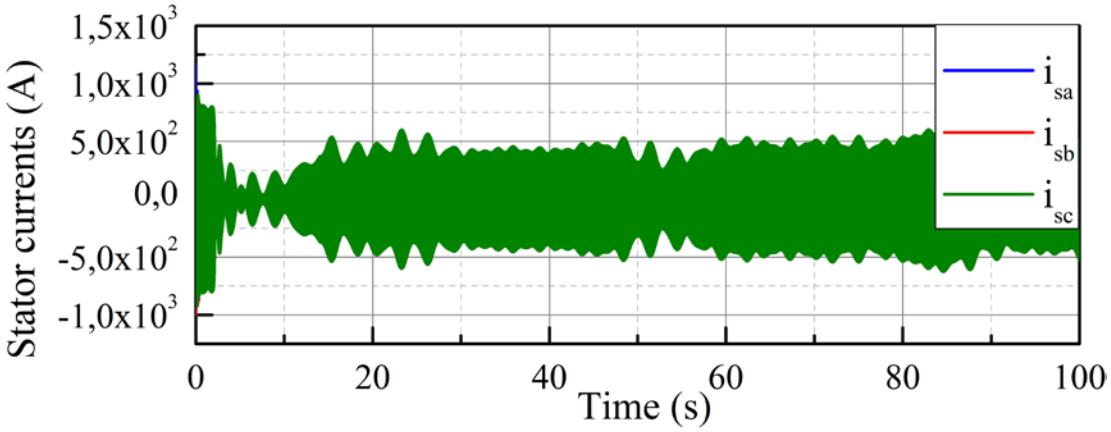

Figure 4.34. Stator currents of generator

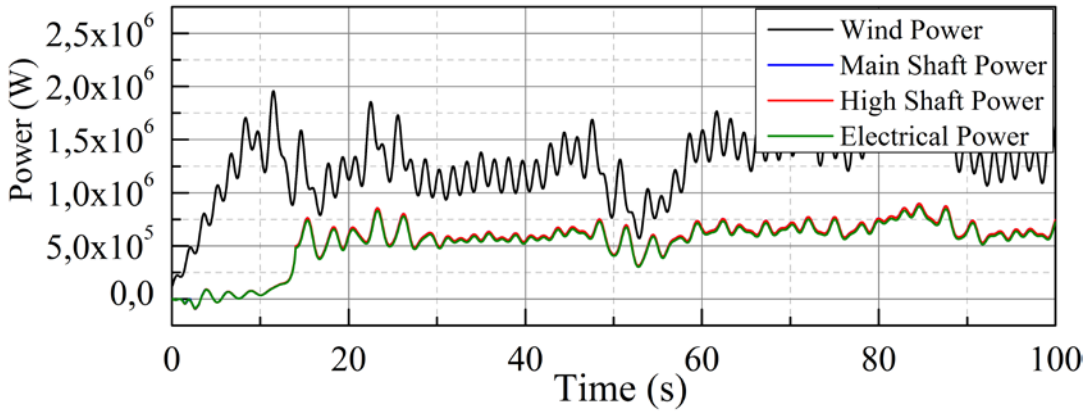

Figure 4.35. Power curves of model

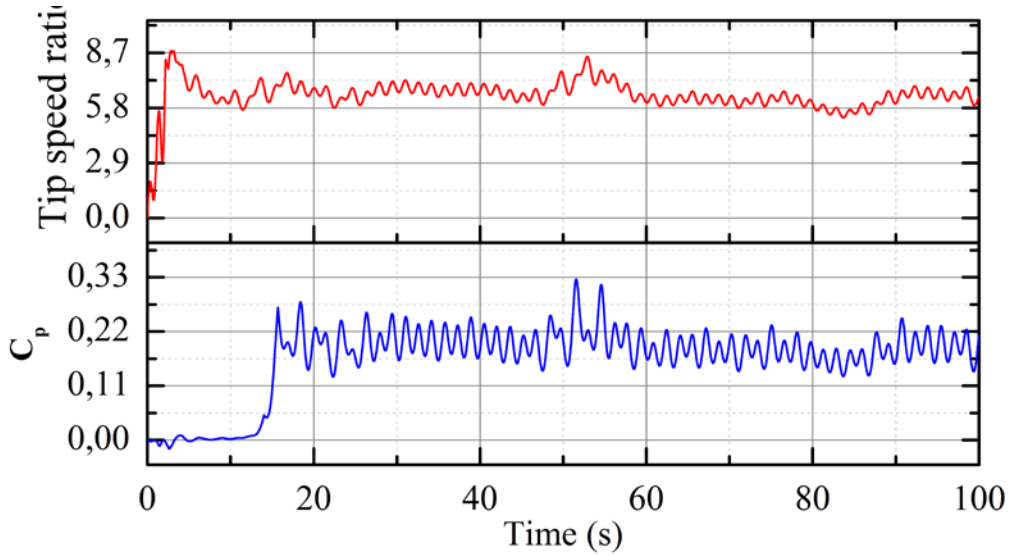

Figure 4.36. Curve C_P,and λ

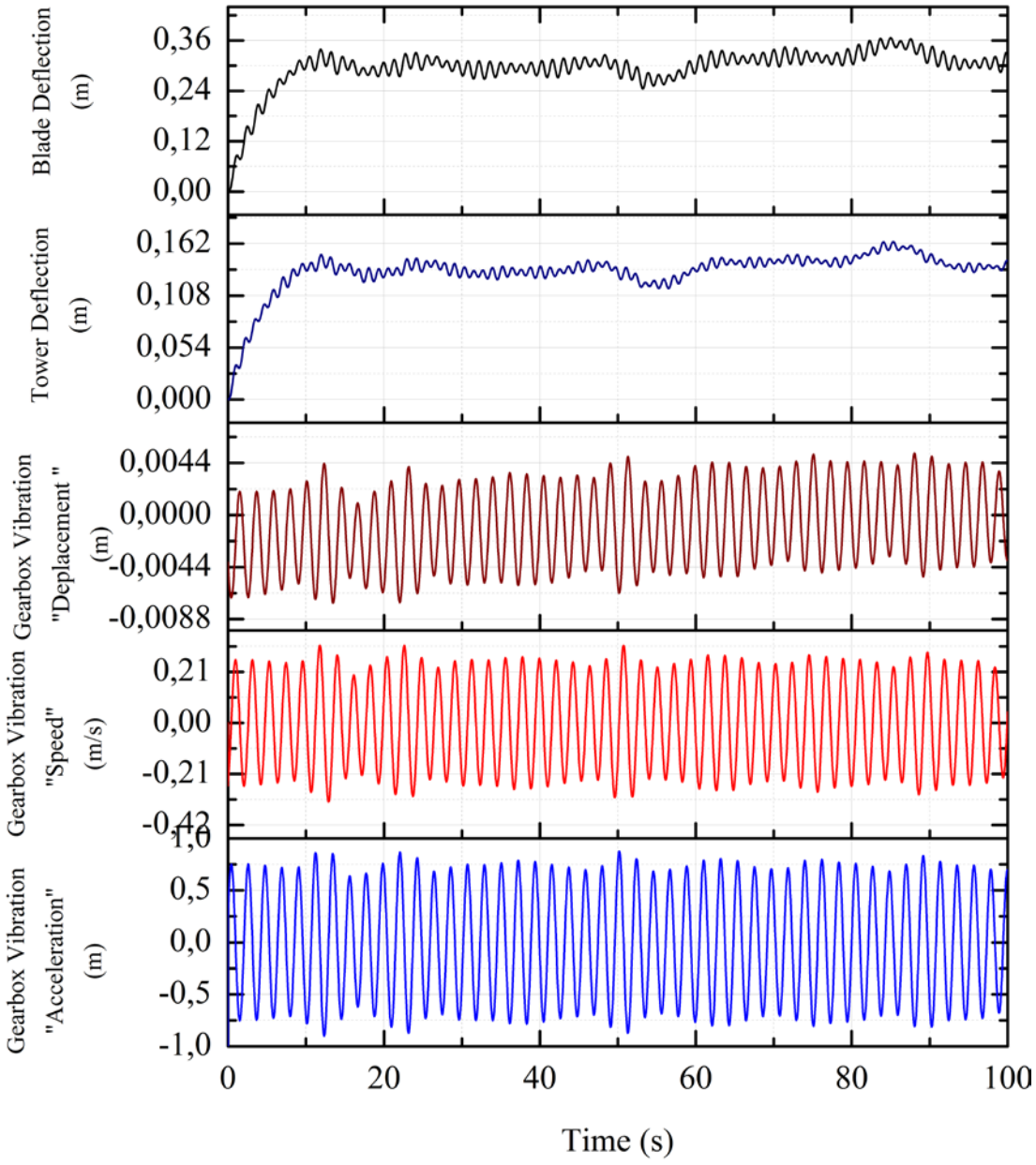

Figure 4.37. Gearbox vibration and Deflection blades and tower

Conclusion

Due to interactions between aerodynamic, mechanical and electrical subsystems, a mechatronic model of a wind turbine generating system using the Bond Graph Approach is proposed to analyze the dynamic behavior of a wind turbine. The close connection between the dynamics of the rotor blade and the pitch actuator requires a certain complexity of the mechanical model. By means of the presented modeling method, a correct load calculation

of the different parts of the system can be carried out. We are not looking to validate a specific turbine system, but we aim to show a suitable way to model it.

Some contributions have used the bong graph implementation, but they involve only one part of the wind turbine, e.g. the gearbox in [20] or blade in [16]. Others [32, 33] have modeled the principal part of the wind turbine but the models are not enough detailed. This "gap" was seemingly filled in [19] but the axial extension deformation of the blade. The deflection of the tower, the vibration of the gearbox and the pitching system were not considered.

This present work highlights the fact that all these parts are considered in one integrated model. This model describes, to a certain extent, the actual behavior of the turbine in that it takes into account the most important dynamics phenomena encountered in the system. We have tried to emphasize that the BGA provides a better understanding of what actually happens in the system.

After simulation for both constant and variable wind speed consideration, good results have been obtained with the proposed model, but comparisons with real measurements are not available at this stage. Research works by other authors are under progress in this direction.

The present model can be used to determine the loads of the wind turbine drive train during the simulation process, and to calculate the deflection of the blade and tower and then develop the law control algorithms, which would minimize the probability of blade tower vibrations. The model can also be used to provide information on the gearbox vibration, as well as an assisting tool in designing the components of the pitching system. Moreover, it is possible to use this model for the system dynamic behavior's optimization. It was also efficiently used for testing new control strategies of wind turbines.

Only a few publications involving all the stages of a wind turbine are available in the open literature. In this context, the model proposed here is an important starting point for the analysis of this complex system.

Based on the results of this work, interesting future prospective research will include performing control design using bond graph and possibly constructing a complete wind turbine model.

References

[1]. Peter C. Breedveld. Port-based modeling of mechatronic systems. Mathematics and Computers in Simulation. 2004;66:99-127.

[2]. Buur, "A theoretical approach to mechatronics design," Ph.D. disserta-tion,1990.

[3]. Ehsanolah Assareh, Mojtaba Biglari. A novel approach to capture the maximum power from variable speed wind turbines using PI controller, RBF neural network and GSA evolutionary algorithm. Renewable and Sustainable Energy Reviews. 2015;51:1023-37.

[4]. Poultangari I, Shahnazi R, Sheikhan M. RBF neural network based PI pitch controller for a class of 5-MW wind turbines using particle swarm optimization algorithm. ISA Trans. 2012;51:641-8.

[5]. Olaf Enge-Resenblatt, Petre Schneider, Modelica wind turbine models with structural charges related to different operating modes, The modelica Association 2008 pp. 610-19.

[6]. Qiong-zhong Chen, Flavio D'Ambrosio, Michel Defourny, Olivier Brüls. Integrated control and structural analysis of DFIG wind turbines using a monolithic approach, 2012.
[7]. [7] G.M. Joselin Herbert, S. Iniyan, D. Amutha, A review of technical issues on the development of wind farms. Renewable and Sustainable Energy Reviews. 2014;32:619-41.
[8]. Jackson G. Njiri, Dirk Söffker. State-of-the-art in wind turbine control: Trends and challenges. Renewable and Sustainable Energy Reviews. 2016;60:377-93.
[9]. M. J. Hoffmann, R. Reuss Ramsay, G.M. Gregorek. Effects of Grit Roughness and Pitch Oscillations on the NACA 4415 Airfoil. The Ohio State University Columbus, Ohio. July 1996.
[10]. Donald Margolis. Bond Graph Modelling of Engineering Systems: Theory, Applications and Software Support 2011.
[11]. Rochdi Merzouki, Arun Kumar Samantaray, Pushparaj Mani Pathak, Belkacem Ould Bouamama. Intelligent Mechatronic Systems: Modeling, Control and Diagnosis. 2013.
[12]. Fernando D. Bianchi, Hernán De Battista and Ricardo J. Mantz. Wind Turbine Control Systems: Principles, Modelling and Gain Scheduling Design. 2007.
[13]. Fernando L. Ponta, Alejandro D. Otero, Lucas I. Lago, Anurag Rajan. Effects of rotor deformation in wind-turbine performance: The Dynamic Rotor Deformation Blade Element Momentum model (DRDeBEM). Renewable Energy. 2016;92:157-70.
[14]. Sungmoon Jung, Sung-Ryul Kim, Atul Patil, Le Chi Hung. Effect of monopile foundation modeling on the structural response of a 5-MW offshore wind turbine tower. Ocean Engineering. 2015;109:479-88.
[15]. Shipley D.E., Miller M.S., Robinson M.C., Luttges M.W., Simms D.A. Evidence that aerodynamic effects, including dynamic stall, dictate HAWT structural loads and power generation in highly transient time frames. In: WINDPOWER, AWEA, Minneapolis,1994, pp. 615-26.
[16]. Lee C.-W., Yun J.-S. Dynamic analysis of flexible rotors subject to torque and force. Journal of Sound and Vibration.1996;192:439-52.
[17]. S. Agarwal, L. Chalal, G. Dauphin-Tanguy, X. Guillaud, Bond Graph Model of Wind Turbine Blade, Bond Graph Modeling: Theory and Practice MathMod Vienna, 2012.
[18]. Christopher J. Spruce and Judith K. Turner, Tower Vibration Control of Active Stall Wind Turbines, JULY 2013.
[19]. GWEC, Global Wind Statistics 2012, Global Wind Energy Council, February 2013.
[20]. N. Coudert, G. Dauphin-Tanguy, A. Rault, Mechatronic Design of an Automatic Gear Box using Bond Graphs, in: Proceedings of the IEEE Systems Man and Cybernetics Conference, 1993.
[21]. Deur Joško, Ivanovic Vladimir, Assadian Francis, Kuang Ming, H. Tseng Eric, Hrovat, Bond graph modeling of automotive transmissions and drivelines, in: Proceedings of 7th Vienna International Conference on Mathematical Modelling (MATHMOD), Vienna, Austria, 2012.
[22]. R. Sanchez, A. Medina. Wind turbine model simulation: A bond graph approach. Simulation Modelling Practice and Theory. 2014;41:28-45.
[23]. F. Chaari, T. Fakhfakh, and M. Haddar, “Dynamic analysis of a planetary gear failure caused by tooth pitting and cracking,” Journal of Failure Analysis and Prevention, vol. 6, 2006, pp. 73-78.
[24]. F. Chaari, W. Baccar, M. S. Abbes, and M. Haddar, “Effect of spalling or tooth breakage on gearmesh stiffness and dynamic response of a onestage spur gear transmission”, European Journal of Mechanics-A/Solids, vol. 27, 2008, pp. 691-705.

[25]. Liu Xiong, Chen Yan, Ye Zhiquan. “Wind turbine computing model of aerodynamic performance with horizontal axis,” Journal of solar, Beijing, vol. 26, 2005, pp. 792-800.
[26]. M.O.L. Hansen, J.N. Sorensen, S. Voutsinas, N. Sorensen, H.A. Madsen, State of the art in wind turbine aerodynamics and aeroelasticity, Progress in Aerospace Sciences. 2006;42:285-330.
[27]. E. Delaleau, J.P. Louis, R. Ortega, Modeling and control of induction motors, International Journal of Applied Mathematics and Computer Science. 2001;11(1):105-29.
[28]. D. Sahm, A two-axis, bond graph model of the dynamics of synchronous electrical machines, Journal of the Franklin Institute. 1979;308(3):205-18.
[29]. G. Dauphin-Tanguy, Les Bond Graphs, Hermès Science Editor, 2000.
[30]. Berthold Schlecht, Samer Mtauweg, Thomas Rosenlöcher. Dynamic design of an electromechanical Pitching System for Wind turbines by Means of Multi-Body Simulation. SIMPACK News 2011.
[31]. Mtauweg, S.; Dynamische Analyse des Pitchsystems der Windenergieanlage GE 1.5 MW, unveröffentlichter Bericht, Tu-Dresden 2010.
[32]. Tore Bakka and Hamid Reza Karimi. Bond graph modeling and simulation of wind turbine systems. Journal of Mechanical Science and Technology 2013;27(6):1843-1852.
[33]. Tore Bakka and Hamid Reza Karimi. Wind Turbine Modeling Using The Bond Graph. IE EE Multi-conference on systems and control. 2011, pp. 28-30.

Chapter 5. Role of VANETs in managing Smart Cities.

5.1 . Introduction

In recent years, large numbers of people moving towards urban environments has been detected, where it has been forecasted that cities inhabitant will represent 60% of the population in future years. This phenomena triggered new challenges for companies and systems that may address these challenges related to the increase and development of the Smart City. The concept The Smart City operates in, may be considered as a complex urban environment, managing and controlling several complex systems including infrastructure, human behavior, technology, social, political structures, communication tools and the economy. A Smart City provides an intelligent way to manage components such as transport, health, energy, homes, buildings and the environment. The data collected by these components are usually generated by wireless networks data collectors. The wireless communication Vehicular Ad-hoc Networks (VANETs) within the Smart City are an essential tool that benefits the network in the Smart City by providing opportunistic communication to the different intelligent systems without the need of pre-installed infrastructures. Vehicular Communications offered new research fields to establish and manage different applications used in Vehicular Communications, to provide network connectivity in environments where wired solutions are impossible. Among these promising and important applications in Vehicular ad hoc Networks, there are road safety, traffic control and entertainment for passengers' applications. VANETs are capable of providing network connectivity inside and outside cities where wired connectivity is impossible or will cost a fortune and a big amount of resources to be established and maintained.

The fact that VANETs afford connectivity in roads inside and outside cities, justifies the importance of road network connectivity and classifies it as an essential tool, especially the connectivity inside the cities that benefits the connected cities and in global the smart cities. VANETs fill a major gap of the existent networks implemented and applied in smart cities, it facilitates the communication between vehicles and infrastructures implemented in the City for different use cases, such as road safety, traffic control and may also transmit different data of different applications used in the Smart City. VANETs offer different type of communications where, it can act as a mobile node that forwards urgent data from source to destination, we may also employ them as data mules, where they can collect and deliver data with low delays from the information collectors in the city, In fact, this solution provides a mobile data infrastructure as a replacement for the fixed infrastructure, especially for those application that are not delay. In this paper, we illustrate the importance of VANETs within a smart city, and how the opportunistic established connections, may benefit the smart city infrastructure. On the other hand, we focus more on the communications that require an acknowledgement of the received data, and make sure that the packet has been correctly delivered to its destination. Recently, more researches propose to have global understanding not only of the physical places, but also of the network systems and flows, where many literatures hint to the global challenges regarding the contribution of the cities such as Intelligent, Wired, Digital or Smart City, in order to develop new ideas and set up applications as well as Smart Monitoring Systems capable of managing and maintaining the basic infrastructures of a Smart City basing their network connectivity on Vehicular Networks.

in this Chapter, we elucidate the importance of VANETs in a Smart City infrastructure, where we propose VANETs as one of the basic networks to be implemented in a Smart City

for a Smart Monitoring System managing the Smart Cities basic infrastructure, by controlling the generated and collected data from the different sensors and servers implemented in multiple places within the Smart City, and we provide a small enhancement implemented to the AODV routing protocol, for data transmission that requires a reception acknowledgement, which enhances the Quality of Service (QoS) of the network performance, we establish some simulations to evaluate the enhancement performed, then present an example of a Smart Application that can be deployed in a Smart City, and how minimizing the data generated from this application may facilitate and rapidly enhance the performance of such application.

5.2 . State of the Art

The rapid growth of population in cities demands an implementation of multiple types of communication tools and technologies in order to satisfy the global needs of the city inhabitants; due to the huge amount of data circulating within the city, multiple communication technologies are implemented in order to minimize the network traffic, due to the increasing demand of services identified in the Smart City, but the implementation within the Smart City of a full connected infrastructure with all the other infrastructures and services cost a fortune and request continuous and costly maintenance, and it is preferable to use flexible, mobile and opportunistic connections between vehicles and nodes(Servers, Sensors, data collectors ...etc.), this is where VANETs can be considered a powerful tool used for network connectivity within a Smart City, and how the VANETs have evolved from the collection of traffic congestion, road safety and emergency data concerning the road to the Internet of Autonomous Vehicles like other instantiations of the Internet of Things (IoT) where they are capable of acting as a regular network that is capable of forwarding data between two different entities and connecting them through The Internet of Vehicles, the Internet of Vehicles represent a part of the Internet that will possess his own storage, intelligence and learning capabilities to anticipate the Smart City needs and intentions.

The Art of Vehicular Communications employed within the Smart Cities, are still far from reaching the ideal desired results. Nevertheless; they act as a powerful communication tool when it concerns the handling of traffic congestion, road safety and emergency data; the next step would be to identify the Internet of Vehicles as a powerful communication tool, that deploy the mobility of its nodes to a better and flexible communication that tolerate short delays.

5.3 . Enhanced Communication

5.3.1. Vehicular Networks Interaction:

For the promising future Smart Cities, global communications between vehicles and the city are required to be constant, including infrastructure-to-infrastructure, car-to-car and infrastructure-to-car communications. Though the Infrastructure-to-Infrastructure require pre-installed tools and continuous maintenance, in the other hand the car-to-car and car-to-infrastructure may overlook the continuous maintenance of the path. Indeed, in the context of smart city one only needs to forward the message to the next nodes(vehicle, station...etc.), but we want to make sure that the information will reach its final destination. Therefore we need to find alternative routes to establish the connection in case unwanted disconnections occur in the Vehicular Network.

The fact that the daily vehicles circulating in the city roads vary from private, public and semi-public transport systems, limit the benefits of vehicles networks and the full potential VANETs may accentuate in Smart Cities. Eventually if all the vehicles in the city were

involved, the quality of service would be optimal; but private vehicles may refuse to share their network connectivity due to the drivers preferences and privacy. So for a realistic alternative, we consider only the public and semi-public moving vehicles. Which means that just part of the vehicules within the city will constitute our Vehicular Network for a Smart City which may represent between 10-30% of all the vehicles in the city roads, and may go sometimes up to 50%, each interacting vehicle in the Vehicular Network is required to have an on-board terminal, that integrates different wireless communication technologies(Wi-Fi, ZigBee, Bluetooth...etc.), to communicate with surrounding vehicles, stations, nodes, sensors or other infrastructures.

The main interest is oriented towards improving the Quality of Service of the communications between source and destinations nodes that require an acknowledgement for the received data packets, with short delays and continuous transmissions. Our proposed approach, deploys an enhanced Ad-hoc On-demand Distance Vector(AODV) routing protocol. Our objective is rather than the focus of distributing the information or flood the data packets in the Vehicular Network, we try to enforce the connection we may require to establish between two nodes (source and destination), that may be represented as two vehicles, storage station and data collector, vehicle and storage station or even storage station and the control server where we need to transmit packets data from source to destination with an acknowledgement received data and go through vehicles as the forwarder nodes. The enhanced AODV routing protocol deploy a new method that specify the time limit of the route we established between the source and destination nodes in order to maximize the Packets Delivery Rate (PDR) and remove any obstacle that may cause packets loss during the exchange of information between the two nodes

5.3.2. The AODV Routing Protocol

Ad-hoc On-demand Distance Vector (AODV) is a reactive routing protocol which discovers a route to the destination when the route is needed; this routing protocol maintains the active routes discovered while they are not stale, which helps solving the network loop problem, where routing packets circulate indefinitely, for each new route requested the source node of the route request broadcast a packet defined as the Route Request Message (RREQ) with a Time To Live (TTL) in order to not keep the RREQ packet in the network for infinite time, the destination node responds to the RREQ message by sending a special packet defined as a Route Reply Message (RREP) to the source node, in case neighbors nodes do not have a route to the requested destination, the node acting as a forwarder, forwards the RREQ, upon reaching the destination node, a RREP is transmitted to the source node and a route is established between the source and destination nodes for data packets transmission. The routing information, the routing protocol AODV collects is limited, thus the node source calculates only the route to the destination node, and for each new node destination, a new route discovery process is necessary, such actions may carry a significant network overhead, and periodically each node broadcast Hello messages to neighbors' nodes in order to determine their connectivity, and update the routing table with the routes to the neighbors' nodes, by adding the not existing nodes and increasing the lifetime of the already existing nodes, once the lifetime of a node expire the route is deleted from the routing table. A broken link between two nodes affects only active paths using this link: AODV does not trigger any process action if the affected link is not used by any active path. Each time a node involved in active route moves out of its neighbor range, that node verifies if the conditions are met to trigger the broken link repair algorithm, in case the conditions are not met the node broadcasts a "Route Error" (RERR) packet in order to inform its precursor nodes about the broken link. This information is conveyed backwards to the source node. Each node that receives the route

error, updates its routing table. Then the node source re-initiates the route discovery process, if the route is still required .

5.3.3. The Enhancement of AODV in VANETs within a Smart City

The AODV routing protocol establishes a connection with the destination node once the route is found and starts transmitting the packets until there are no more packets in the source node, then he puts down the route, but there are cases where the link between source and destination nodes is broken due to the mobility, disconnection or other causes, so either the AODV try to reestablish the connection or find another route, which cause in cases when there are a lot of disconnections, a huge amount of packets loss, that requires the retransmission of the packets when there is a new connection between source and destination nodes.

In this paper we approach the problem of the route disconnections, with an aim of completely removing the packets loss as the ideal objective, and interrupting the packets transmission whenever there are problems within the route due to a disconnection, to remove the problem of packets loss and additional routing packets generated in order to reestablish the route or report the failure of the route due to a disconnection; in this paper we illustrate our first step towards achieving this goal, where we define to the route a timestamp Route Time To Live (RTTL), this RTTL represents the predicted Time between the hop and next hop nodes before they get out of range of each other's broadcast range, in order to reduce the failure problem and unnecessary and unwanted routing packets broadcast in the network.

The RTTL time represent the time limit of each route between the hop node and next hop node and whenever the routing time through these two nodes reach the RTTL we put down this link between these two nodes and we rediscover the route to destination node, without the requirement of sending route error packets to source node which reduces the unwanted routing packets and also reduces the packets loss due to the routing protocol route rediscovery before the route failure occurs, which will minimize the normal huge packet queuing at the hop where the disconnection is predicted to appear, that causes us a great amount of packets loss within the network.

In order to compute the RTTL for each two node link in the Enhanced AODV we defined to VANETs, multiple characteristics interfere during the computing time:

Speed: each vehicle (node) within the vehicular network traverse the road with a variable speed depending on the road limit speed and the driver's preferences, this speed affect the connectivity with the next hop node depending on the direction of each node.

Direction: each node has a trajectory that it will take, this trajectory may happen to be random or predicted or even a fixed trajectory (bus, trams, trains...etc.), the link between the two nodes may be in same direction, opposite direction or even distancing or regrouping with each other with a random angle, that is determined by the route each node (vehicle) is crossing.

Mobility Pattern: vehicles (nodes) normally in roads may change the direction of their route depending on the driver which alters the distance and the RTTL between the two nodes randomly, and may cause an unpredicted disconnection between the two nodes.

Road Environment: traffic lights, accidents, road maintenance works...etc; all these obstacles may alter the speed and direction as well as the mobility pattern of the vehicle (node) within the road, which also may cause an unpredicted disconnection due to lack of knowledge regarding the route environment.

Driver's Behavior: finally the major and most random characteristic that affects the link connection, is the driver's behavior that we are incapable of predicting and sometimes even for the nodes (vehicles) with fixed trajectory (bus, tram, train...etc.) their direction is altered, which causes the link disconnection between the two nodes (vehicles).

In order to evaluate the enhancement implemented onto AODV routing protocol, we will perform our data transmission of the Smart Diagnosis Application presented in the next paragraph, over a casual Smart city map, and Agdal District Map from Rabat City.

5.4 . Smart Diagnosis

5.4.1. System Architecture.

The Smart diagnosis Application paves the way to a new way of preventive maintenance where the vehicle/machine does not need to have built-in dedicated devices. Such system can be easily deployed in all kind of vehicles especially old models and those working on hostile areas. The platform consists of a set of sensors and data collectors connected to an intelligent device that can process and analyses, locally, the data received. The device is controlled and monitored by a server through a two ways communication system. The vibration/noise sensors are fixed on the equipments and parts to be monitored. The measurements are done automatically and continuously, and the data is sent to the onboard device for filtering and processing. The server, jointly with the onboard device, will give warning if the vibration/noise values exceed set limits. The technique is based the number of summits that exceeds the threshold within the desired frequency range in the spectrum.

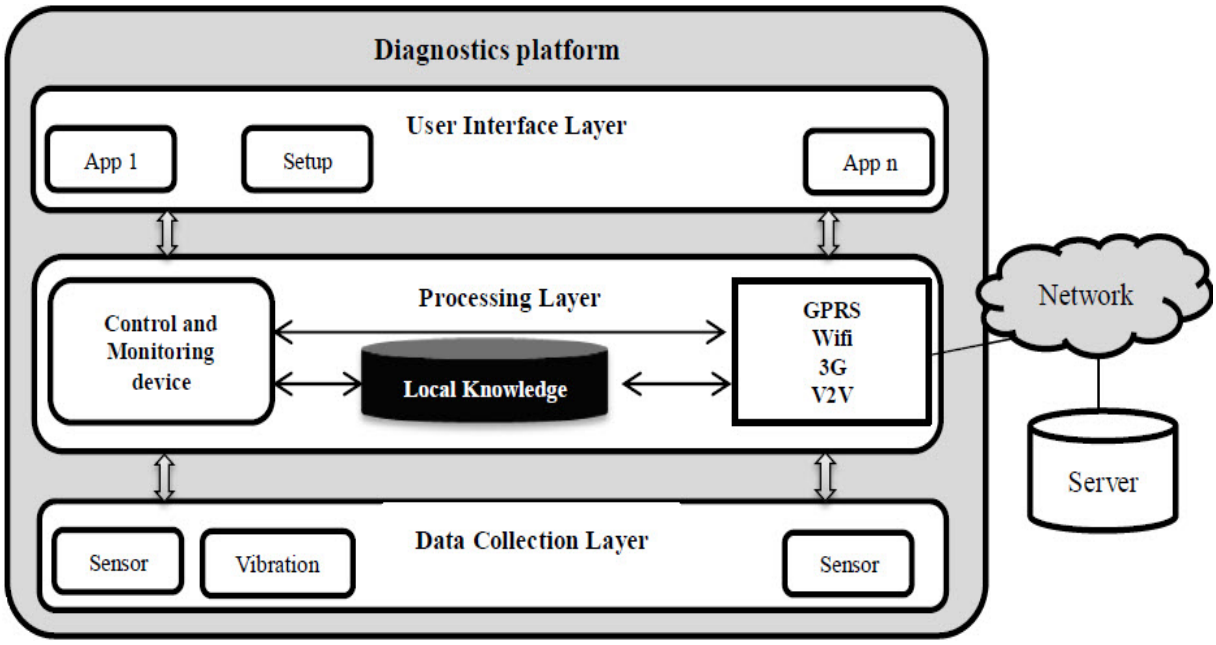

Figure 5.1. The Different Layers of the Smart Diagnosis Application

As shown in Figure 5.1 the proposed system consists of the following layers:

The sensing layer: it is a set of data collectors, mainly the vibration and noise sensors deployed around the targeted parts and equipments to be monitored within a vehicle or a machine. Various types and technologies of sensors may be used and hence one needs to care only about the range of the measurements and the way these values are sent to the device. The data collectors are connected to the device through wired or wireless local system in

client/server architecture. The information flow is controlled and synchronised by the device to get the right information at the right time. The information is sent continuously or on demand.

The processing layer: It consists of an on-board device that is a combination of hardware and software. This part is the heart beat of the platform, in charge of the coordination and the preliminary processor of the received data. It is also the proxy and the tool of the server onboard. The hardware part is composed of electronic controller with processing and buffering capabilities and junctions that can support all kind of sensors regarding the sensing technology used and the sensors communication protocols. The device needs to be connected to the server. For this purpose it has communication components such as GPRS,Wi-Fi and 3G to allow a long range communication through the Internet. The software part is in charge of processing and analysing the received data. This task uses the knowledge available locally. Further processing and intelligence is provided by the server.

The user interface layer: It consists of a set of applications that allow interacting locally with the system. Indeed the system can send messages and alerts to the user of the vehicle/machine. It can even operate and control the machine such as stopping the engine or reducing the speed if it was programmed to do so. This interface also could be used to set and configure the system. This layer maybe composed of monitors and speaker for the outputs and buttons and keyboards for inputs.

Server: The server, is the intelligence center of the system, performs further processing and analysis on the results, provides the knowledge to the device such as parameters and limits set, also updates the local database embedded in the device. We keep all the information called the knowledge base on the server. The knowledge base includes historical information regarding the monitored part and other technical information provided by the manufacturer such as the profile of the vibrations and the noises in normal conditions. These profiles are used by the server to compare it to those received from the data collectors to detect any gap between them. The server may request specific data from the platform regarding the monitored part, saves new results obtained from the analysis of the targeted part as historical information for future monitoring.

5.4.2. Smart diagnosis implementation.

The system performs remote diagnosis and track the targeted part within the vehicle, preventing incoming failures or defects to the targeted part. The smart diagnosis are based on the vibration data collected from the targeted parts, processed and analyzed in the middleware before presenting the results or requesting additional information from the server. The main function of the system is the surveillance and analysis in order to identify all kind of fatigue at their early stage. The main objective of the Smart Diagnosis Application is the reduce of the huge volume of the vibration data and minimizing the informative data without altering the results of the diagnosis performed on the monitored gear to “One Single Value” that represents the state of the targeted gear. This value is obtained by counting the number of summits exceeding the threshold within the desired frequency range from the Fast Fourier Transformation vibration signal; this value represent the profile of the gear and simplifies the data transmission between the platform and the server.

5.5 . Simulation

In this paragraph we evaluate the PDR (Packet Delivery Ratio) as well as the QoS (Quality of Service) of the network during the transmission of the data packets from the different sources (the data collectors installed within the Smart City streets, or the data

storages installed in the most known junctions within the District) to their one and only final destination, the Control Server.

5.5.1. Configuration of the Data Storages and the Vehicles

The Data Storages are installed on Agdal streets using Multi-interface nodes at fixed positions to ensure communications with both vehicles and the other sensors and nodes (Data Collectors).

To ensure high connectivity of the stations, we install them nearby a group of blocks and at famous junctions known for their traffic congestion and covers a range of 150m for the interface communicating with vehicles, as for the interface connecting with sensors and nodes that collect informative data we used a range of 200m. The control server act in our simulation as the end line of the data transmission where the transmission range is set at 150m. As for the vehicles, we divide them into two groups, where the Blue and White Taxis implement one interface that interact with other vehicles or the interface of the server or the interface of the stations that communicate with the vehicles, while the Buses, Trucks and Trams use two interfaces to interact with the stations and the server, where they use an interface identical to Blue and White Taxis, they use also another interface where they are capable of communicating and storing data received from each sensors, data nodes installed at bus, tram stop or blocks and keep it in their data base until they are closer to the server and transmit the data, in the simulation we are performing we are interested only on the first interface, that communicate like the Blue and White Taxis, we set the transmission range to 100m, taking into consideration the transmission range disturbances due to buildings.

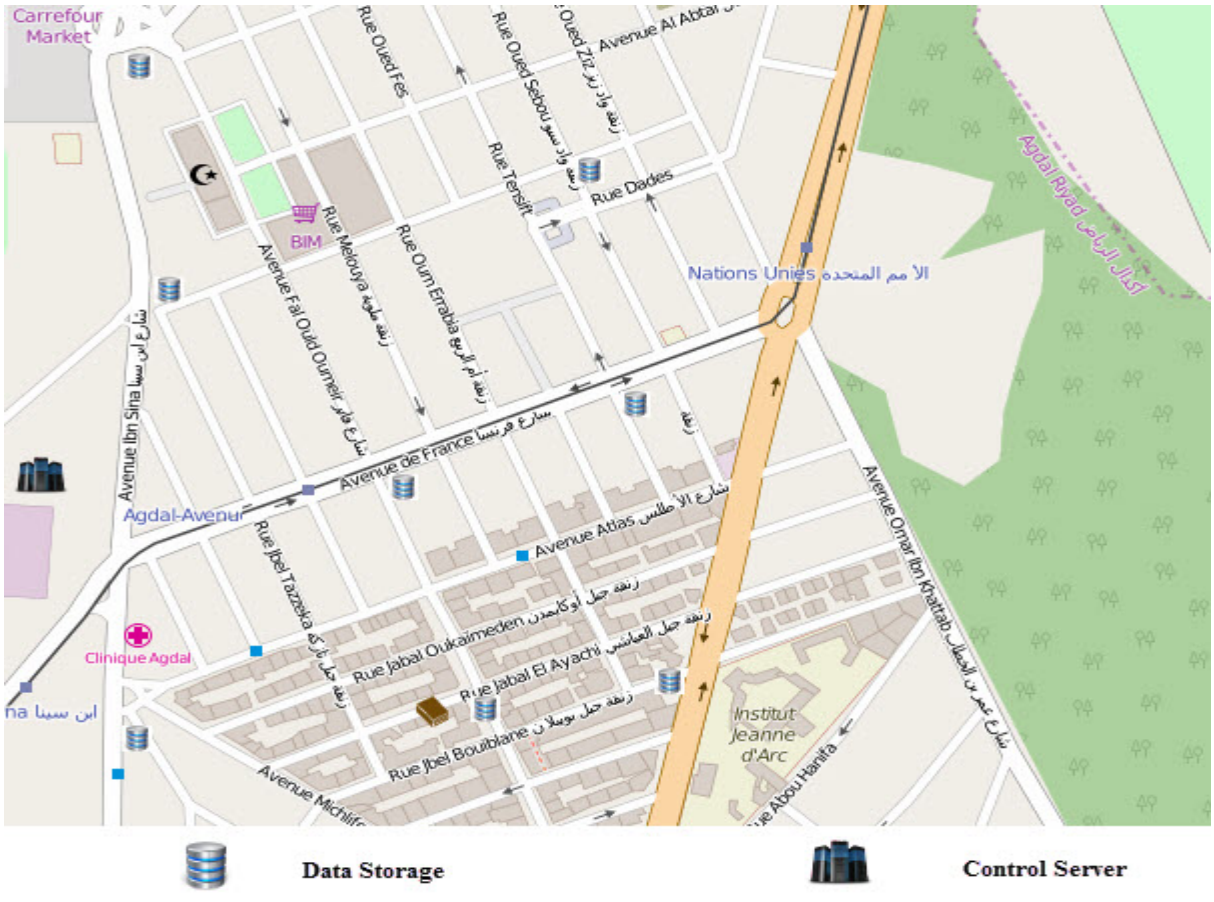

Figure 5.2. Part of Agdal District Taken by OpenMapStreet, Illustrating The Locations of some Data Storages and The Control Server

5.5.2. Maps Configuration

To evaluate the utility of VANETs in Smart Cities, we use two different maps, the first one represent an urban scenario of the Full Agdal district from Rabat city, to show how the VANETs are capable of acting as a transportation system between the stations and the server, Fig.2 above shows some of the stations location in the map as well as the server. The Simulation recreates the full Agdal district in Rabat city, the length of the streets varies from 50m to 300m with multiple junctions that connect from 2 streets to 7 streets with higher traffic congestion at junctions with 5 to 7 streets connections, and at junctions where the tram passes, due to the priority is always given to trams.

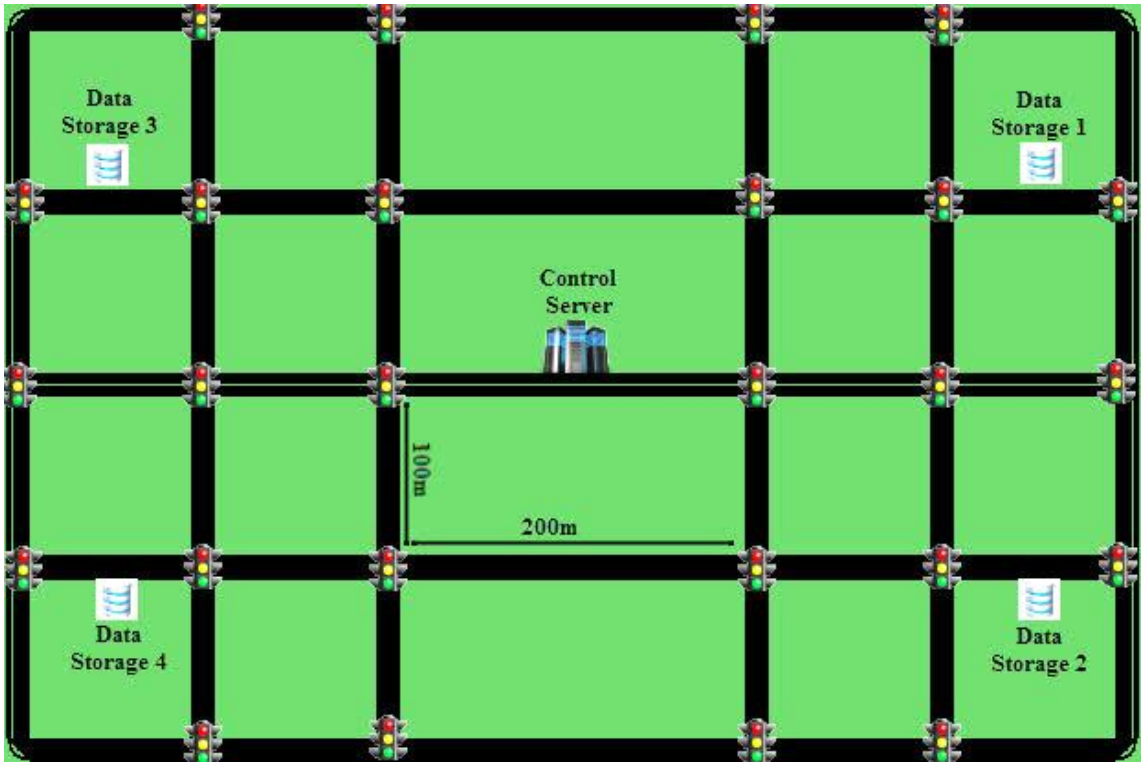

Figure 5.3. Intelligent Map of a Smart City with 4 Data Storages and a Control Server Installed

While the second map illustrate a casual number of blocks and streets we may encounter in a normal Smart City, as shown in Fig.3 we pre-install four data storages and the control server, the length of the streets differ from 100m to 200m as shown in the Fig.2.

5.5.3. Simulation Configuration:

The Simulation scenario for Agdal District map generates 1000 vehicle that includes a ratio of taxis, buses and public trucks, as well as trams, the Simulation scenario is using Agdal district map taken from OpenStreetMap, as for the second Simulation scenario we generate a 300 vehicles distributed between public, semi-public and private transportation systems, both scenarios are configured in the Simulation of Urban MObility(SUMO), this simulator generates a realistic scenario of vehicles mobility that can be used in the Network Simulator 2(NS2), where we set the Initial Energy used by the vehicles to 0 unless the vehicle represent public or semi-public transport system, or a private transport system that allows the forwarding of data packets, we keep altering the ratio and the number of vehicles influencing

the VANET networks within the Smart City where we change the ratio of the number of nodes(vehicles) interacting in the network between (10%, 20%, 50%, 100%) , the Initial Energy is set to 100 Joules, to make the vehicle capable of receiving and transmitting data.

For both maps The data storages stations will broadcast 512 bytes messages every 0.5 second (2 messages each second), whenever they find route to the server using the public and semi-public and some private transportation tools depending on the ratio of the vehicles interacting in the VANET Network as forwarders for their messages while they are roaming the city according to the customers' requests or due to their trajectory, the simulation will continue for a period of 82 seconds taken between 9A.M and 11A.M during the period of time where Agdal roads are active with vehicles, but with no huge traffic congestions for the first map, while in second map we simulate for a duration of 60 seconds during a upper traffic compared to the first one.

In the Simulation scenarios presented we use the AODV routing protocol and an Enhancement of the latter routing protocol as described above in this paper, the main objective of both simulations is to evaluate if the Vehicles Networks may act as strong network connectivity tool that is capable of transmitting data within the city between stations placed in the city streets and the control server within the Smart City as well as the improvement of our approach to the AODV routing protocol to improve the PDR as well as the QoS.

Table 1: SIMULATION SETTINGS

Parameter	Value
Packet Size	512 bytes
Simulation Time	82 seconds
Agdal District Map	3500*3500 m2
Map 2	640*440 m2
Number of Nodes in Agdal Map	1011
Number of Nodes in Map 2	305
Maximum Average Speed	20-50 (km/h)
Mobility Model	CarAgentMod (SUMO)
Vehicles Transmission Range	100m
Data Storages Transmission Range	200m
Routing Protocol	AODV

5.5.4. Results & Analysis

As shown from Table.2 and Table.3, the utility of VANET Networks within the Smart City is not negligible and can be implemented as a basic network within the Smart City, from the same figures we can see the improvement the proposed approach present to AODV routing protocol regarding the PDR and QoS, where our enhanced routing protocol in the same scenario as the normal routing protocol transmit lesser packets but with a higher ratio of

the received data packets due to the RTTL indicator that represent a major factor in the results.

Tableau 2: Results of Agdal District Map

Nodes Ratio	PDR (%)		Throughtput [kbps]		EED (ms)	
	AODV	RTTL-AODV	AODV	RTTL-AODV	AODV	RTTL-AODV
100%	80,59% S: 1602 R: 1291	87,36% S: 1512 R: 1321	65,69	70,28	135,95	104,04
50%	78,95% S: 1592 R: 1257	86,1% S: 1510 R: 1300	63,67	68,71	263,87	206,14
20%	64,19% S: 1578 R: 1013	70,65% S: 1489 R: 1052	59,12	62,52	312,41	451,21
10%	62,59% S: 1524 R: 954	66,59% S: 1485 R: 989	46,4	55,12	792,24	851,52

Tableau 3: Results of Map 2

Nodes Ratio	PDR (%)		Throughtput [kbps]		EED (ms)	
	AODV	RTTL-AODV	AODV	RTTL-AODV	AODV	RTTL-AODV
100%	82,66% S: 623 R: 515	90,04% S: 623 R: 561	27,87	30,53	75,19	86,61
50%	81,03% S: 643 R: 521	85,62% S: 640 R: 548	27,7	29,2	263,87	116,36
20%	65,07% S: 647 R: 421	71,29% S: 620 R: 442	22,44	24,64	704,56	624,04
10%	47,42% S: 639 R: 303	55,82% S: 541 R: 302	16,81	18,45	1210,8	728,03

As shown from both Table.2 and Table.3 the RTTL-AODV outperforms the standard AODV routing protocol, where as seen from the results obtained in both Tables there is a reduce of the data packets send and an increase of the received data packets due to the Route being put down whenever the RTTL reach the zero to avoid a link failure before it occurs, but the results are still non-satisfactory where we are trying to achieve a result as close as possible to the optimal solution where PDR should be close to 100% (Transmission/ Reception) in any VANET Network scenario within a Smart City, where all send data packets need to reach their destination with the same characteristics the AODV routing protocol but with a better

improvement to the RTTL that determines the route time to live before the route may encounter disconnections or other problems that disturb the transmission of data packets.

5.6 . Conclusion

In this Chapter, we displayed how Vehicular Networks in Smart Cities offer a very satisfactory and alternative network. The simulation results confirm how the vehicular networks are capable of acting as a connectivity tool between the stations and the back-end server. The goal of this work, is considered to be achieved, since the transmission delays between the stations and the back-end server are negligible when we are interested on informative data transmission that do not require delays and require instantaneous update of information for Smart Applications like the already presented Smart Diagnosis Application, we used the AODV routing protocol that satisfies this charge, and we presented the enhancement we performed on the AODV routing protocol where we identified a new metric known by the RTTL that time out the route before its failure, to avoid a huge drop-out of data packets. The simulation results confirm how the idea we presented as an enhancement is applicable and may still be reinforced, by adding more metrics and characteristics to improve the performance of the network.

CONCLUSION

In this « Thesis of Works », the author has reported the summary of his research activities in two different fields within two entities.

The first one was about developing a new multidomain and multilevel approach for designing and controlling a Wind Energy Conversion System. It encompasses various physics areas such as Aerodynamics, Mechanics, Vibrations, Strength of Materials, Power Electronics, Electrical Circuits and Control Theory. The Bond Graph Approach has been proved to be an excellent tool in dealing with this complex problem. The outcomes were two publications which make up the main contribution in this present report.

The author intends to explore the experimental side of this exciting topic if the conditions of having a full functioning facility within our Lab or eventually with another partner entity are met. Alternatively, there is a trend also to examine this BGA applicability to the new trend within the automotive industry in the field of the Internal Combustion Engines (ICE)'s Diesel Common Rail Injection Systems.

The second topic deals with the increasingly crucial role played by the so-called VANETs (=wireless communication Vehicular Ad-hoc Networks) in managing the Smart City. It has been put forward how Vehicular Networks in Smart Cities offer a very satisfactory and alternative network. The simulation results confirm how the vehicular networks are capable of acting as a connectivity tool between the stations and the back-end server.